Faculty of Electrical and Electronic Engineering Technology

DEVELOPMENT OF A LOW-COST WATER BASED TRANSPARENT ANTENNA FOR SUB 6 GHZ 5G COMMUNICATION SYSTEMS

AINA FARISAH BINTI RAHMAT

Bachelor of Electronics Engineering Technology (Telecommunications) with Honours

2023

DEVELOPMENT OF A LOW-COST WATER BASED TRANSPARENT ANTENNA FOR SUB 6 GHZ 5G COMMUNICATION SYSTEMS

AINA FARISAH BINTI RAHMAT

A project report submitted
in partial fulfillment of the requirements for the degree of
Bachelor of Electronics Engineering Technology (Telecommunications) with Honours

Faculty of Electrical and Electronic Engineering Technology

UNIVERSITI TEKNIKAL MALAYSIA MELAKA

2023

DECLARATION

I declare that this project report entitled "Development of a Low-Cost Water Based Transparent Antenna for Sub 6 GHz 5G Communication System" is the result of my own research except as cited in the references. The project report has not been accepted for any degree and is not concurrently submitted in candidature of any other degree.

Signature : 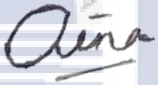

Student Name : AINA FARISAH BINTI RAHMAT

Date : 15 JANUARY 2023

APPROVAL

I hereby declare that I have checked this project report and in my opinion, this project report is adequate in terms of scope and quality for the award of the degree of Bachelor of Electronics Engineering Technology (Telecommunications) with Honours.

Signature : 

Supervisor Name : DR. MUHAMMAD INAM ABBASI

Date : 15 JANUARY 2023

DEDICATION

Thanks to Allah,

For giving me good health and strength to finish this work.

To my beloved mother and my lovely father,

I dedicate this study

to all of those who patiently stood by and comforted and encouraged me

during difficult and turbulent times.

They instilled in me desire to learn and made sacrifice.

They always support their moral, spiritual, emotional, and financial support.

They are also my source of inspiration and my source of strength when I wanted to give up.

To my brothers,

Thanks, with shared their words of advice and encouragement to finish this study.

To Dr. Muhammad Inam Abbasi,

Thanks for the guidance given. Hopefully I will be remembered.

and also,

this dedicated to my infinite friends

who have always supported me throughout my years of studies.

ABSTRACT

In this day and age, many people know about technology because with the advent of technology, it can make human life more enjoyable in doing daily activities. So, communication system is one of the technologies that can give a lot of impact in life. For example, in the old days, communication systems such as telephones that had a 3G bottom line, did not get response because they did not know about communication technology. So now, technology systems have evolved rapidly in the technology era and have evolved to 5G communication systems so that human beings can communicate with outsiders without restrictions. 5G communication systems provide many potentials and challenges for antenna designers. One of the challenges is to develop transparent antennas to provide freedom of antenna integration with other components. Many researchers have proposed different techniques for the design of transparent antennas. However, most of the proposed techniques use high -cost materials that make the antenna and the overall system, expensive. Therefore, in this work the development of a low -cost water -based transparent antenna for a 5G Sub 6 GHz Communication System has been proposed. In this paper, the design of water-based antenna has used CST Microwave Software to obtain the results that have been shown.

ABSTRAK

Pada zaman ini, ramai orang mengetahui tentang teknologi kerana dengan adanya teknologi, ianya dapat menyenangkan hidup manusia dalam melakukan aktiviti seharian. Jadinya, sistem komunikasi adalah salah satu teknologi yang dapat memberikan kesan yang banyak dalam kehidupan. Contohnya, pada zaman dulu, sistem komunikasi seperti telefon yang mempunyai line bawah 3G, tidak mendapat sambutan kerana mereka tidak mengetahui tentang teknologi komunikasi. Jadi sekarang, sistem teknologi telah berkembang pesat dalam era teknologi dan sudah meningkat kepada sistem komunikasi 5G supaya manusia dapat berhubung dengan orang luar tanpa sekatan. Sistem komunikasi 5G menyediakan banyak potensi dan cabaran untuk pereka antena. Salah satu cabaran adalah untuk membangunkan antena telus untuk memberikan kebebasan integrasi antena dengan komponen lain. Ramai penyelidik telah mencadangkan teknik yang berbeza untuk reka bentuk antena lutsinar. Walau bagaimanapun, kebanyakan teknik yang dicadangkan menggunakan bahan kos tinggi yang menjadikan antena dan sistem keseluruhan, mahal. Oleh itu, dalam kerja ini pembangunan antena lutsinar berasaskan air kos rendah untuk Sistem Komunikasi 5G Sub 6 GHz telah dicadangkan. Dalam kertas kerja ini, reka bentuk antenna berasaskan air telah menggunakan Perisian Gelombang Mikro CST untuk mendapatkan keputusan yang telah ditunjukkan.

ACKNOWLEDGEMENTS

First and foremost, I want to say thanks to Almighty Allah for giving me good health and strength so I can achieve this undertaking. In addition, I would like to express my gratitude to my supervisor, Dr. Muhammad Inam Abbasi for his precious guidance, words of wisdom and patient throughout this project.

My highest appreciation goes to my parents and family members for their love and prayer during the period of my study. An honourable mention also goes to my close friend for all the motivation and understanding.

Finally, I would like to thank all the staffs at the FTKEE, fellow colleagues and classmates, the faculty members, as well as other individuals who are not listed here for being co-operative and helpful.

TABLE OF CONTENT

LIST OF TABLES

LIST OF FIGURES

TABLE **TITLE** **PAGE**

CHAPTER 1

INTRODUCTION

1.1 Background

An antenna that uses water to transmit and receive electromagnetic signals is known as a water-based antenna. Therefore, it is safe and simple to create, water has become a more preferred liquid medium for making low-cost antennas. Transparent antennas are useful for integrating antenna functions into surfaces such as automotive windshields and windows while maintaining visibility. The transparent antenna additionally includes a radiation patch is placed above the clear glass substrate and a frequency selective surface on the surface of the glass provides as the ground for a microstrip antenna.

1.2 Problem Statement

For the designers of antennas, 5G communication systems present a wide range of opportunities and difficulties. To enable the freedom of antenna integration with other components, one issue is to design transparent antennas. Numerous academics have put forth various design methods for transparent antennas. However, the majority of the suggested approaches utilize pricey components, which raises the cost of the antenna and the entire system. Therefore, it has been suggested in this work to create a low-cost, transparent water-based antenna for sub 6 GHz 5G communication systems.

1.3 Project Objective

The primary objective of this study is to develop a method for building a transparent low-cost antenna for sub 6 GHz 5G Communication Systems that is both effective and scientific. Specifically, the objectives are the following:

a) To investigate the possibility of designing a water-based antenna for sub 6 GHz 5G communication system.
b) To design the water-based antenna at 3.5 GHz using different types of water.
c) To optimize the cost and performance of the proposed water-based antenna.

1.4 Scope of Project

The following is the project's scope:

a) Water based antenna design using CST Microwaves.
b) Anlayze and optimize this performances using CST Microwaves.
c) Measure the conductivity of different types of water sample using dielectric probe.
d) Measure the scattering parameter using Network Analyze.

1.5 Expecting Outcome

In this project, the water-based antenna will be discussed to propose a systematic and effective methodology to develop the system which is transparent and low-cost for 5G communication systems operating at sub 6 GHz. Based on this project, this paper is investigating the possibility of designing a water-based antenna for sub 6GHz 5G communication system. Then, this paper is showing how to design the water-based antenna at 3.5 GHz using different types of water such as pure water, salt is water, sugar in water, sea water, water bottle and oil gas water. Lastly, in this paper also show how depending on the material used that improve the cost and performance of the proposed water-based antenna.

CHAPTER 2

LITERATURE REVIEW

2.1 Introduction

Nowadays, many people are interested in designing antennas using liquids such as water because they are flexible and reconfigurable. Therefore, the antennas that were built are expensive, difficult and high level. So, for this project, the antenna that was built is low cost using 6 GHz with the x-band is 3.5GHz. There are many kinds of material that are used in the transparent patch antenna.

In addition, the materials that others used are high cost and difficult to develop, so, we are using the water based transparent antenna to cut off the cost to become a low-cost water based transparent antenna. In recent years, water has become a more common liquid medium for antenna fabrication at low cost because it is safe and easy to develop. The materials that affect the cost are using microstrip with multilayer and metal mesh films, wideband water and dual-polarized stacked.

Furthermore, transparent antennas are helpful for integrating antenna functions into surfaces while keeping visibility, such as automobile windshields, windows and others. The transparent antenna is also made includes a radiation patch above the transparent glass substrate and a frequency-selective surface on the back of glass that operates as the ground of microstrip antenna. Therefore, for antenna designers, 5G communication technologies present several opportunities and problems. Developing transparent antennas that enable integration with other components is one of the issues with this project. Transparent antennas have been created using a variety of methods suggested by many researchers. However, the majority of the suggested methods need for pricey components, making the antenna and complete system expensive. This paper presents the development of a low-cost water-based transparent antenna for sub 6 GHz 5G communication systems.

2.2 Transparent Antenna

The antenna is made up of rectangular shaped branches that have been tuned for wideband performance. Using CST software to design the antenna and using the dielectric to construct it, it is composed of a radiation patch and a ground plane. One of the most critical elements to consider in order to fully exploit 5G technology is antenna design. However, the performance of an antenna can be harmed by a few design flaws. Aside from that, mechanical flaws and mistakes in the fabrication process might have an impact on antenna performance.

2.2.1 Conductivity of Water

Water that is pure does not conduct electricity because it is an insulator. There are no ions in water that has been thoroughly particularly when it comes, or water that is absolutely clean. As a result, because no charge flows through pure water, it cannot transmit electricity. In distilled water, there are no particles and hence no ions. There are only neutral molecules, and these neutral molecules have no charge. As a result, distilled water is not electrically conductible.

Unwanted substances such as sodium, calcium and magnesium ions can be found in tap water, rainwater, and ocean. When they are present in water, they get charged, allowing electricity to flow through the liquid. To operate as a good conductor of electricity, water does not require a huge number of contaminants even a small number of ions can enable a water source to conduct electricity. In summary, the dissolved ions and contaminants in water allow it to conduct electricity. When a battery with positive and negative poles is submerged in water, positive ions are drawn to the positive pole, providing a closed circuit, whereas negative ions are drawn to the negative pole, creating a positive charge. Water has the ability of being amphoteric, which means it can perform as a solvent.[1]

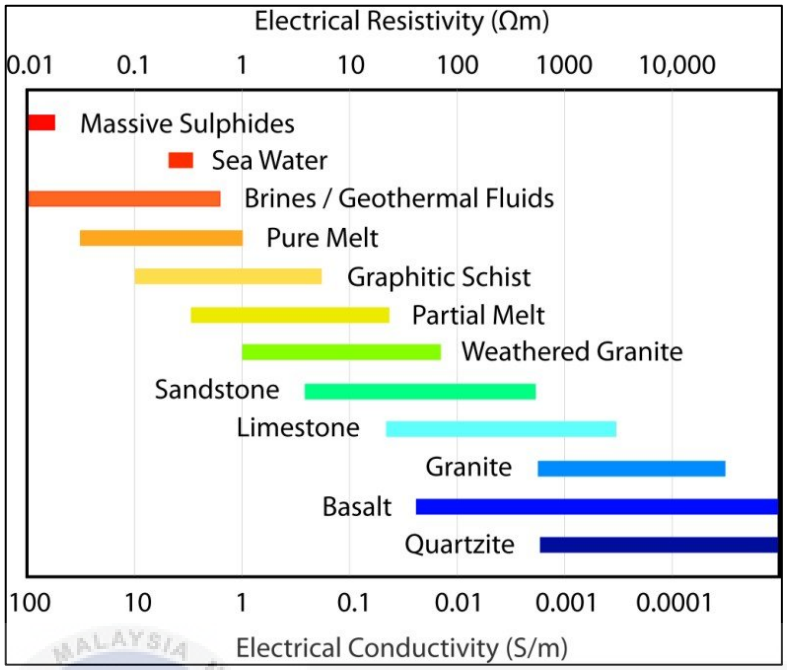

Figure 1: Electrical Conducting Water

In figure 1, it shows the electrical resistivity and conductivity values. Simpson and Bahr (2005) and their sources provided the values. Electrical conductivity is a valuable characteristic for defining different Earth materials because this varies by many orders of magnitude. Value ranges are represented as bars, with blue representing high resistivity and red representing low resistivity that is conductive.

	Types	Conductivity (S/cm)
[17]	Pure Water	400
[18]	Salt in Water	0.018
[18]	Sugar in Water	0
[19]	Sea Water	400
[20]	Water Bottle	26.7
[21]	Oil Gas Water	0.008

Table 1: Conductivity Water

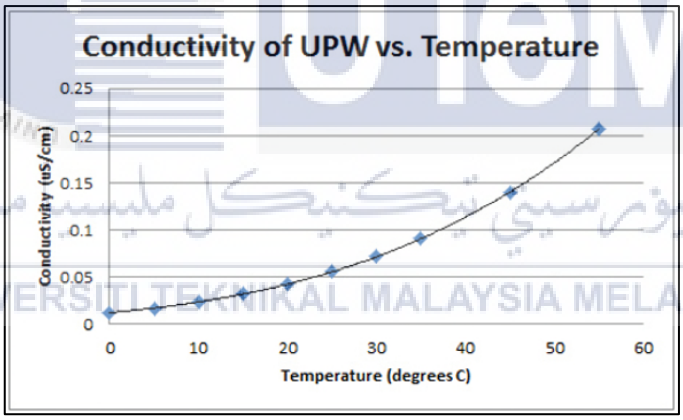

Figure 1. 1: Conductivity of Pure Water

In figure 1.1, the graph shows conductivity of pure water increasing because it starts from 0.01uS/cm and end with 0.21uS/cm. When the values of temperature increase, the conductivity is also increase.

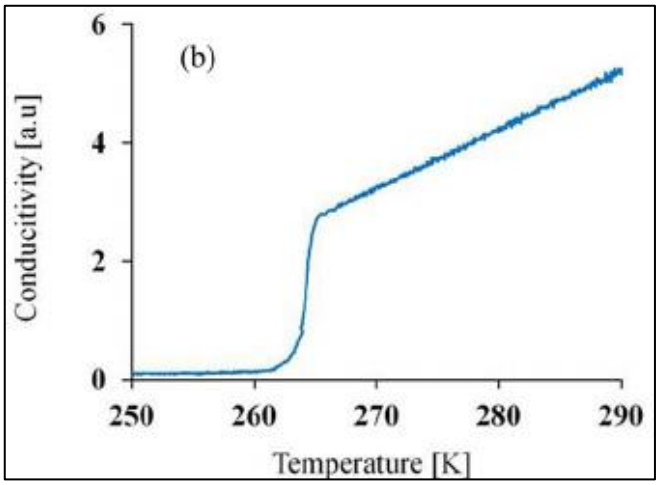

Figure 1. 2: Conductivity of Salt in Water

In figure 1.2, the graph shows conductivity of salt in water. Then, temperature from 250K to 262K constant at conductivity which is 0.2. Then, the graph increase start with 263K because when temperature increase, the conductivity is also increase.

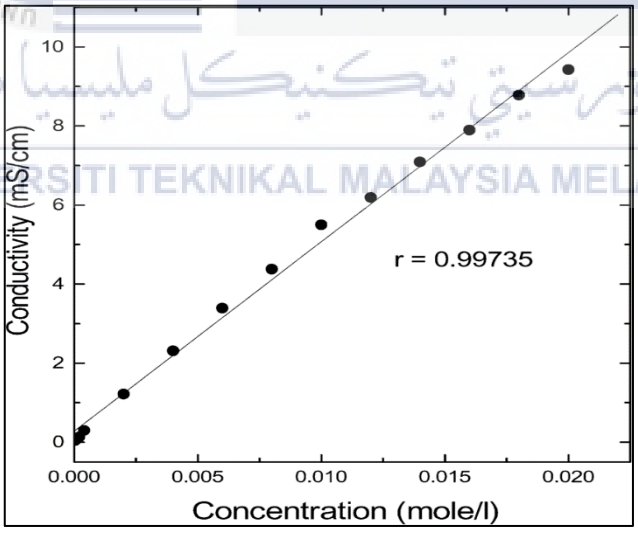

Figure 1. 3: Conductivity of Sugar in Water

In figure 1.3, the graph shows conductivity of sugar in water is increasing. When the values of concentration increase, the conductivity is also increase.

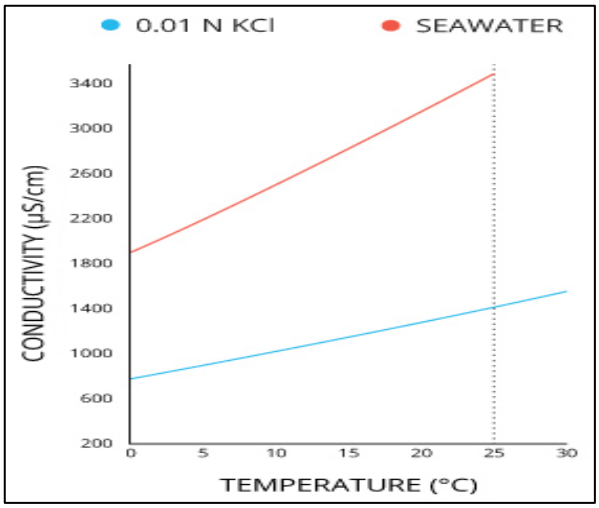

Figure 1. 4: Conductivity of Sea Water

In figure 1.4, the graph shows conductivity of sea water increasing. When the temperature increases, the conductivity is also increase.

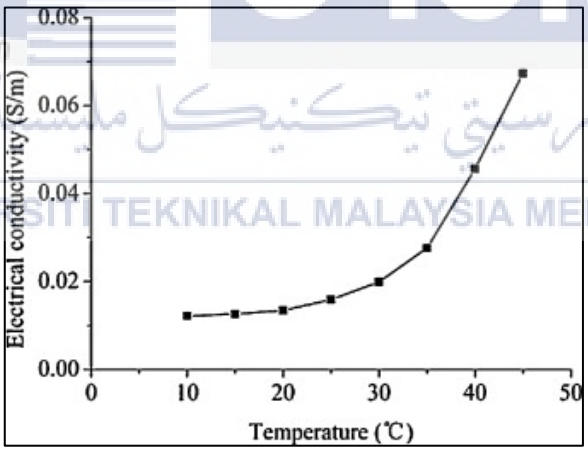

Figure 1. 5: Conductivity of Water Bottle

In figure 1.5, the graph shows conductivity of water bottle. The temperature from 10 Celsius to 20 Celsius is constant. Then, values of temperature increase, electrical conductivity is also increase.

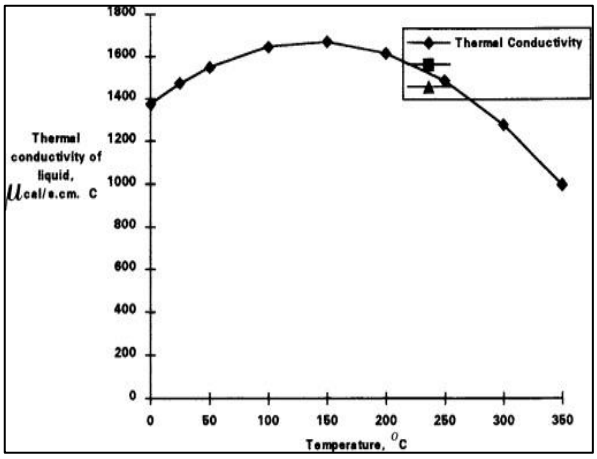

Figure 1. 6: Conductivity of Oil Gas Water

In figure 1.6, the graph shows conductivity of oil gas water. When the temperature 0 Celsius to 140 Celsius, the conductivity is increasing. Then, the graph starts decrease at 150 Celsius.

2.2.2 Transparent Microstrip Patch Antenna

The transparent microstrip patch antenna has two types of conductive sheets that are transparent multiplayer films and metal mesh films. The multiplayer films have over 80% at 550 nm wavelength respectively while metal mesh films have over 60% at 550 nm wavelength respectively. The transparent conductive films are a common component of solar cells solar cells and displays it because it is electrically conductive films and also optically transparent. Usually, the transparent patch antenna that uses microstrip is applied in the Wi-Fi service band. At figure 2, it shows the microstrip patch antenna that is one of the transparent antennas but using different material.[2]

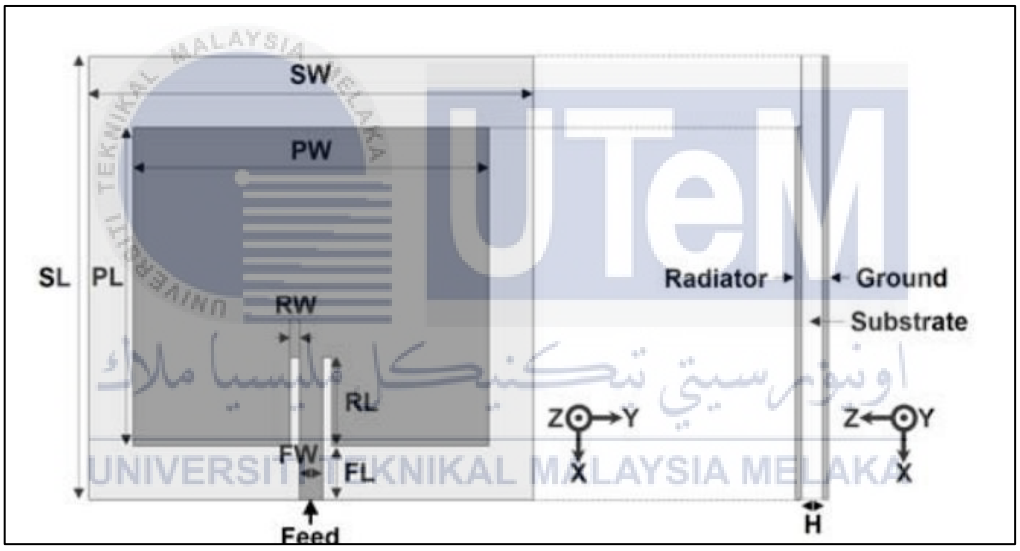

Figure 2: The microstrip patch antenna.[2]

Table 2: Composition of proposed antennas[2]

Type of film	Material
Copper Sheet	Copper
Multiplayer Film	IZTO/Ag/IZTO
Metal Mesh Film	Copper

In table 2, for the transparent microstrip patch antenna, it uses different types of film in this project such as copper sheet, multiplayer film and metal mesh film. For copper sheets, copper is an extremely effective conductor of electrical energy, which makes it an excellent option for antennas. In fact, silver is the only common element that is more conductive than copper. It also can make silver antennas which would be costly. Then, metal is soft and flexible although relatively solid, providing copper the optimum material for base antennas. Stainless steel has hard tensile strength, so thin wire can be used. This makes steel ideal for mobile whip antennas where flexibility is essential.[2]

Table 2. 1: Dimensions of proposed antennas[2]

	PL	**PW**	**RL**	**RW**	**FL**	**FW**	**t**
Copper Sheet	36	40	10	1	6	2.65	0.0180
Multiplayer Film	36	40	-	-	6	2.65	0.0001
Metal Mesh Film	36	40	-	-	6	2.65	0.0050

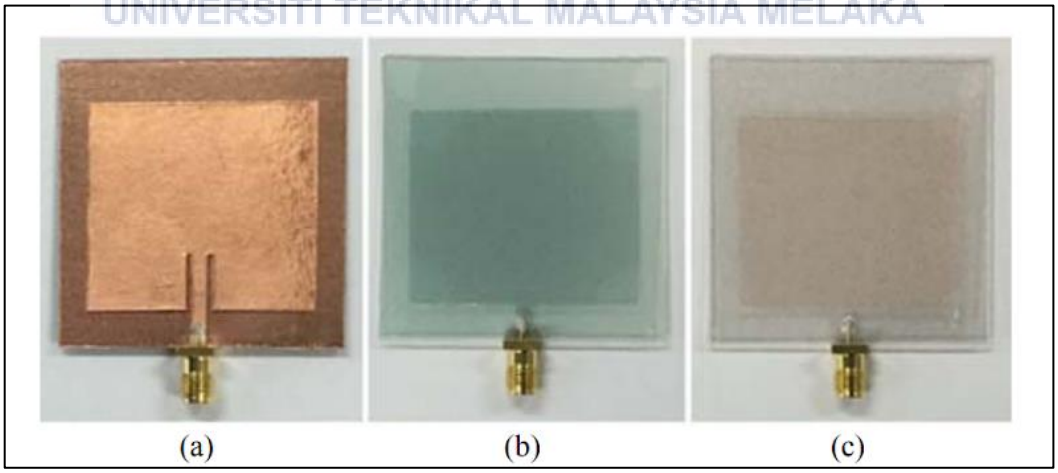

Figure 2. 1: (a) Copper sheet, (b) Multiplayer films, (c) Metal mesh films[2]

The suggested antenna is based on a traditional microstrip patch antenna design. The substrate's whole side is covered by the ground plane. The parameters of the acrylic substrate used to build each of the advised antennas are SL SW H = 50 mm 50 mm 0.5 mm (r = 2.81, tangent = 0.008). The patch antenna's dimensions are determined using the formula PL PW = 36 mm 40 mm, which has a resonance frequency of 2.45 GHz. The feeding line measures FL FW = 6 mm 2.65 mm in length and FL FW = 6 mm 2.65 mm in width and has a characteristic impedance of 50.[2]

For improved impedance matching, it uses the recessed lines on either side of the microstrip line. The lack of recessed lines improves the dimensions of both the multiplayer film and metal mesh film transparent antennas, which are transparent antennas with dimensions of RL RW = 10 mm 1 mm in the copper sheet..[2]

In table 2.1, it shows the suggested dimensions of antennas. The conductive parts (t) of the suggested antennas have thicknesses of 18 m for copper sheet, 100 nm for multilayer film, and 5 m for metal mesh film, respectively. Figure 1.1 illustrates the fabrication of antennas made of three materials, all of which are transparent, including the ground plane and the transparent radiator.[2]

Table 2. 2: Electrical and optical properties of conductive films.[2]

	Sheet resistance (Ω)	**Transparency (%)**	**TA (%)**
Copper Sheet	0.02	-	-
Multiplayer Film	2.52	80.78	68.63
Metal Mesh Film	0.18	61.46	62.10

In table 2.2, it shows the proposed antennas that include the conductive sheets' electrical and optical characteristics. The multiplayer film has a larger sheet resistance than the metal mesh film, which is 0.18, at 2.52. The sheet resistance is essential for antenna applications and is associated with the reduction in antenna signal transmission loss. The transmission of 550 nm light is the definition of transparency. Over 80% of the multiplayer film is transparent, compared to over 60% of the metal mesh film. The average wavelength transmittance in the visible region is thus between 400 and 800 nm and is 68.63% for multiplayer film and 62.10% for metal mesh film.[2]

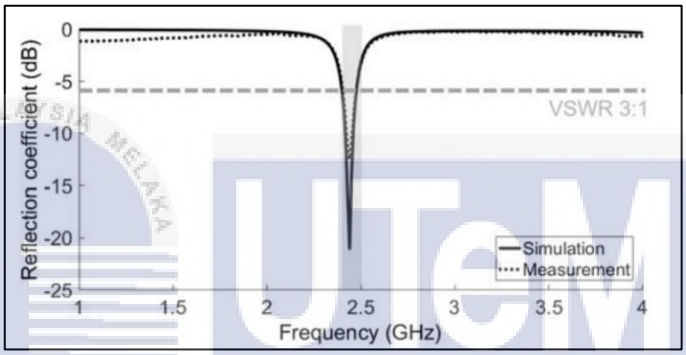

(a)

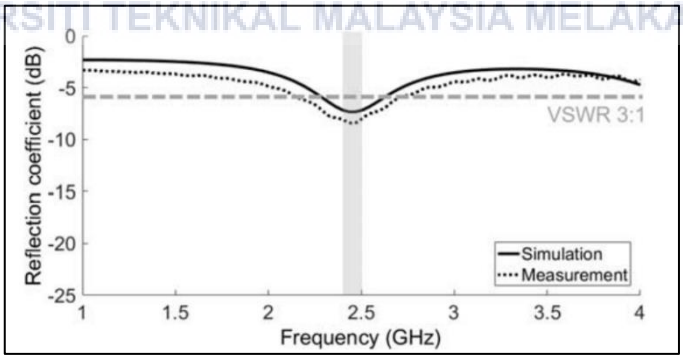

(b)

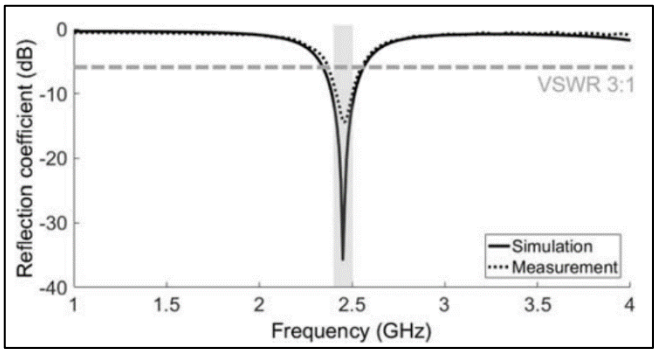

(c)

Figure 2. 2: Simulated and measured reflection coefficients of proposed antennas. (a) Copper sheet. (b) Multiplayer film. (c) Metal mesh film[2]

In figure 2.2, it shows suggested antennas simulated and observed reflection coefficients for copper sheet, multiplayer film and metal mesh film. For the copper sheet, it has a narrow band width. Next, for the multiplayer film, it has a measured frequency range that makes it losses because among the others, it has the greatest resistance to sheets. Then, the pattern of metal mesh film that is exactly equivalent to a copper sheet.[2]

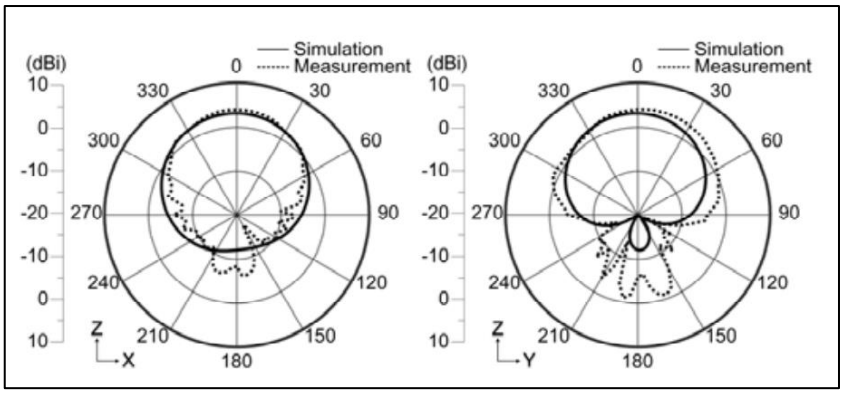

(a)

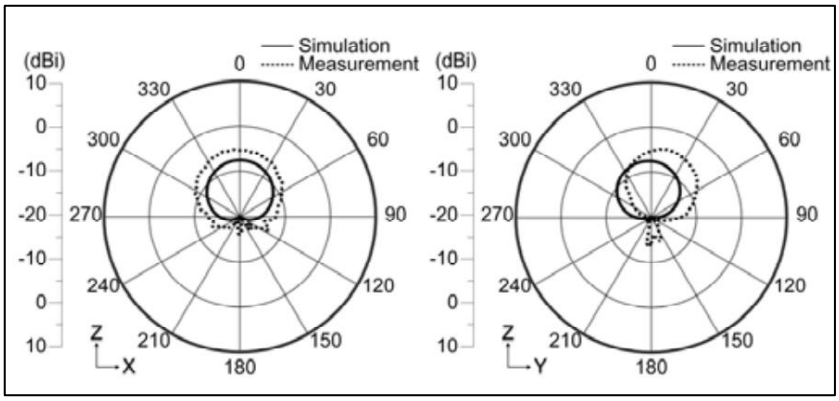

(b)

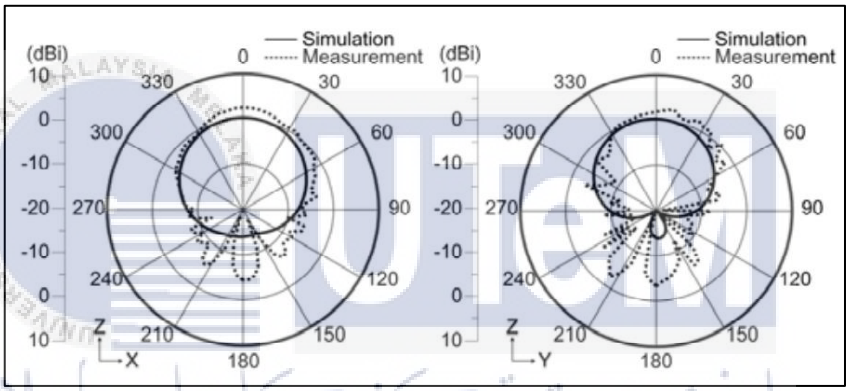

(c)

Figure 2. 3: Measured 2d radiation patterns of xz and yz planes at 2.45 GHz.

(a)Copper sheet. (b)Multiplayer film. (c) Meta mesh film[2]

Table 2. 3: Measured performances of the proposed antennas[2]

	S11 (dB)	**Peak gain (dB)**	**Efficiency (&)**
Copper Sheet	-12.5	4.75	66.32
Multiplayer Film	-8.4	-4.23	7.76
Metal Mesh Film	-14.5	2.63	42.69

In figure 2.3, it shows the pattern that suggested antennas' radiation patterns match the results rather well. of simulation because the measurements of all shape's antenna radiation patterns are similar. Next, in table 2.3, a copper sheet is the highest of peak antennas and efficiency while the lowest is multiplayer film.[2]

2.2.3 Transparent Dual-Polarized Stacked Patch Antenna

The optically transparent metal-mesh films used in the transparent dual-polarized stacked patch antenna. The metal plate has been replaced with a transparent conductive film that was made by printing a metal grid on polyethylene terephthalate with a 0.5ohm side resistance. Generally, most of the surface of the antenna has high light transmission. The stacked round microstrip patch provides a wide impedance bandwidth. The disks probe has a limited obstruction area and good impedance matching. The optical transparency adds further functionality to antennas such as inner examination and soft visual impact. Figure 3, shows the construction of transparent dual-polarized stacking patch antenna where (a) is showing from the explosion view while (b) is showing from the front view.[3]

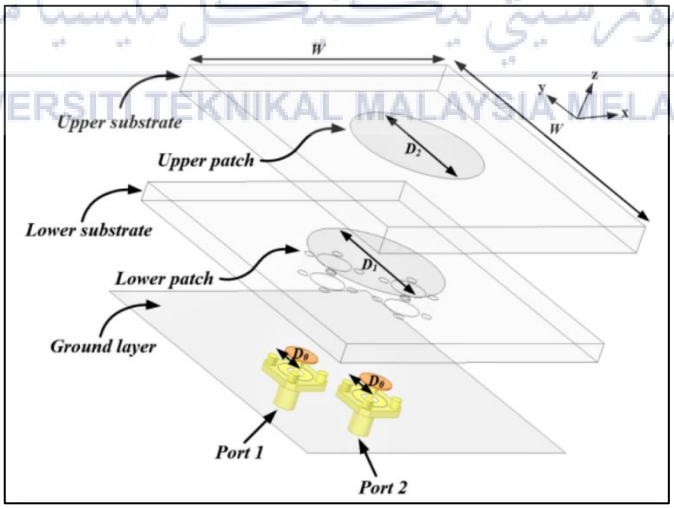

(a)

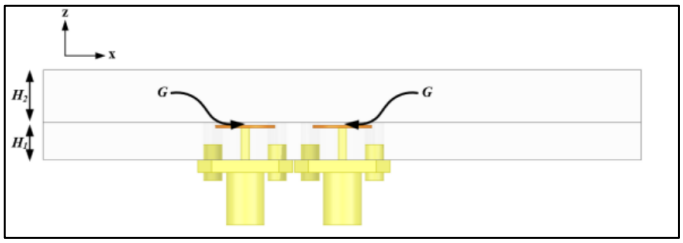

(b)

Figure 3 : Structure the transparent dual-polarized stacked patch antenna.

(a) Explosion view. (b) Front view[3]

Table 3: Dimension for the proposed dual-polarized stacked patch antenna[3]

Parameter	D1	D2	D3	D4	G	D0	W
Value (mm)	34	33	4	5	0.4	8	100

Table 3 shows all dimensions of the proposed design that have been optimized through modelling using the High Frequency Structure Simulator (HFSS). The major components of the antenna are conductive films, transparent substrate and feeding probes have been composed.[3]

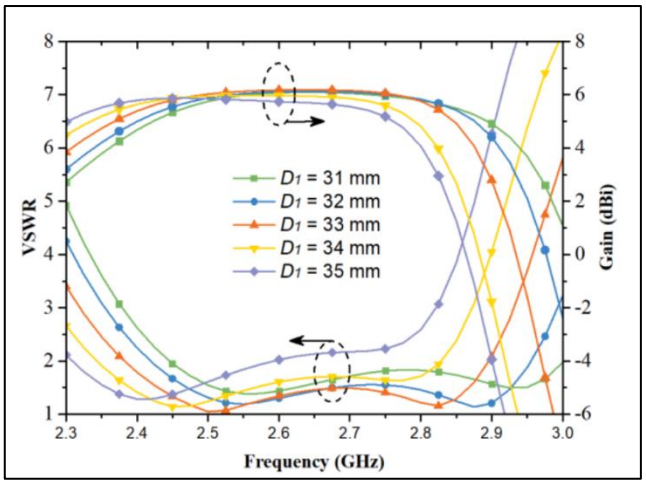

Figure 3. 1: Effect of the diameter of the lower round patch[3]

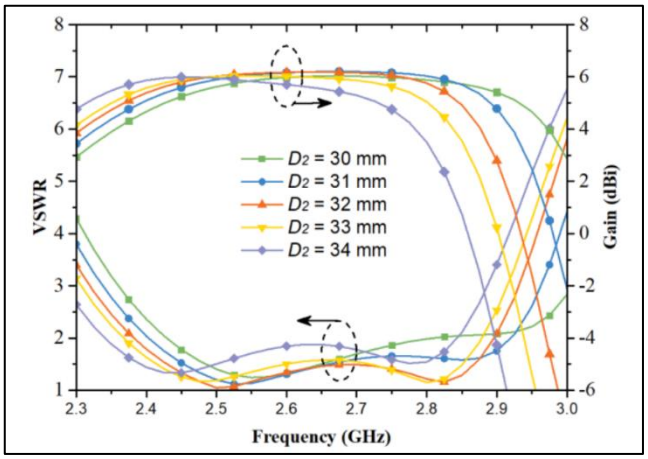

Figure 3. 2: Effect of the diameter of the upper round patch[3]

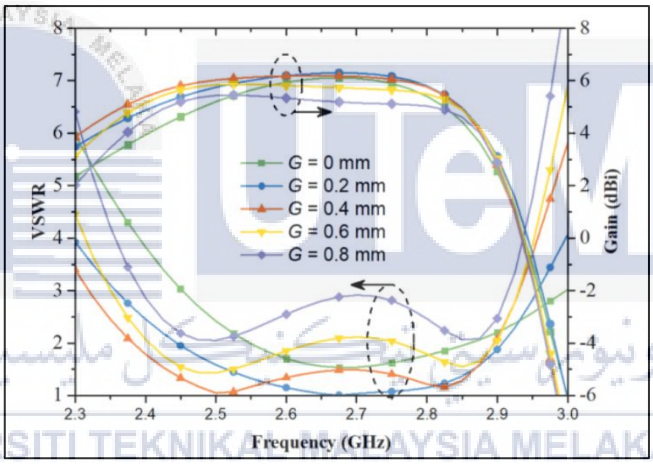

Figure 3. 3: Effect of the gap distance between the probe disk and the lower patch[3]

In figure 3.1, it shows the effect of changing the lower patch diameter D1 on VSWR and gain while keeping the other parameters constant. In figure 3.2, it shows the effect of changing the upper parasitic patch diameter D2 on VSWR and gain while keeping the other parameters constant. In figure 3.3, it displays the effect of G on the antenna's SWR and gain because the gap G is observed to have a significant impact on impedance matching.[3]

By selecting appropriate patch sizes D1 and D2, the operation frequency can be successfully regulated. The separation distance between the disc and lower patch controls the impedance matching between the round patches and the feeding probe.[3]

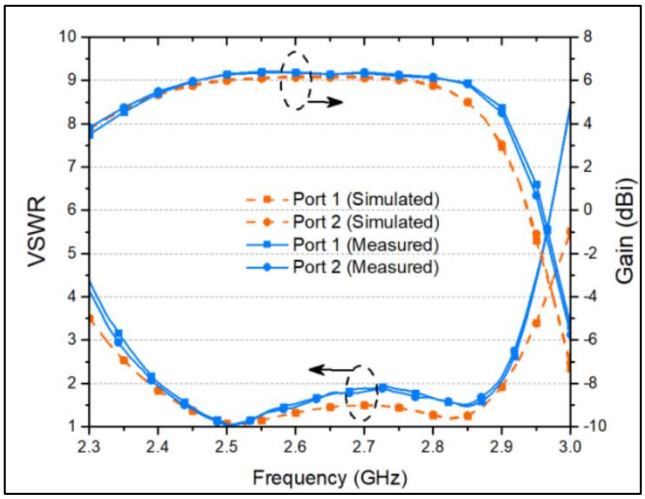

Figure 3. 4: Measured and simulated VSMRs and gains of the proposed transparent dual-polarized stacked patch antenna[3]

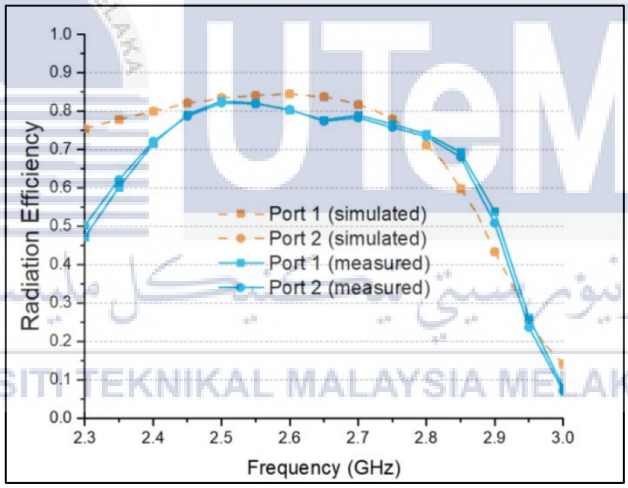

Figure 3. 5: Measured and simulated efficiencies for both ports of the proposed transparent dual-polarized antenna[3]

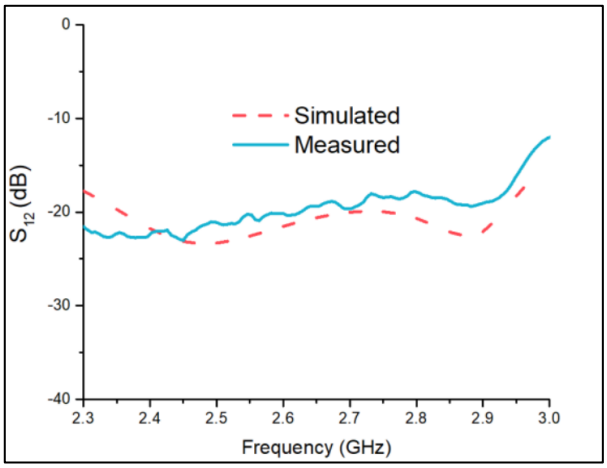

Figure 3. 6: Measured and simulated port isolations of the proposed transparent dual-polarized antenna[3]

In figure 3.4, from 2.4 to 2.9 GHz, the measured impedance of bandwidths is 19% (SWR2) for both ports. The measured boresight gains for both ports vary from 5 to 6.4 within the working frequency range. In figure 3.5, from 2.4 to 2.9 GHz, he measured impedance bandwidths of 19 percent (SWR2) for both ports. The measured boresight gains for both ports vary from 5 to 6.4 within the working frequency range. In figure 3.6, it shows that across the operational frequency range, the observed isolation between the two ports is greater than 18 dB, which is consistent with the simulation. [3]

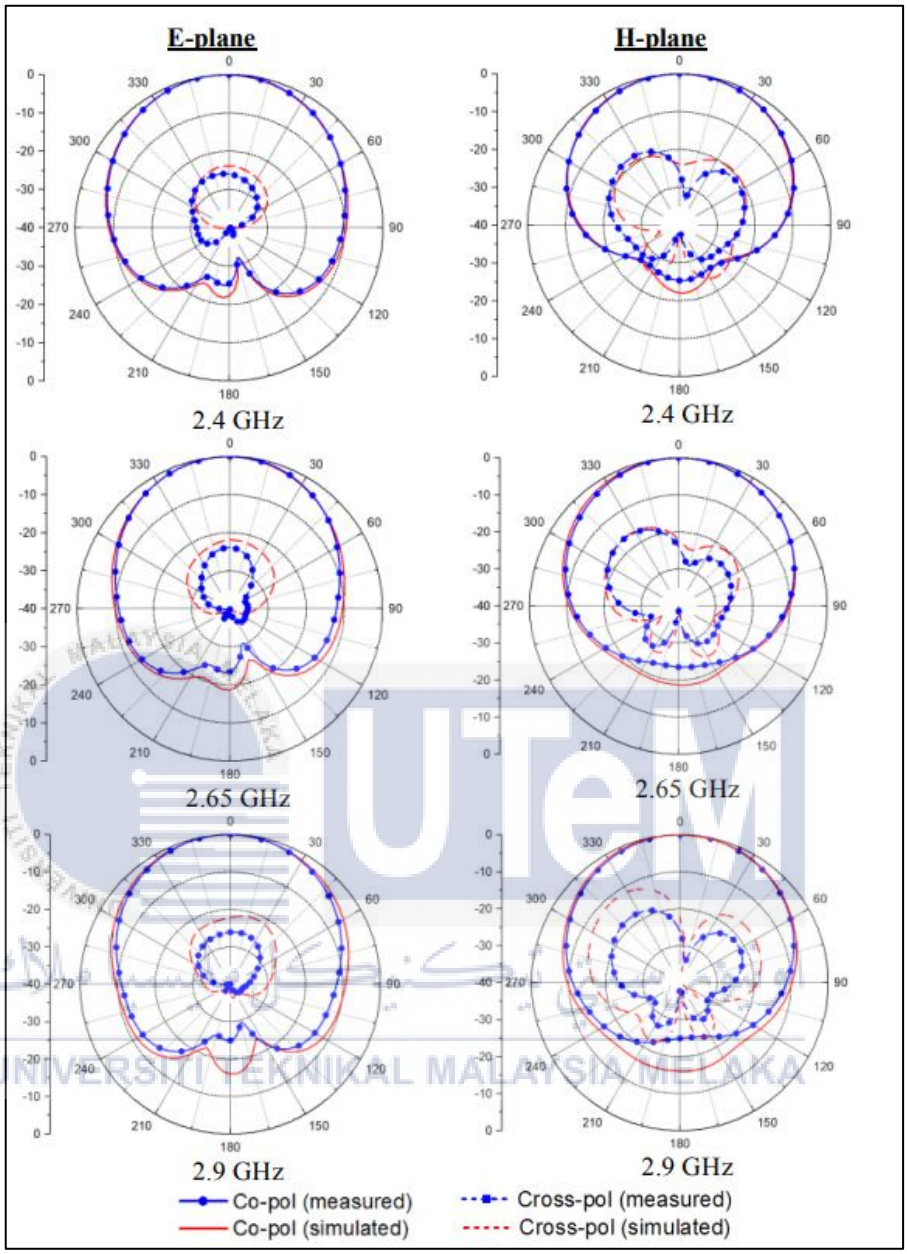

Figure 3. 7: Measured and simulated radiation patterns for the port 1 of the proposed transparent dual-polarized antenna[3]

In figure 3.7, for port 1, the measured and simulated radiation patterns at 2.4, 2.65 and 2.9 GHz. The radiation characteristic of the antenna has been exhibited. Over the working frequency range, the observed front to back ratios is over 20 dB. In both the E- and H-planes, the 3-dB bandwidth remains constant with frequency. Because of the axial symmetry of the construction, the radiation patterns of port 2 are identical to those of port 1.[3]

2.3 Transparent Water Antenna

Water has recently been a prominent liquid material used in the fabrication of antennas due to its low cost, ease of availability, and safety. In general, there are two types of water used for antenna design: salt water and clean water. The former is commonly employed as a conductor to facilitate current flow. Based on this concept, many water monopoles have been created. Pure water, on the other hand, is often used as a dielectric in the construction of dielectric resonator antennas. The substantial dielectric loss of water, on the other hand, reduces antenna efficiency.[4]

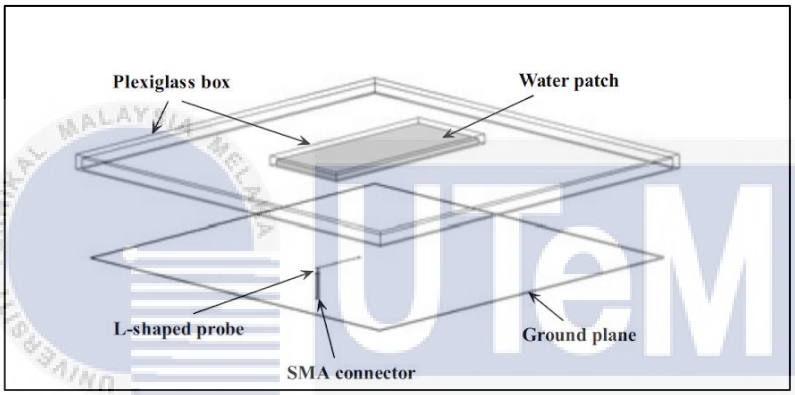

Figure 4: The water dielectric patch antenna[4]

In figure 4, the proposed shape of water dielectric patch antenna is shown. Two plexiglass boxes are linked together to produce the design. The top smaller rectangle box prevents the water and is used to construct the water dielectric patch, meanwhile the bottom larger square box is empty and provides as a supporting framework. As a result, the substrate between the water patch and the ground plane in this design is air. A square metallic ground plane is installed on the bottom surface of the large box, where the L-shaped probe is located. A short section of coaxial cable with a SMA connector is connected to the L-probe for measurement.[4]

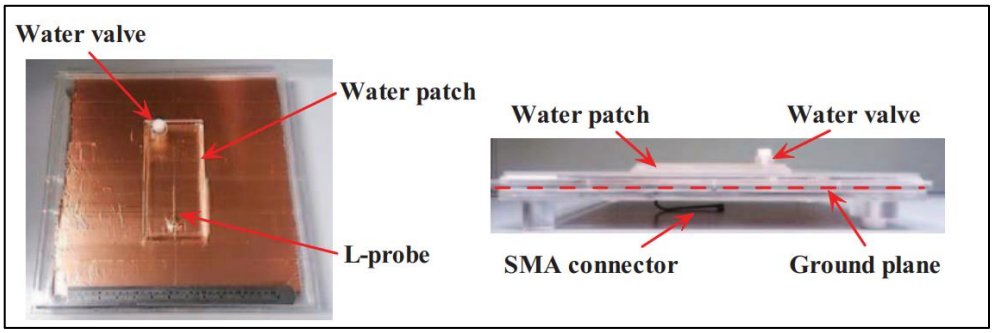

Figure 4. 1: Photographs of the fabricated water dielectric patch antenna

(a) Whole structure, (b) Slide view.[4]

In figure 4.1, it shows the fabricated water dielectric patch antenna which (a) is showing the entire structure and (b) is showing the slide view. The entire antenna arrangement retains a low profile, as can be seen in the side view in (b). At 0.93 GHz, the total antenna height is 0.0590.[4]

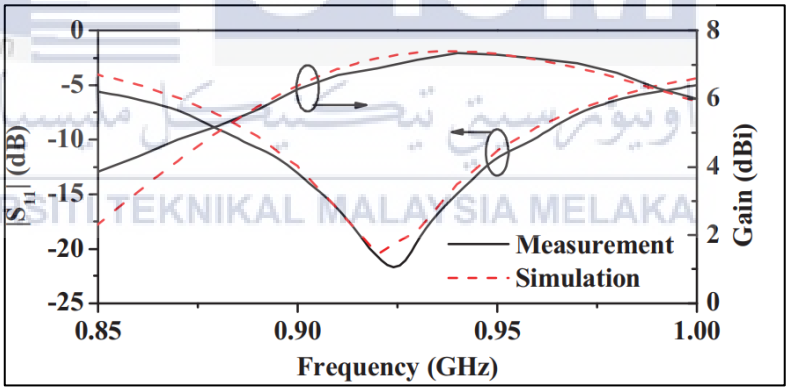

Figure 4. 2: Measured and simulated |S11| and gain of the proposed water dielectric patch antenna[4]

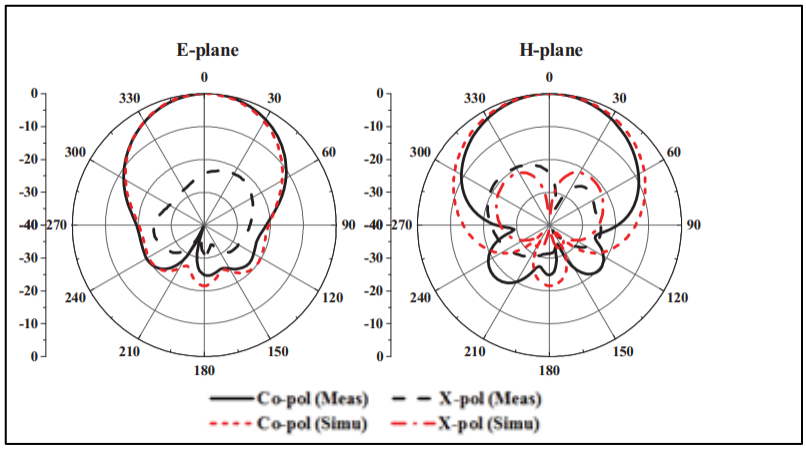

Figure 4. 3: Measured and simulation radiation patterns of proposed water dielectric patch antenna[4]

In figure 4.2, for |S11| -10 dB, the simulated and observed bandwidths are 7.05 percent and 8.02 percent, respectively. Gains of up to 7.4 and 7.34 dBi have been simulated and measured, respectively. By modelling and testing, the 3-dB gain bandwidths are 17.0 percent and 18.5 percent, respectively. [4]

Furthermore, at centre frequency, the simulated and observed efficiencies are both 70%. Because the suggested antenna operates in a patch mode, only a small fraction of the energy is absorbed by the water patch, the antenna's efficiency is not significantly harmed by water loss.[4]

In figure 4.3, in both the E- and H-planes, symmetrically unidirectional patterns are created. The back lobe and cross polarization levels measured are less than -20dB.[4]

Table 4: Comparison of various patch antennas[14]

	Material of patch	Substrate dielectric constant	Polarization	Centre frequency (GHz)	Diameter of circular patch	Substrate thickness	Imp. BW% (|S11<-10 dB or SWR < 2)	Max. Gain (dBi or dBic)
[5]	Metal	2.55	LP	5.20	1.17	0.04	3.3%	4.2
[6]	Metal	2.33	LP	2.26	1.10	0.037	18%	6.0
[7]	Metal	2.65	LP	5.76	2.03	0.047	27.4%	6.0
[8]	Metal	1.00	LP	2.15	1.00	0.172	52%	5.0
[9]	Metal	1.00	LP	1.91	0.955	0.13	30%	6.5
[10]	Metal	2.94	LP	6.05	2.14	0.05	12.8%	5.7
[11]	Metal	2.94	CP	5.70	0.98	0.1	28%	4.9
[12]	Metal	2.33	LP	1.88	1.45	0.06	25.5%	5.9
[13]	Metal	2.20	CP	2.45	1.14	0.042	16.6%	1.1
[14]	Water	3.00	LP	1.95	0.89	0.19	42%	1.56

2.3.1 Water Based Horn Antenna

In recent years, it is recommended that a water-based antenna based on a water waveguide be used. The entire antenna is constructed of pure water covered in transparent resin. Because of the deployment of clean water, the proposed antenna is optically clear and low-cost. A water horn antenna with pattern reconfigurability is also being developed for demonstration purposes. By directing the flow of water to fill various layers, the suggested antenna may be modified between an H-plane horn of pencil radiation beam and a leaky-wave mode of conical-like radiation beam, and the open angle of the horn can be controlled. The reflection and transmission coefficients of dielectric layers were investigated using Airy's calculations. In figure 6, it shows the configuration of back-to-back transition water waveguide transition which a is perspective view and b is side view.[15]

(a)

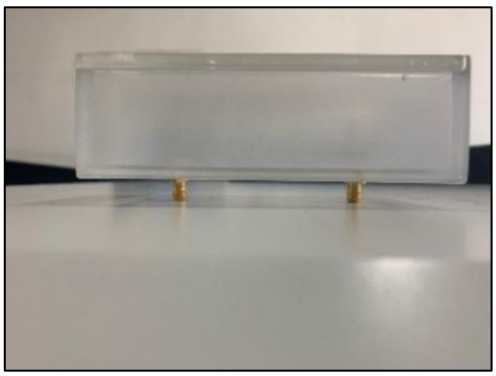

(b)

Figure 5: Configuration of back-to-back transition water waveguide transition.

(a) Perspective view, (c) Side view[15]

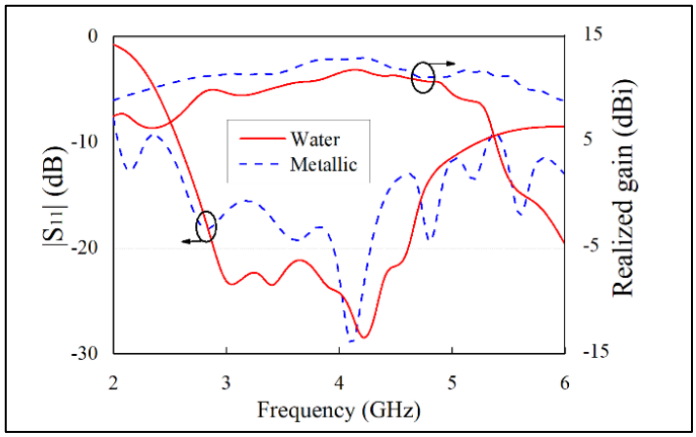

Figure 5. 1: Simulated reflection coefficient and gain of the water and metallic[15]

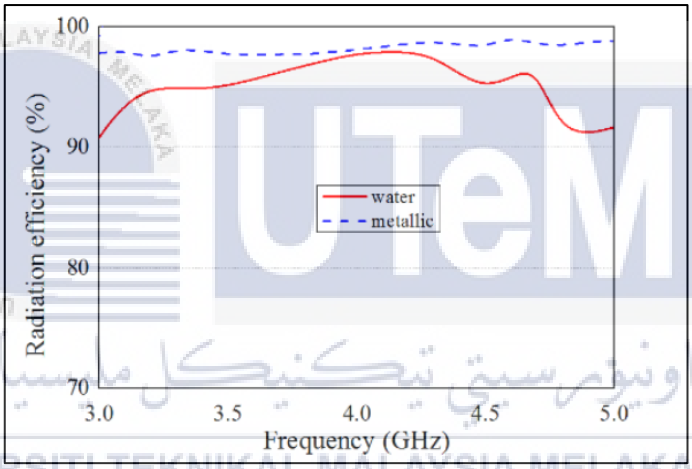

Figure 5. 2: Simulated radiation efficiency of the water and metallic[15]

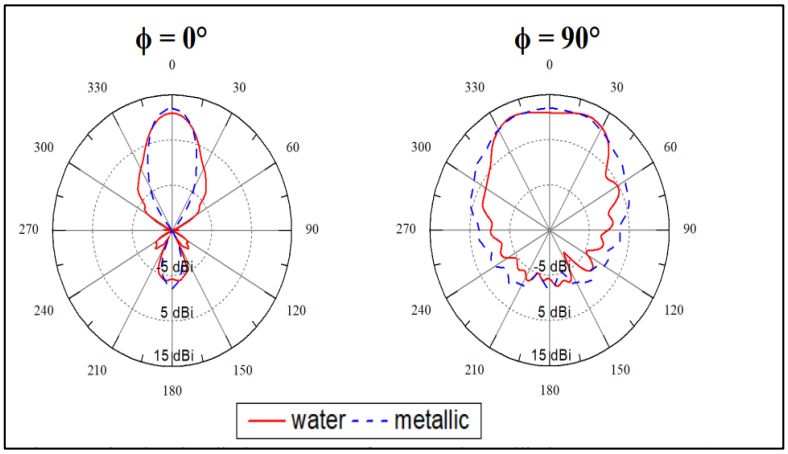

Figure 5. 3: Simulated radiation patterns of water and metallic[15]

Figure 6.1 illustrates the proposed reflection coefficients and gains of water and metallic horn antennas. The simulated impedance bandwidth of the water horn is 66.7 percent from 2.6 GHz to 5.2 GHz, whereas the metallic horn's is 71.8 percent from 2.5 GHz to 5.3 GHz. The maximum gain of the water horn is 11.8 dBi, whereas the maximum gain of the metallic horn is 12.9 dBi.[15]

Figure 6.2 shows their radiation efficiency findings. Both horn antennas appear to have attained broadband performance. Figure 6.3 shows and compares the radiation patterns of these two horn antennas. Despite the fact that the leakage has been decreased due to the horn's massive sectional size, the leaky mode persists. When the angle is 90 degrees, the design of a water horn becomes flat at the top, as opposed to a metallic trumpet.[15]

2.3.2 Water Based Antenna

The feed structure of the transparent wideband water patch antenna is an L-shaped distilled water probe. The L-shaped can increase the transparency of the water patch antenna by replacing the bigger metallic L-shaped with the transparent water L-probe. Distilled or pure water is used in patch antennas primarily because it is a pure liquid dielectric substrate with an 80% dielectric constant at very high microwave frequencies. In figure 6, it shows the water patch antenna using the L-shaped water probe.[14]

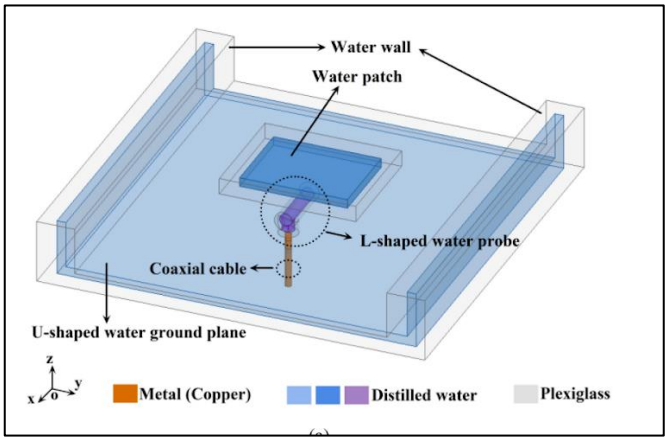

Figure 6: The water patch antenna by L-shaped water probe[16]

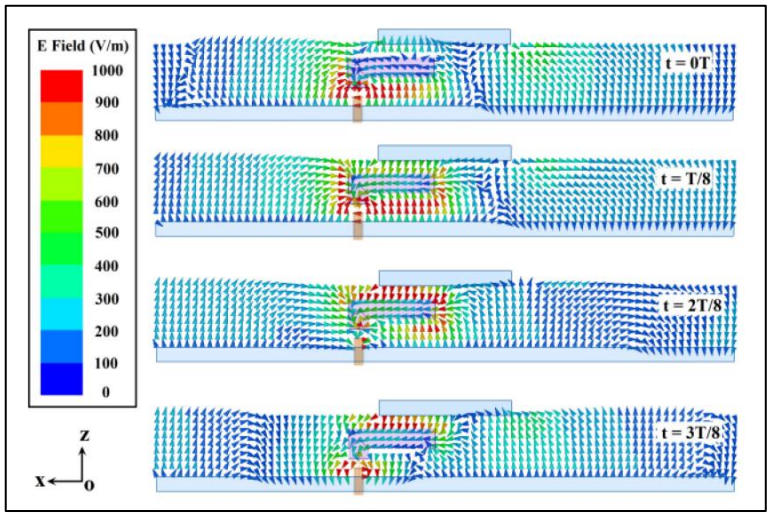

Figure 6. 1: Electric field distribution in the E-plane[16]

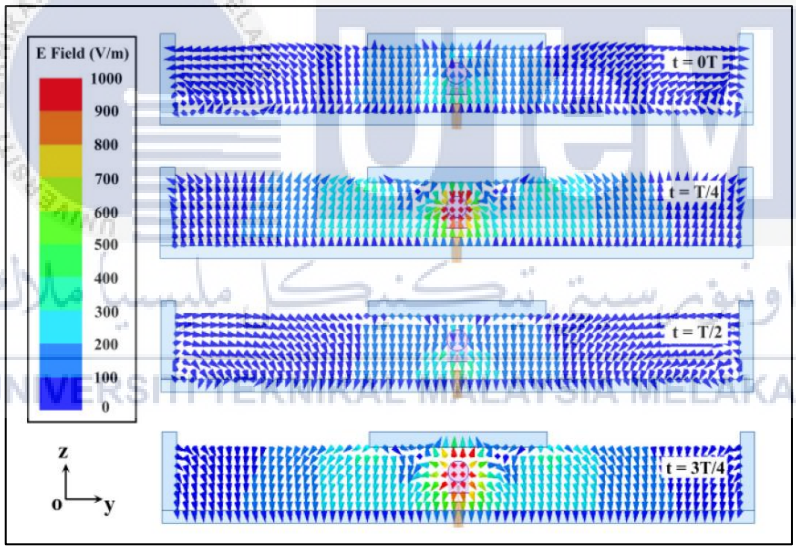

Figure 6. 2: Electric field distribution in the H-plane[16]

In figure 6.1 and figure 6.2, it shows the electric field distribution at 1.8 GHz. The time at t = 0T and t = T/8 where T is refers to one period of time, the E-fields in the E-plane have a very strong magnitude among the bottom area of the water probe, and the E-fields have an opposite direction under the edge of the water patch. [16]

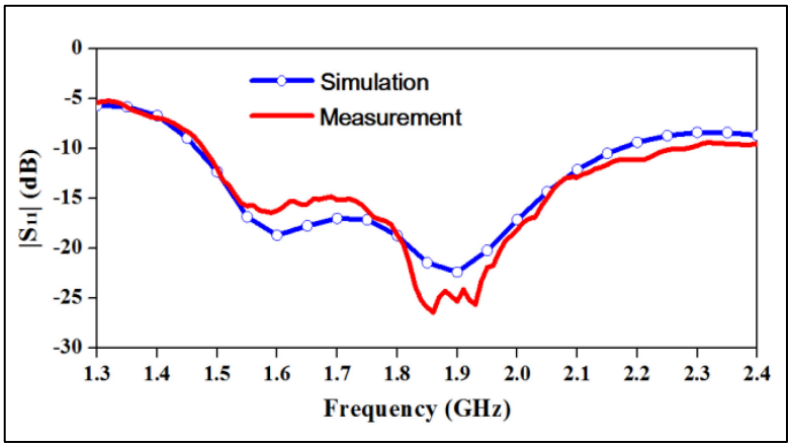

Figure 6. 3: Simulated and measure |S11| of the proposed water patch antenna[16]

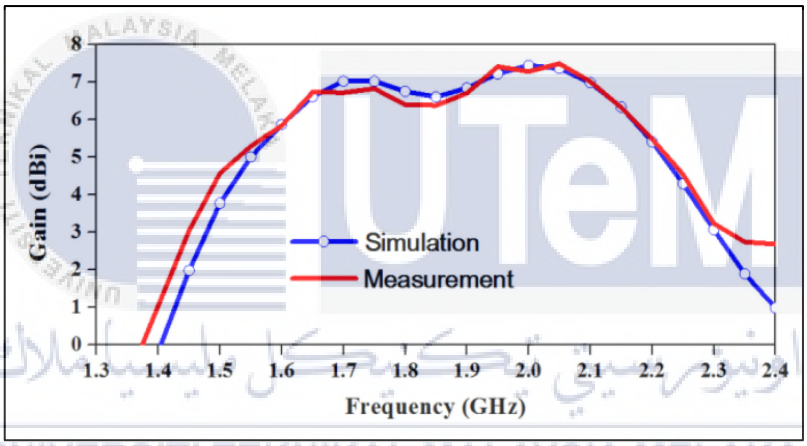

Figure 6. 4: Simulated and measured gain of the proposed water patch antenna[16]

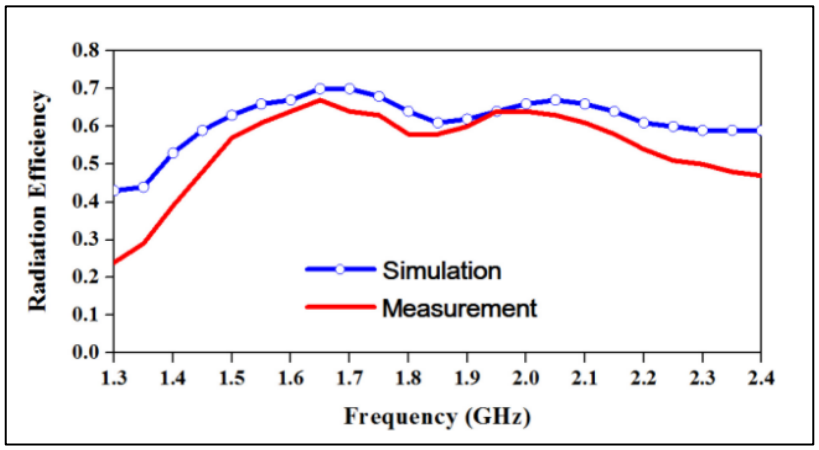

Figure 6. 5: Simulated and measured radiation efficiency of the proposed water patch antenna[16]

In figure 6.3, the simulation bandwidth is 38.5%, varying from 1.47 to 2.17 GHz, while the measurement bandwidth is 42.6%, varying from 1.48 to 2.28 GHz. There are two minimum locations around 1.6 GHz and 1.9 GHz. The patch mode produces the first minimum point, while the L-shaped water probe produces the second. The two minimum points provide a large impedance bandwidth of more than 40% when combined.[16]

In figure 6.4, between the measurement and simulation, the good agreement is achieved and it is similar with the metallic patch antenna. It is because the simulated gain shifts from 2.5 dBi to 7.45 dBi while the actual gain shifts from 3 dBi to 7.5 dBi. At lower frequencies, the gain is minimal, but it climbs to 5.85 dBi at 1.6 GHz. Both the simulated and observed increases are greater than 6.0 dBi over the frequency range of 1.6 GHz to 2.15 GHz.[16]

In figure 6.5, over their respective impedance bandwidths, the simulated radiation efficiency ranges from 60% to 70%, while the measured one ranges from 50% to 67%. [16]

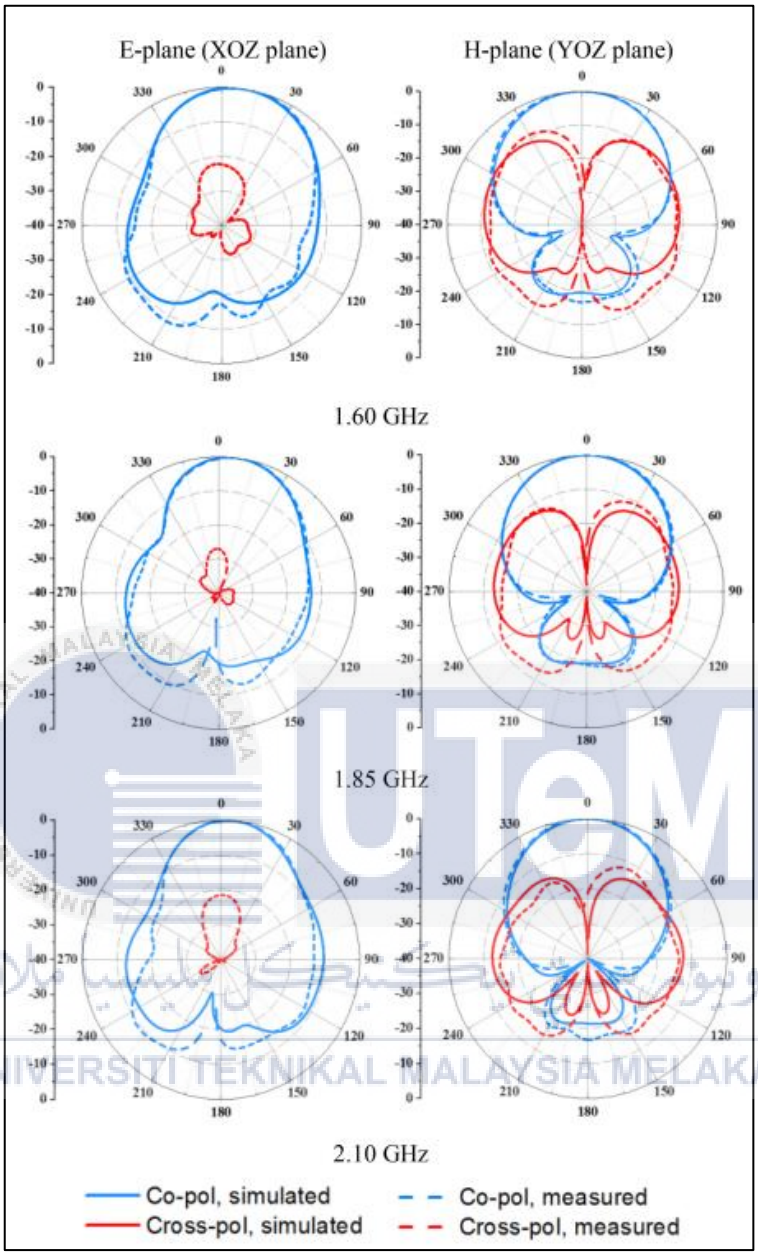

Figure 6. 6: Simulated and measured radiation patterns over the operating band[16]

In figure 6.6, the beam shifts into theta = 8 degree in the E-plane caused by the existence of the water probe which is leading to the asymmetry of the E-fields along the two apertures under the edges of the water patch.[16]

Table 5: Comparison types of water

	Types	**Conductivity (S/cm)**	**Tuning Range (GHz)**	**Relative Permittivity**
[17]	Pure Water	400	1.07-2.04	87.90
[18]	Salt in Water	0.018	0.20-1.40	80.00
[18]	Sugar in Water	0	2.50-18.00	80.10
[19]	Sea Water	400	0.04-0.10	2.70
[20]	Water Bottle	26.7	0.8-1.00	2.19
[21]	Oil Gas Water	0.008	2.34-2.40	2.30

2.4 Summary

	Material of patch	Substrate dielectric constant	Polarization	Centre frequency (GHz)	Diameter of circular patch	Substrate thickness	Imp. BW% (|S11<-10 dB or SWR < 2)	Max. Gain (dBi or dBic)
[5]	Metal	2.55	LP	5.20	1.17	0.04	3.3%	4.2
[6]	Metal	2.33	LP	2.26	1.10	0.037	18%	6.0
[7]	Metal	2.65	LP	5.76	2.03	0.047	27.4%	6.0
[8]	Metal	1.00	LP	2.15	1.00	0.172	52%	5.0
[9]	Metal	1.00	LP	1.91	0.955	0.13	30%	6.5
[10]	Metal	2.94	LP	6.05	2.14	0.05	12.8%	5.7
[11]	Metal	2.94	CP	5.70	0.98	0.1	28%	4.9
[12]	Metal	2.33	LP	1.88	1.45	0.06	25.5%	5.9
[13]	Metal	2.20	CP	2.45	1.14	0.042	16.6%	1.1
[14]	Water	3.00	LP	1.95	0.89	0.19	42%	1.56

CHAPTER 3

METHODOLOGY

3.1 Introduction

In this chapter, the methodology of this project which includes the flow of the project and the process that is flow chart will be discussed.

3.2 Methodology

Based on this paper, this thesis presents a new and integrated analytical approach to optimize the designing of water-based antenna. The different of water samples such as pure water, salt is water, sugar in water, sea water, water bottle and oil gas water will be collected to distribute the result of water-based antenna. In figure 7.0, it shows the research design of this paper.

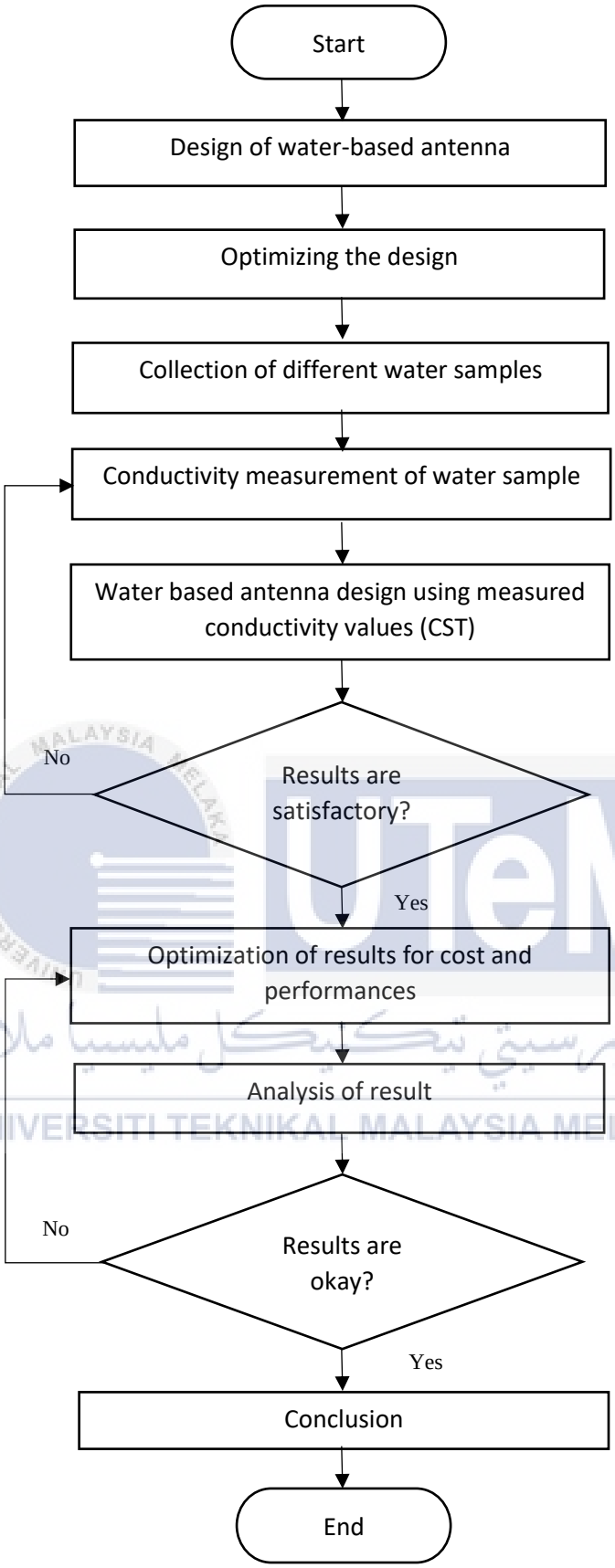

Figure 7: Water based antenna general process flow

3.3 Equipment

3.3.1 Simulation

Figure 7. 1: CST Microwaves Software

In this project, the designing of water-based antenna is using the CST Microwaves Software that shows in figure 7.1. Therefore, this software is to design the microstrip antenna that uses water and optimization the design of antenna.

3.2.2 Collection of water samples

Based on this paper, the transparent patch antenna is using the water for low-cost because some researcher using the high-cost material that makes the system expensive. Thus, in this project, the material is changing to the low-cost material such as pure water, salt is water, sugar in water, sea water, water bottle and oil gas water.

3.2.3 Conductivity Measurement of water samples

In this measurement, the design is using the dielectric probe to measure the conductivity of water samples such as pure water, salt is water, sugar in water, sea water, water bottle and oil gas water.

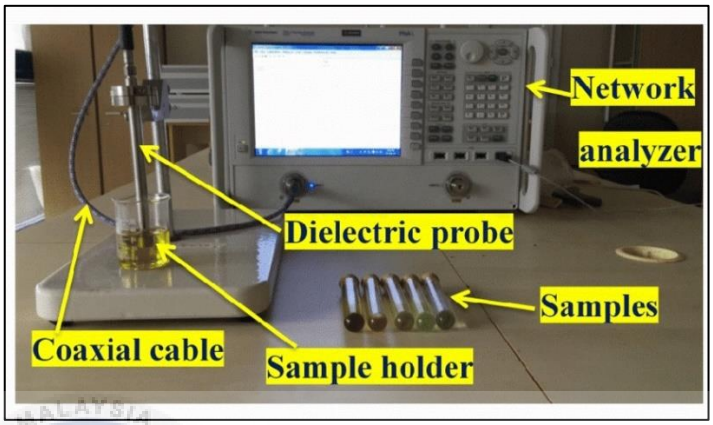

Figure 7. 2: Dielectric probe

3.3.4 Fabrication of Antenna

In this paper, the design is using the glass for substrate and using the different water samples to optimize the result of antenna. Then, it also shows the steps of designing the antenna.

When printing circuits, ensuring that the size of the circuit fits the positive board size by conducting x mirror on the logo, picture, or any text for the group name. To define the region that will be employed, tick bottom copper, board edge, scale 100 percent rotation x horizontal, and reflection normal on the circuit and print the configuration. Set the colour scheme to monochromatic.

Figure 7. 3:PCB Developer Machines

In figure 7.3, to turn on the mains, the PCB developer uses a chemical procedure. Set the temperature to 40°C and the time of the development to 2 minutes. After that, wash it with water and dry it with tissue paper. This method necessitates the use of safety equipment such as gloves, goggles, and an apron.

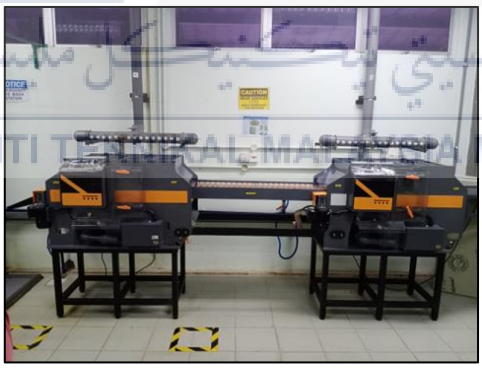

Figure 7. 4: Etching Developer Machines

In figure 7.4, mega electronics are used in the etcher machines (model FAPC 300). At the input roller, assign the +VE board. Then, keep the temperature between 40°C and 46°C. Depending on the size of the board, the etching procedure may be repeated 2-4 times. However, after the etching process is complete, the surrounding copper in the non-circuit region will no longer be visible. Wear safety equipment such as gloves, goggles, and an apron before beginning this activity.

Figure 7. 5: Photoresist Stripper Machines

Based on figure 7.5, the photoresist stripper chemical is used by the etcher machine Mega electronics (model PA320) to assign the +VE board in the networks and execute up and down soaking. The circuit line will be made from green lining to copper lining at the end of the procedure. When doing this procedure, wear safety equipment such as gloves, goggles, and an apron.

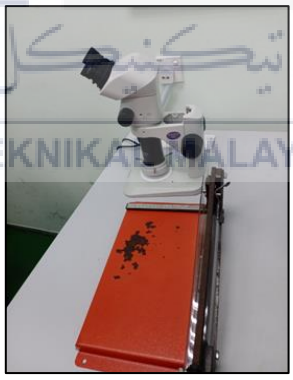

Figure 7. 6: PCB Cutter

In figure 7.6, before beginning the cutting process, this printed circuit board (PCB) cutter must check that the board is dry. To achieve perfect cutting, align the unwanted PCB region towards the cutting area and move the cutter handler down quickly. If you go too slowly during the cutting operation, the board edge will crack. During this process, safety protective equipment like as goggles must be used. When it's finished, toss the remaining piece into the trash and clean up the workspace.

3.3.5 Measurements

In this paper, the design is using Vector Network Analyzer (VNA) to measure the result of water-based antenna based on different water samples such as pure water, salt is water, sugar in water, sea water, water bottle and oil gas water in figure 7.7.

Figure 7. 7: Vector Network Analyzer (VNA)

3.4 Summary

Based on this project, a literature evaluation of printed water-based antennas, return loss analysis of water-based antennas, and radiation patterns of water-based antennas is required from the journal. There are a few pieces of equipment that will be used to complete this project. To begin, design the antenna using CST microwave software to optimise the antenna design. Then, applying the antenna equipment fabrication machinery on the site. The last one measured the S11 using a Vector Network Analyzer (VNA).

CHAPTER 4

RESULT AND DISCUSSIONS

4.1 Introduction

In this chapter, the result present and analysis on the development of low-cost water based transparent antenna that using water. Then, the simulation is using the CST Microwaves Software to design the water-based antenna. Based in the simulation, case studies are carried out to illustrate the applicability of the proposed water-based antenna system. It shows the difference of material that using in the simulation of CST Software. The types of material that I using in this result are FR4, Rogers RT5880 and glass to provide water based transparent antenna that using water.

4.2 Result and Analysis

4.2.1 FR4 and Copper

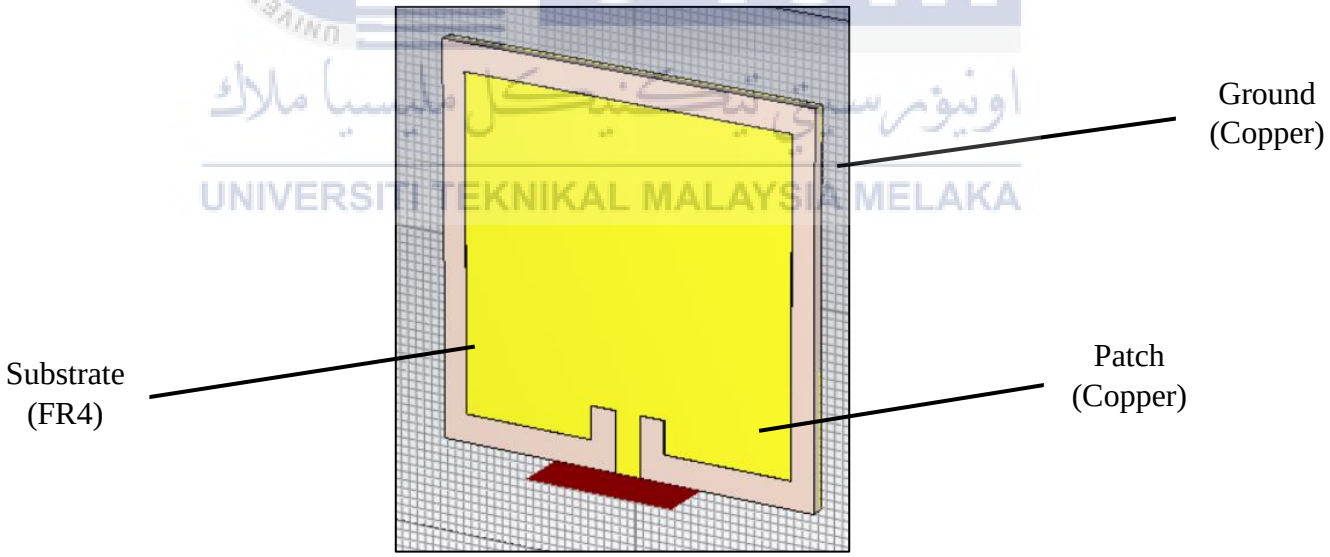

Figure 8: Transparent patch antenna using FR4 and Copper

Calculation of FR4

fr = 3.5 GHz, $\varepsilon_r = 4.3$*, c = 3x*10^8 *m/s, h = 1.6 mm*

$$w = \frac{c}{2fr\left(\sqrt{\frac{\varepsilon_r+1}{2}}\right)}$$

$$= \frac{3x10^8}{2(3.5\ G)\left(\sqrt{\frac{4.3+1}{2}}\right)}$$

= 0.02633 m

= 26.33 mm

$$\varepsilon_{reff} = \frac{\varepsilon_r+1}{2} + \frac{\varepsilon_r-1}{2}\left[1 + 12\left(\frac{h}{w}\right)\right]^{-\frac{1}{2}}$$

$$= \frac{4.3+1}{2} + \frac{4.3-1}{2}\left[1 + 12\left(\frac{1.6}{26.33}\right)\right]^{-\frac{1}{2}}$$

= 3.90

$$L_{eff} = \frac{c}{2fr\left(\sqrt{\varepsilon_{reff}}\right)}$$

$$= \frac{3x10^8}{2(3.5\ G)(\sqrt{3.90})}$$

= 0.02170 m

= 21.70 mm

$$\Delta L = 0.412\ h\ \left[\frac{(\varepsilon_{reff}+0.3)(\frac{w}{h}+0.264)}{(\varepsilon_{reff}-0.258)(\frac{w}{h}+0.8)}\right]$$

$$= 0.412(1.6)\ \left[\frac{(3.90+0.3)(\frac{26.33}{1.6}+0.264)}{(3.90-0.258)(\frac{26.33}{1.6}+0.8)}\right]$$

= 0.7366 mm

$$L_p = L_{eff} - 2\Delta L$$

= 21.70 – 2(0.7366)

= 20.23 mm

$$w_g = L_g = w_s = L_s = \frac{c}{2f_r}$$

$$= \frac{3x10^8}{2(3.5\ G)}$$

$$= 42.86\ mm$$

$$DL = \frac{L_s}{2} - \frac{L_p}{2}$$

$$= \frac{42.86}{2} - \frac{20.23}{2}$$

$$= 11.23\ mm$$

Table 6: Comparison value of parameters using FR4

Parameters	Theoretical Calculation Value (mm)	Simulation Value (mm)
Patch Height, Hp	0.035	0.035
Substrate Height, Hs	1.600	1.600
Feed Width, Wf	3.065	3.065
Insert Length, Yo	4.000	4.000
Patch Length, Lp	20.230	40.000
Patch Width, Wp	26.330	41.000
Substrate Width, Ws	42.860	46.600
Substrate Length, Ls	42.860	46.600
Delta L, DL	11.230	3.300

In table 6, it shows the comparison value of parameters between values of theoretical calculation and values of simulation using FR4. Based on the values of table, there are significant difference between theoretical calculation value and simulation value. Furthermore, the differences between theoretical and experimental probability are that theoretical is based on knowledge and mathematics, while experimental is based on observation. It also effects from sensitivity of human error and numerical error when doing this simulation.

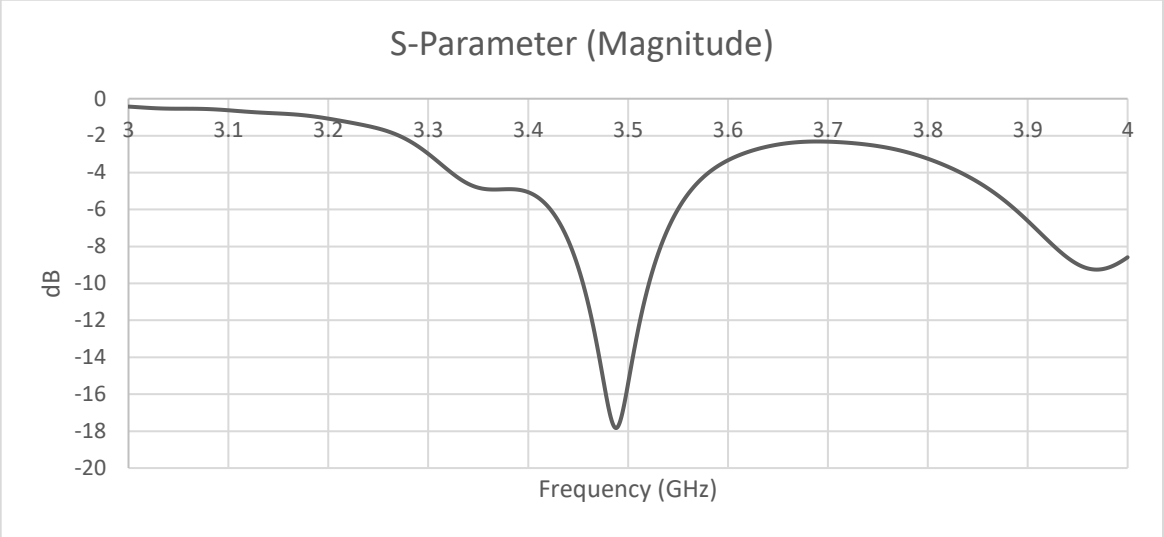

Figure 8. 1: S-Parameter |S11| of FR4 at 3.5 GHz

In figure 8.1, it shows the S-Parameter |S11| that using material which is FR4 at resonant frequency that chooses is 3.5 GHz. However, the value of return loss is must below -10 dB for antenna. When the performance gets below -10 dB, it shows the better performance because it depends on the measurement value of return loss that we get in the measurement of simulation. Therefore, the return loss of simulate for this transparent antenna using FR4 is below -10 dB which is -16.88 dB at 3.49 GHz. From the result of S-Parameter, it shows the better performance of FR4 at 3.5 GHz.

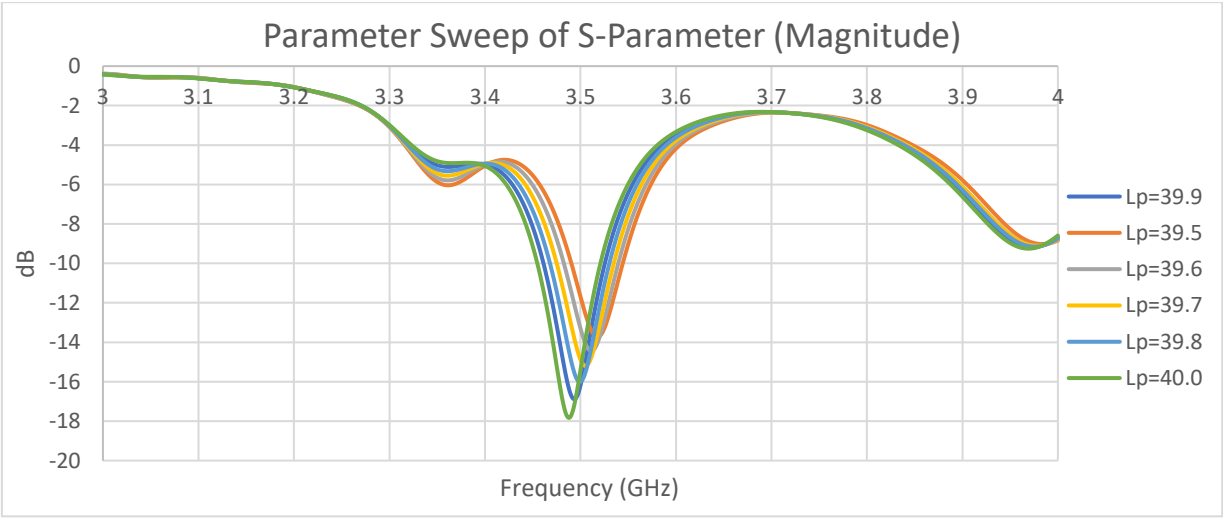

Figure 8. 2: Parameter Sweep of FR4

In figure 8.2, it shows the parameter sweep using FR4 with difference value of return loss. It is because of using difference value of length of patch that to see the difference value of return loss. Based on calculation above, the value of length patch is 20.23 mm. Therefore, using varified the value of length patch is to show the difference value of variety return loss that must below -10 dB which is -17.79, -16.70, -15.83, -15.13, -14.43 and -13.73.

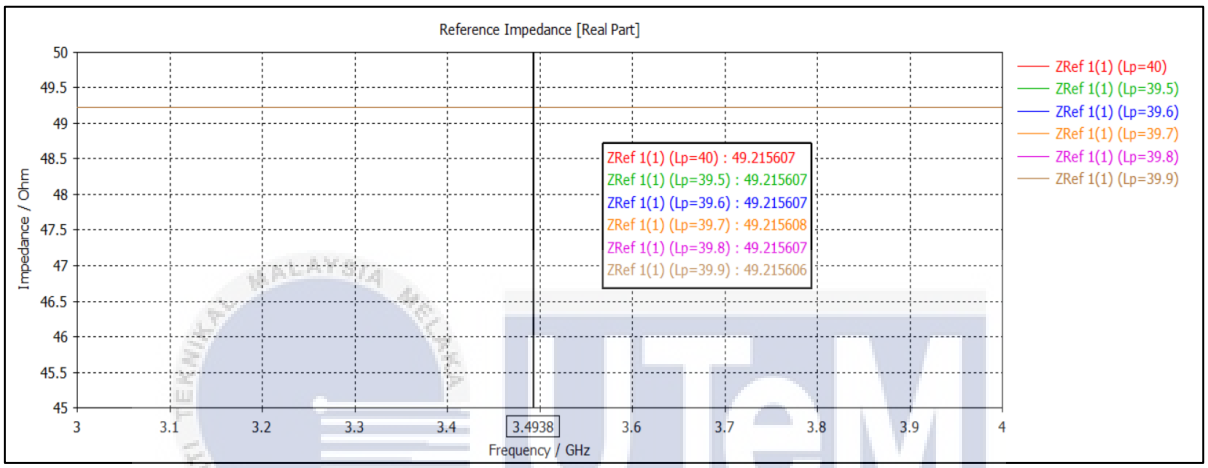

Figure 8. 3: Reference Impedance of FR4

In figure 8.3, it shows the reference impedance that using FR4. The exactly value of impedance in antenna is 50 Ohm. It is because the voltage and current at the input of antenna are related by its impedance. Furthermore, 50 Ohm cables are designed to transport voltage and power such as the output of a transmitter. When antenna with 50 Ohm impedance, that shows the sinusoidal voltage with an amplitude of 1V is applied at the antenna terminals with the current will have an amplitude of 0.02A. Therefore, the results that get in the simulation is below 50 Ohm which is 49.22 for all value measurement.

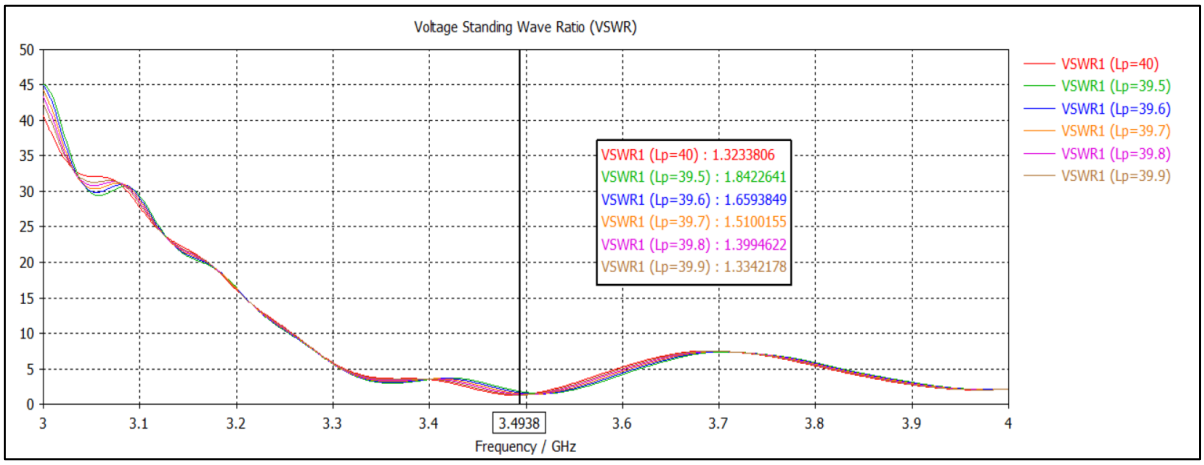

Figure 8. 4: VSWR of FR4

In figure 8.4, it shows the voltage standing wave radio that using FR4. It is a measurement of the performance of radio frequency power transmission from a power source to a load through a transmission line. The value of voltage standing wave radio is must below 2. Therefore, the value of simulation of voltage standing wave radio is 1.32, 1.84, 1.66, 1.51, 1.40 and 1.33.

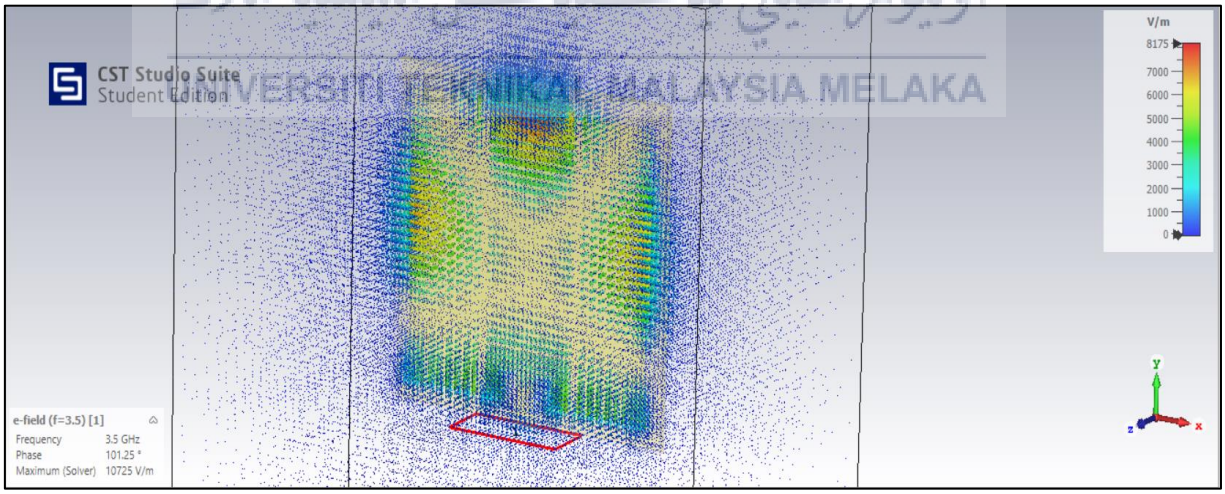

Figure 8. 5: E-field of FR4 at 3.5 GHz

In figure 8.5, it shows the e-field that using FR4. E-field is standing for the electric field that surrounds electrically charged particles and interacts with them to either attract or repel other charged particles in the field. Therefore, at 3.5 GHz, the maximum value of e-field in this simulation is 10725 V/m.

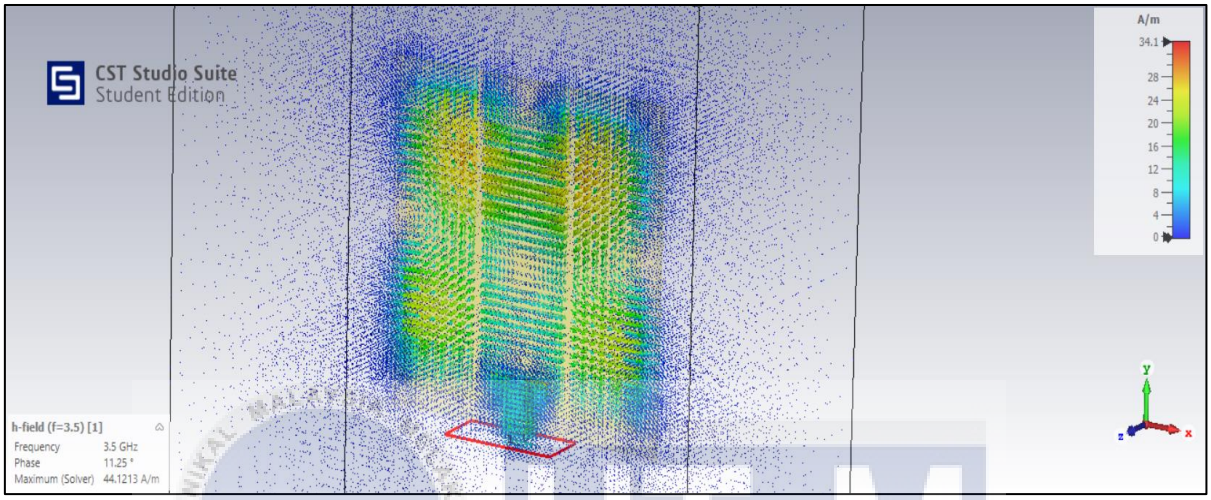

Figure 8. 6: H-field of FR4 at 3.5 GHz

In figure 8.6 GHz, it shows the h-filed that using FR4. H-filed is standing for magnetic fields that what shows the antenna's greatest radiation direction. Therefore, the maximum value of h-field in this simulation at 3.5 GHz is 44.12 A/m.

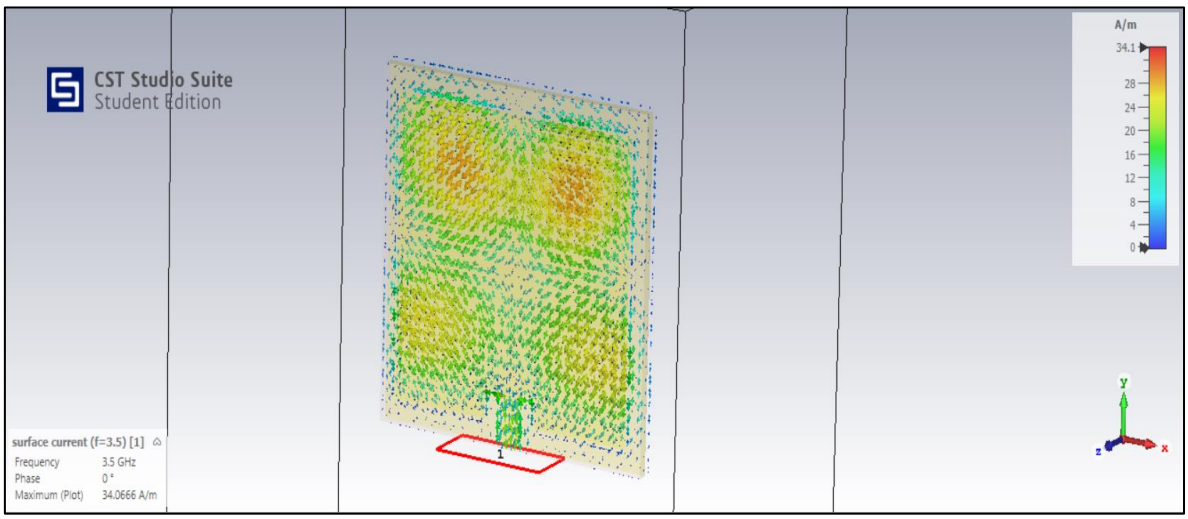

Figure 8. 7: Surface Current of FR4 at 3.5 GHz

In figure 8.7 GHz, it shows the surface current that using FR4. It is an electromagnetic field that used to create a real electric current. Therefore, the maximum value of surface current in this simulation at 3.5 GHz is 34.07 A/m.

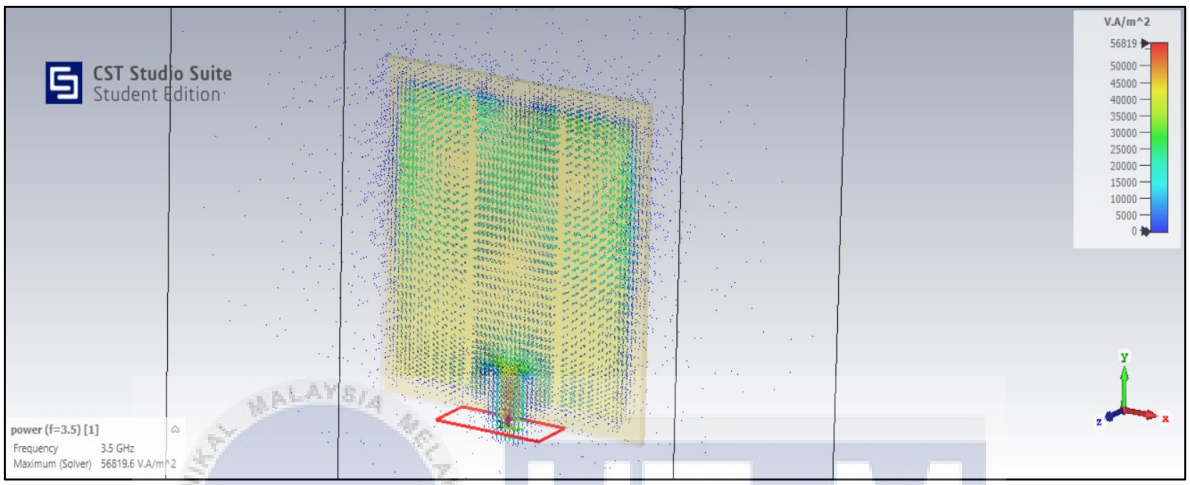

Figure 8. 8: Power of FR4 at 3.5 GHz

In figure 8.8, it shows the power that using FR4. It is showing how the antenna obtains energy by radiating energy into space. Therefore, the maximum value of power in this simulation at 3.5 GHz is 56819.60 VA/m^2.

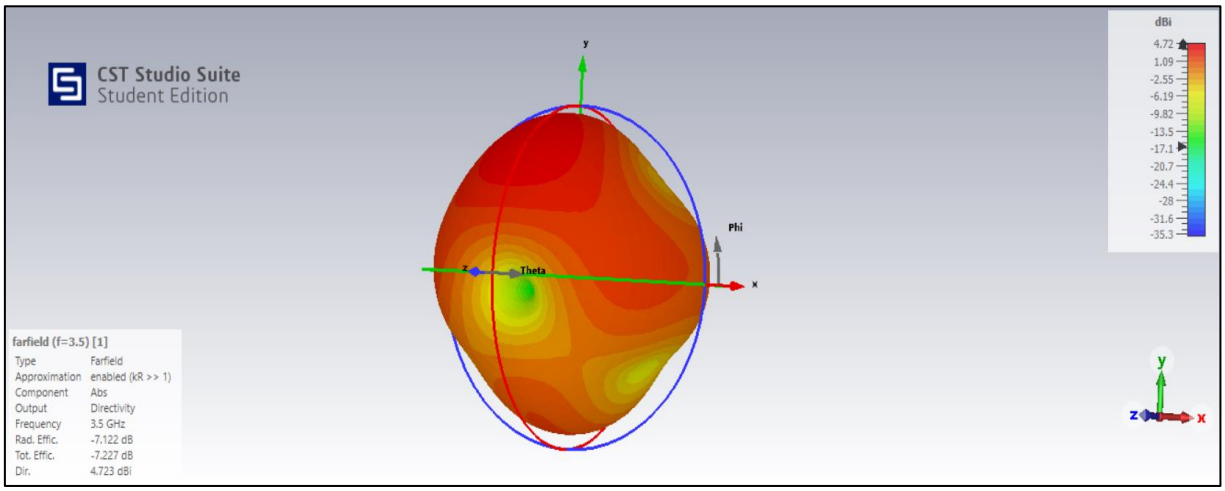

Figure 8. 9: 3D Farfield of FR4 at 3.5 GHz

In figure 8.9, it shows the 3D farfield that using FR4. It shows the region where the antenna radiation pattern has a polarity variation and is independent of distance from the antenna is typically thought to be this one. Based on that, it can see the polar of theta and phi at 3.5 GHz. Therefore, the value of efficiency is -7.23 dB and the value of directivity is 4.72 dB.

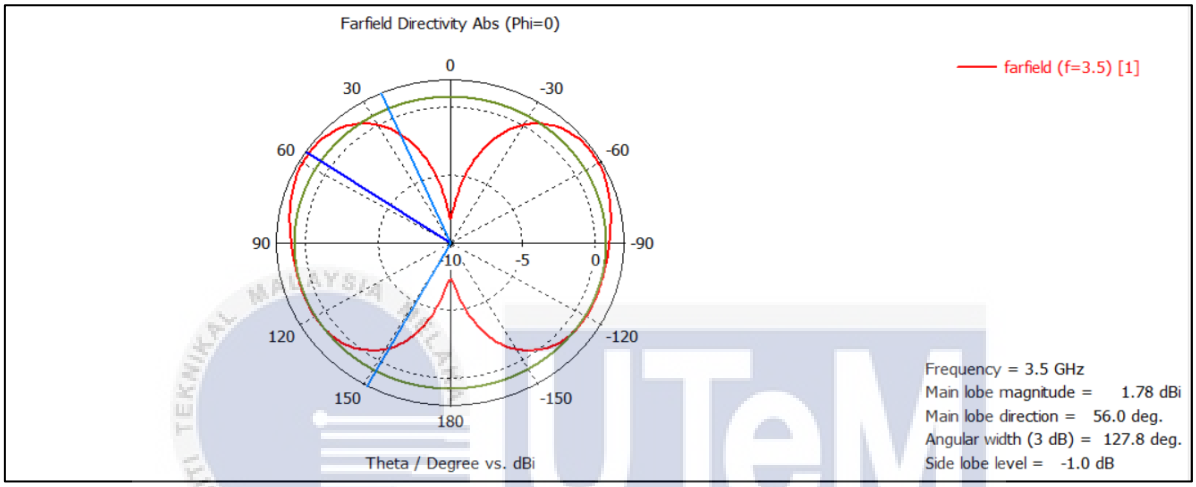

Figure 8. 10: 2D Farfield of FR4 at 3.5 GHz when π=0

In figure 8.10, it shows 2D farfield that using FR4. Based on that, the value of phi is 0 that shows in the farfield directivity abs. Therefore, when phi is 0, the gain is 1.78 dB at 3.5 GHz.

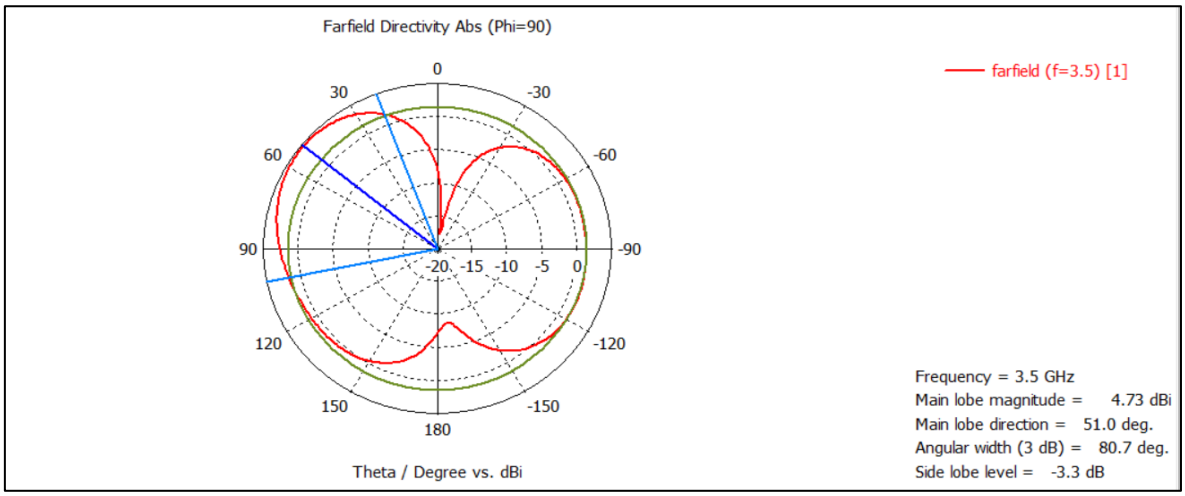

Figure 8. 11: 2D Farfield of FR4 at 3.5 GHz when π=90

In figure 8.11, it shows 2D farfield that using FR4. Based on that, the value of phi is 90 that shows in the farfield directivity abs. Therefore, when phi is 90, the gain is 4.73 dB at 3.5 GHz.

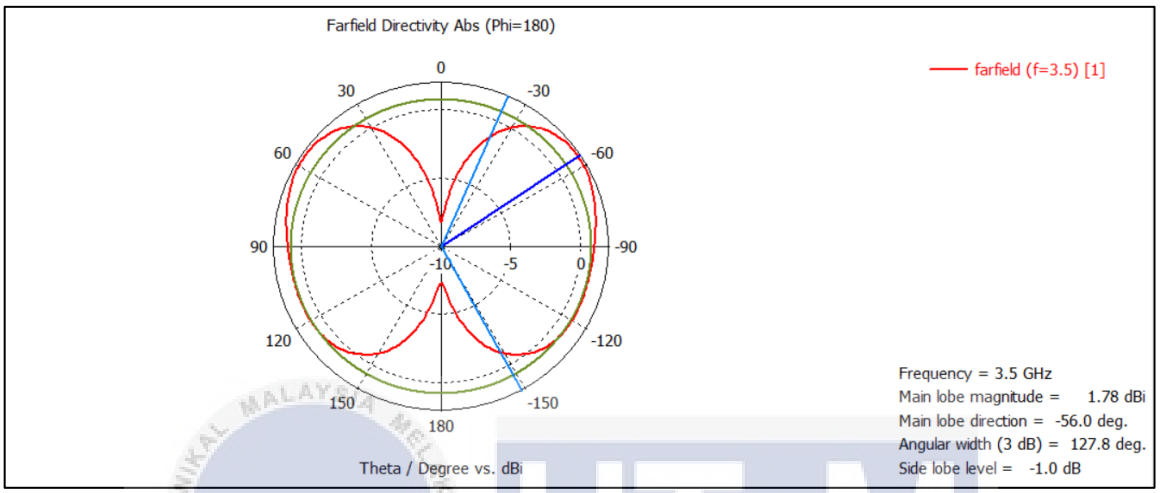

Figure 8. 12: 2D Farfield of FR4 at 3.5 GHz when π=180

In figure 8.12, it shows 2D farfield that using FR4. Based on that, the value of phi is 180 that shows in the farfield directivity abs. Therefore, when phi is 180, the gain is 1.78 dB at 3.5 GHz.

4.2.2 Rogers RT5880 and Copper

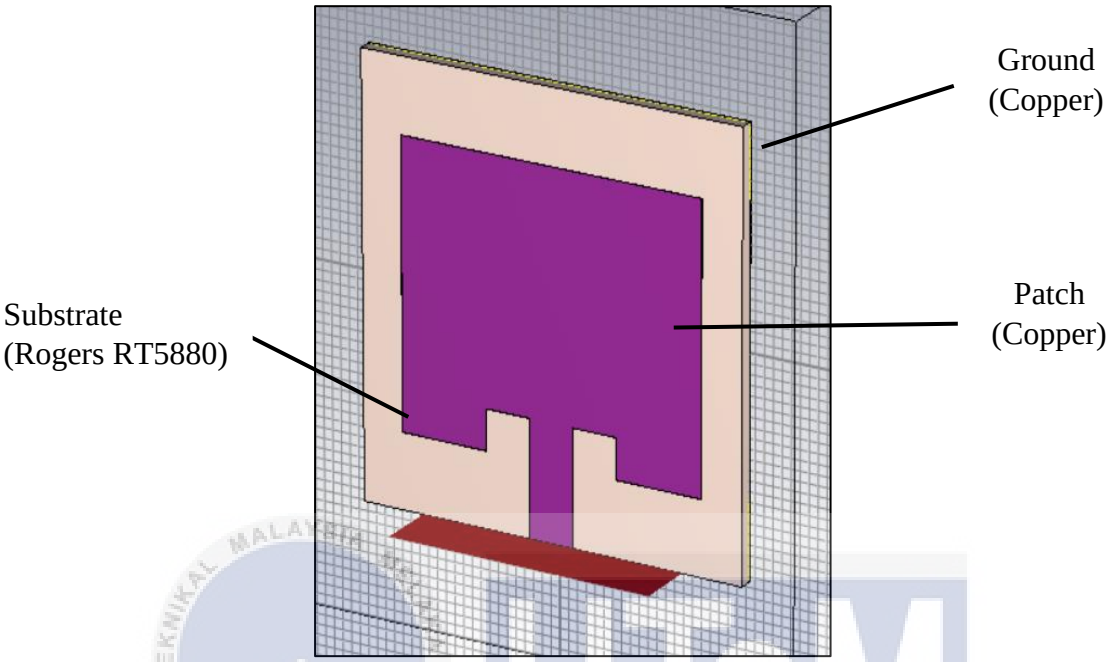

Figure 9: Transparent patch antenna using Rogers RT5880 and Copper

Calculation of Rogers 5880

fr = 3.5 GHz, ε_r *= 2.2, c = 3x*10^8 *m/s, h = 1.6 mm*

$$w = \frac{c}{2fr\left(\sqrt{\frac{\varepsilon_r+1}{2}}\right)}$$

$$= \frac{3x10^8}{2(3.5\ G)\left(\sqrt{\frac{2.2+1}{2}}\right)}$$

$$= 0.03388\ m$$

$$= 33.88\ mm$$

$$\varepsilon_{reff} = \frac{\varepsilon_r+1}{2} + \frac{\varepsilon_r-1}{2}\left[1 + 12\left(\frac{h}{w}\right)\right]^{-\frac{1}{2}}$$

$$= \frac{2.2+1}{2} + \frac{2.2-1}{2}\left[1 + 12\left(\frac{1.6}{33.88}\right)\right]^{-\frac{1}{2}}$$

$$= 2.08$$

$$L_{eff} = \frac{c}{2fr(\sqrt{\varepsilon_{reff}})}$$

$$= \frac{3x10^8}{2(3.5\ G)(\sqrt{2.08})}$$

$$= 0.02972\ m$$

$$= 29.72\ mm$$

$$\Delta L = 0.412\ h\ \left[\frac{(\varepsilon_{reff}+0.3)(\frac{w}{h}+0.264)}{(\varepsilon_{reff}-0.258)(\frac{w}{h}+0.8)}\right]$$

$$= 0.412(1.6)\ \left[\frac{(2.08+0.3)(\frac{33.88}{1.6}+0.264)}{(2.08-0.258)(\frac{33.88}{1.6}+0.8)}\right]$$

$$= 0.8401\ mm$$

$$L_p = L_{eff} - 2\Delta L$$

$$= 29.72 - 2(0.8401)$$

$$= 28.04\ mm$$

$$w_g = L_g = w_s = L_s = \frac{c}{2f_r}$$

$$= \frac{3x10^8}{2(3.5\ G)}$$

$$= 42.86\ mm$$

$$DL = \frac{L_s}{2} - \frac{L_p}{2}$$

$$= \frac{42.86}{2} - \frac{28.04}{2}$$

$$= 7.41\ mm$$

Table 7: Comparison value of parameters using Rogers RT5880

Parameters	Theoretical Calculation Value (mm)	Simulation Value (mm)
Patch Height, Hp	0.035	0.035
Substrate Height, Hs	1.600	1.600
Feed Width, Wf	3.065	4.897
Insert Length, Yo	4.000	4.000
Patch Length, Lp	28.040	27.040
Patch Width, Wp	33.880	38.880
Substrate Width, Ws	42.860	42.860
Substrate Length, Ls	42.860	42.860
Delta L, DL	7.410	7.910

In table 7, it shows the comparison value of parameters between values of theoretical calculation and values of simulation using Rogers RT5880. Based on the values of table, there are narrow difference between theoretical calculation value and simulation value. Therefore, it also effects from sensitivity of human error and numerical error when doing this simulation.

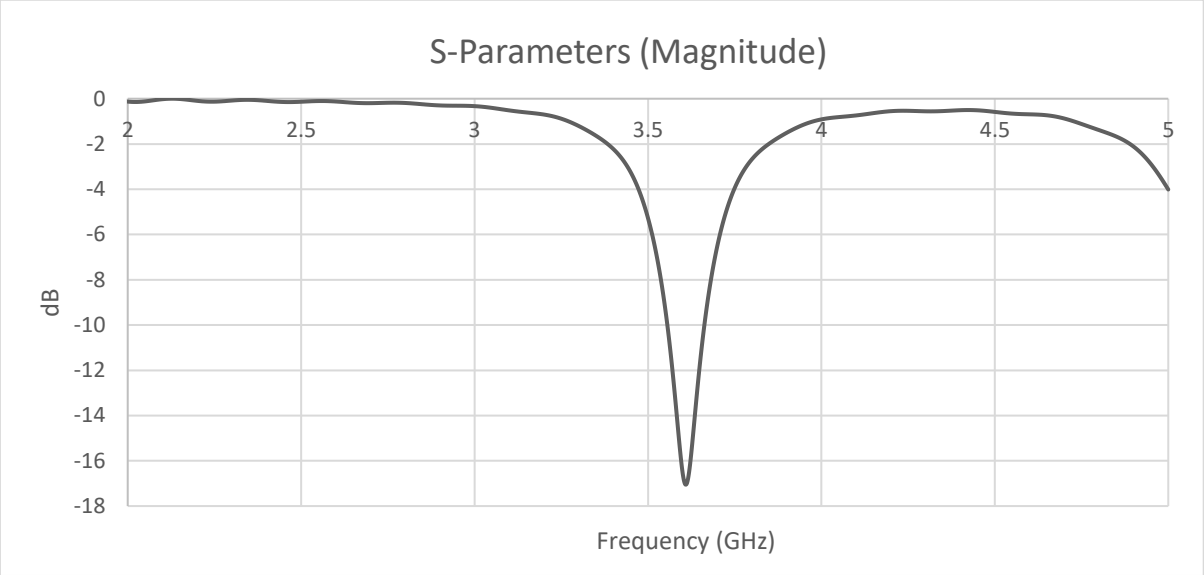

Figure 9. 1: S-Parameter |S11| of Rogers RT5880 at 3.5 GHz

In figure 9.1, it shows the S-Parameter |S11| that using material which is Rogers RT5880 at resonant frequency that chooses is 3.5 GHz. Furthermore, the value of return loss is also must below -10 dB for antenna. When the performance gets below -10 dB, it shows the better performance because it depends on the measurement value of return loss that we get in the measurement of simulation. Therefore, the return loss of simulate for this transparent antenna using Rogers RT5880 is below -10 dB which is -20.23 dB at 3.60 GHz. From the result of S-Parameter, it shows the better performance of Rogers RT5880 at 3.5 GHz.

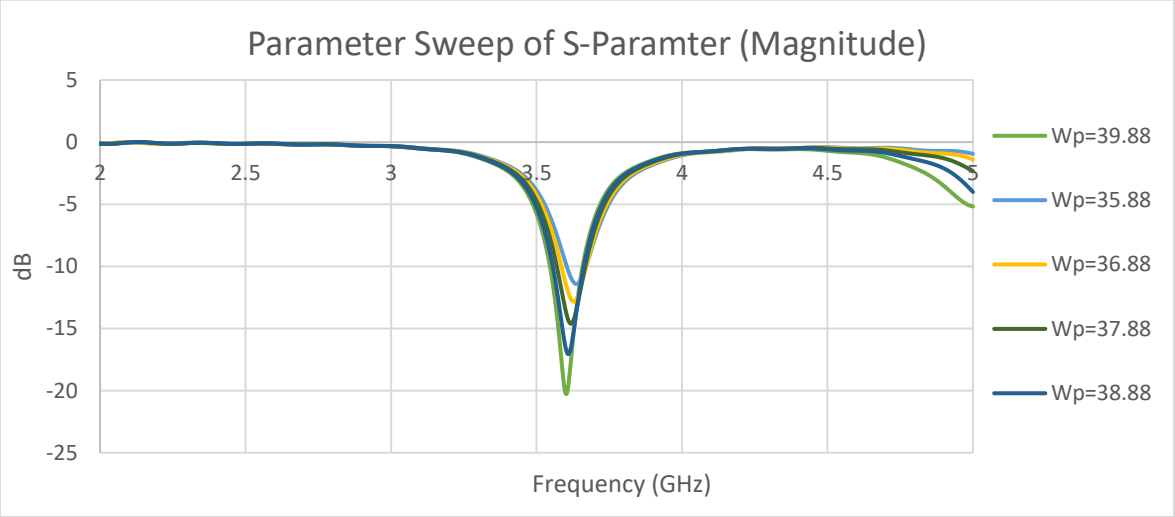

Figure 9. 2: Parameter Sweep of Rogers RT5880

In figure 9.2, it shows the parameter sweep using Rogers RT5880 with difference value of return loss. It is because of using difference value of length of patch that to see the difference value of return loss. Based on calculation above, the value of length patch is 28.04 mm. Therefore, using varified the value of length patch is to show the difference value of variety return loss that must below -10 dB which is -20.02, -16.74, -14.56, -12.83 and -11.40.

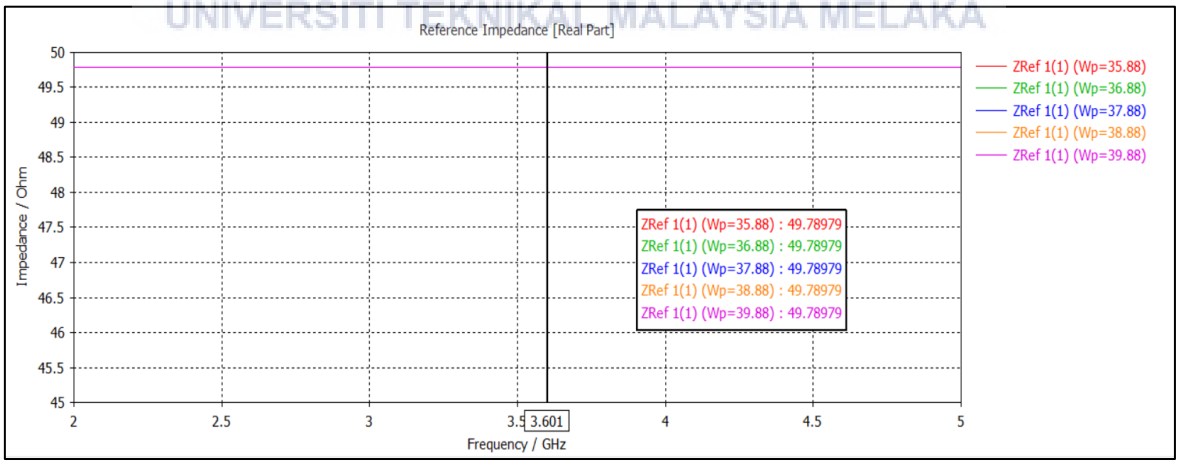

Figure 9. 3: Reference Impedance of Rogers RT5880

In figure 9.3, it shows the reference impedance that using Rogers RT5880. The exactly value of impedance in antenna is 50 Ohm. When antenna with 50 Ohm impedance, it shows the sinusoidal voltage with an amplitude of 1V is applied at the antenna terminals with the current will have an amplitude of 0.02A. Therefore, the results that get in the simulation is below 50 Ohm which is 49.79 for all value measurement.

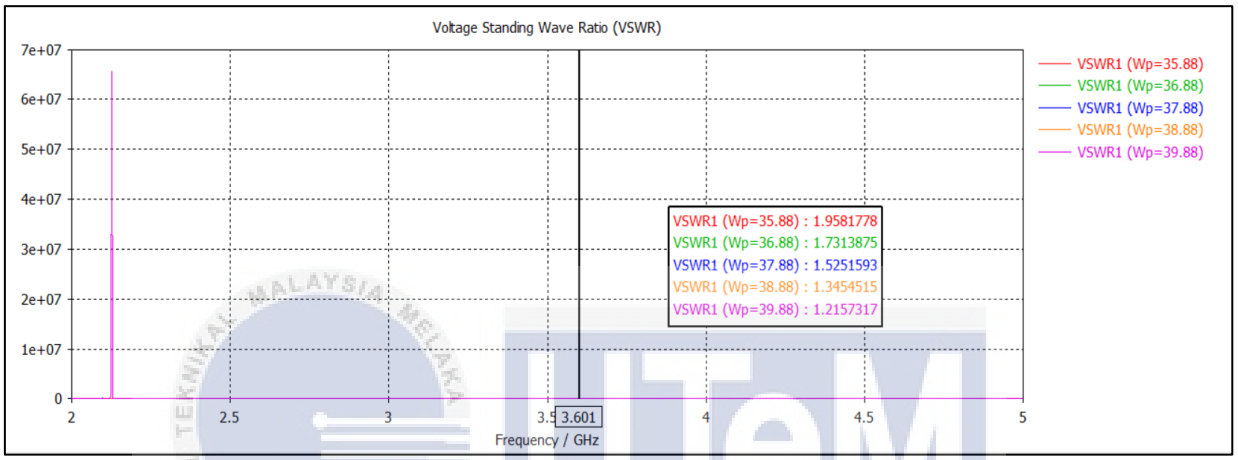

Figure 9. 4: VSWR of Rogers RT5880

In figure 9.4, it shows the voltage standing wave radio that using Rogers RT5880. It is a measurement of the efficiency with which radio frequency power is transmitted from a power source to a load through a transmission line. The voltage standing wave radio value must be less than 2. Therefore, the value of simulation of voltage standing wave radio is 1.96, 1.73, 1.53, 1.34 and 1.22.

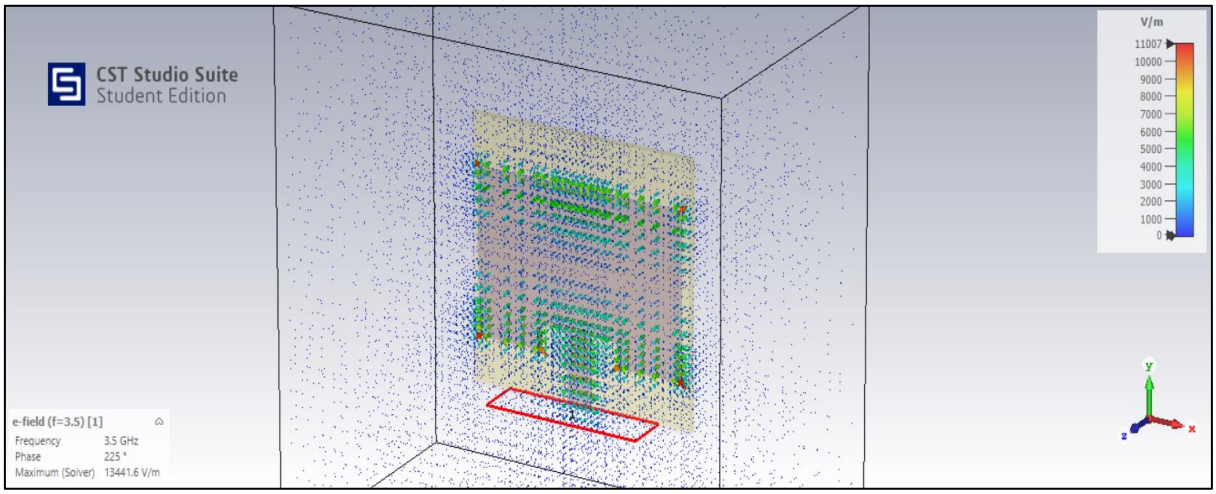

Figure 9. 5: E-field of Rogers RT5880 at 3.5 GHz

In figure 9.5, it shows the e-field that using Rogers RT5880. E-field is standing for the electric field that surrounds electrically charged particles and interacts with them to either attract or repel other charged particles in the field. Therefore, at 3.5 GHz, the maximum value of e-field in this simulation is 13441.6 V/m.

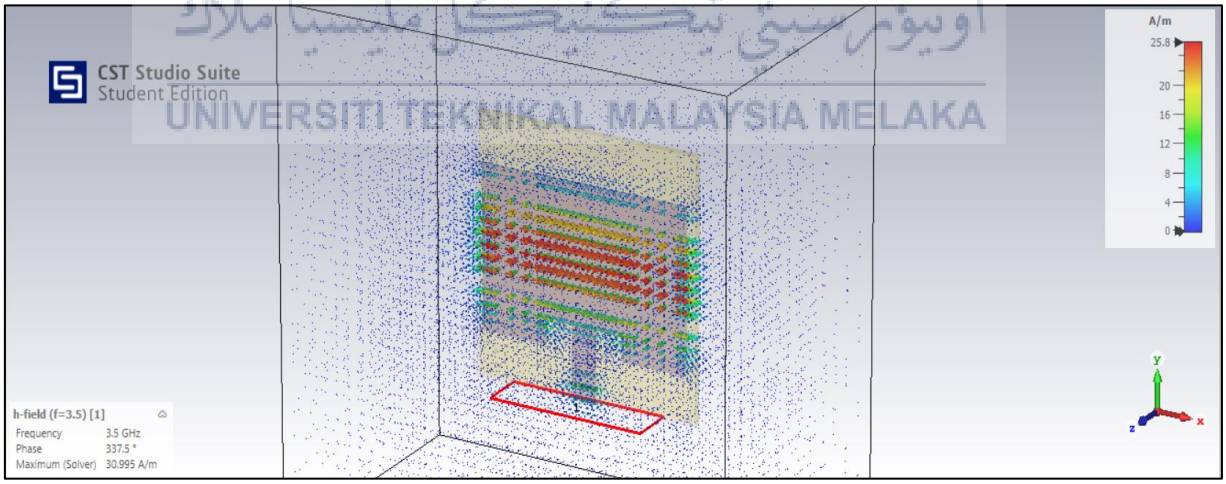

Figure 9. 6: H-field of Rogers RT5880 at 3.5 GHz

In figure 9.6 GHz, it shows the h-filed that using Rogers RT5880. H-filed is standing for magnetic fields that what shows the antenna's greatest radiation direction. Therefore, the maximum value of h-field in this simulation at 3.5 GHz is 30.995 A/m.

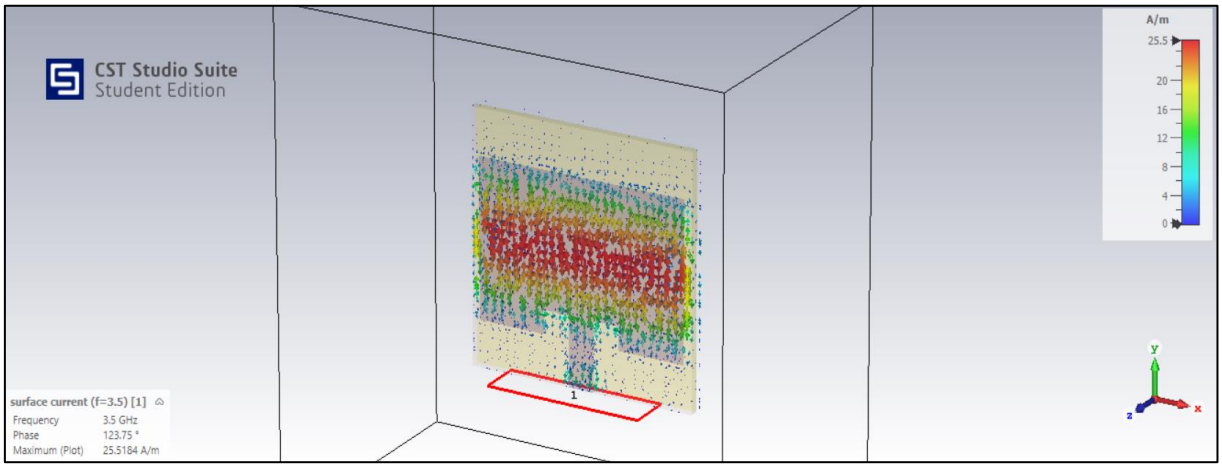

Figure 9. 7: Surface Current of Rogers RT5880 at 3.5 GHz

In figure 9.7 GHz, it shows the surface current that using Rogers RT5880. It is an electromagnetic field that used to create a real electric current. Therefore, the maximum value of surface current in this simulation at 3.5 GHz is 25.52 A/m.

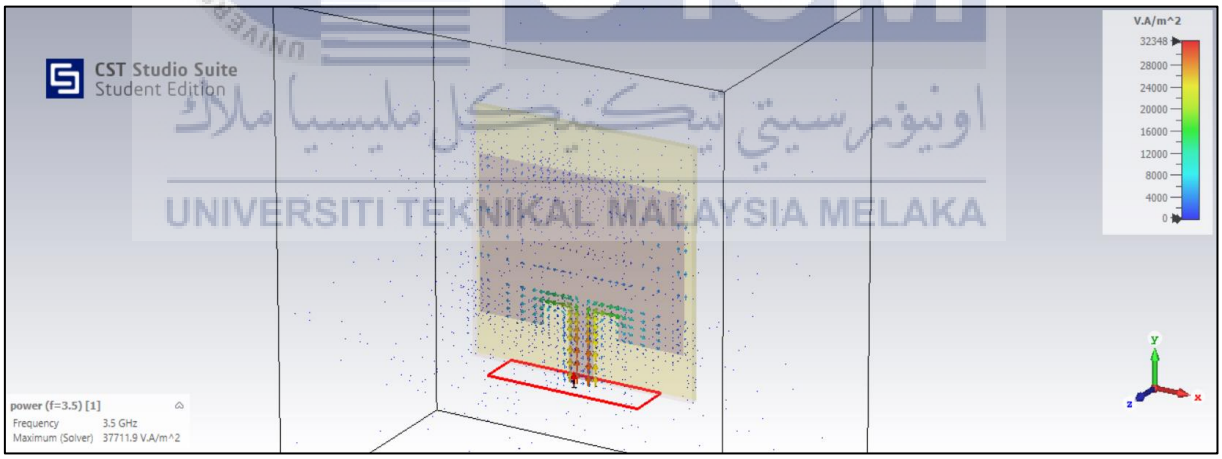

Figure 9. 8: Power of Rogers RT5880 at 3.5 GHz

In figure 9.8, it shows the power that using Rogers RT5880. It is showing how the antenna obtains energy by radiating energy into space. Therefore, the maximum value of power in this simulation at 3.5 GHz is 37711.90 VA/m^2.

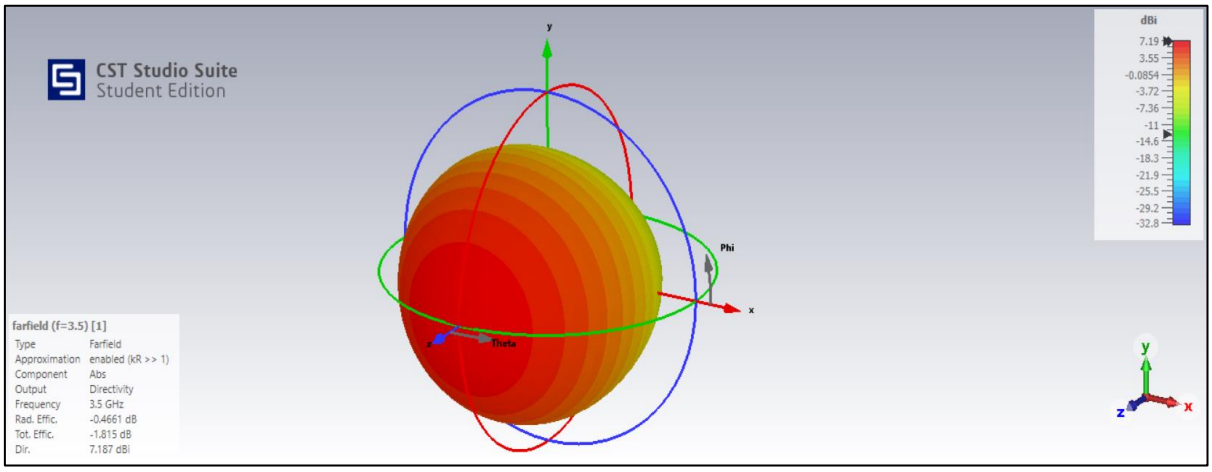

Figure 9. 9: 3D Farfield of Rogers RT5880 at 3.5 GHz

In figure 9.9, it shows the 3D farfield that using Rogers RT5880. It shows the region where the antenna radiation pattern has a polarity variation and is independent of distance from the antenna is typically thought to be this one. Based on that, it can see the polar of theta and phi at 3.5 GHz. Therefore, the value of efficiency is -1.82 dB and the value of directivity is 7.19 dB.

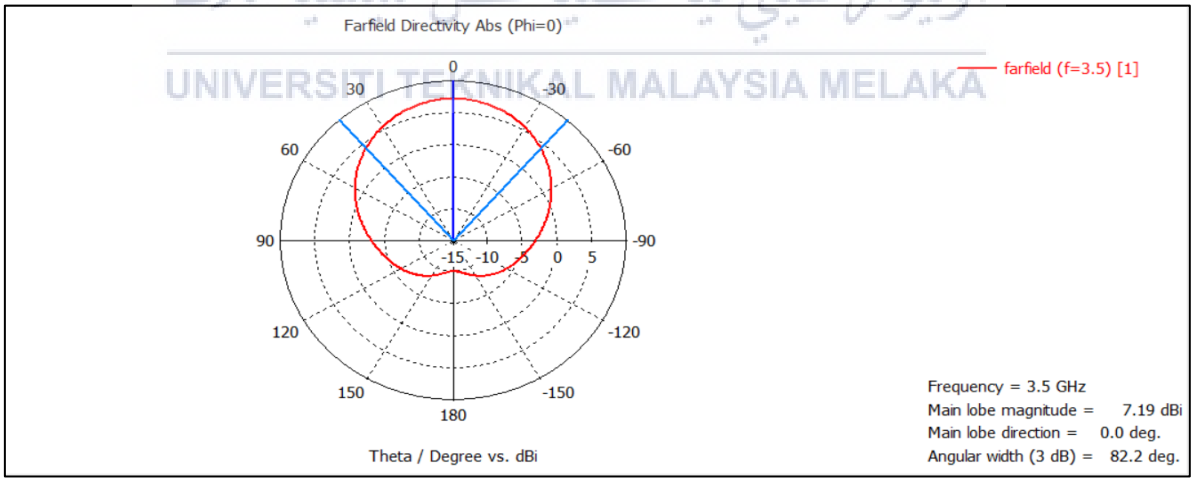

Figure 9. 10: 2D Farfield of Rogers RT5880 at 3.5 GHz when π=0

In figure 9.10, it shows 2D farfield that using Rogers RT5880. Based on that, the value of phi is 0 that shows in the farfield directivity abs. Therefore, when phi is 0, the gain is 7.19 dB at 3.5 GHz.

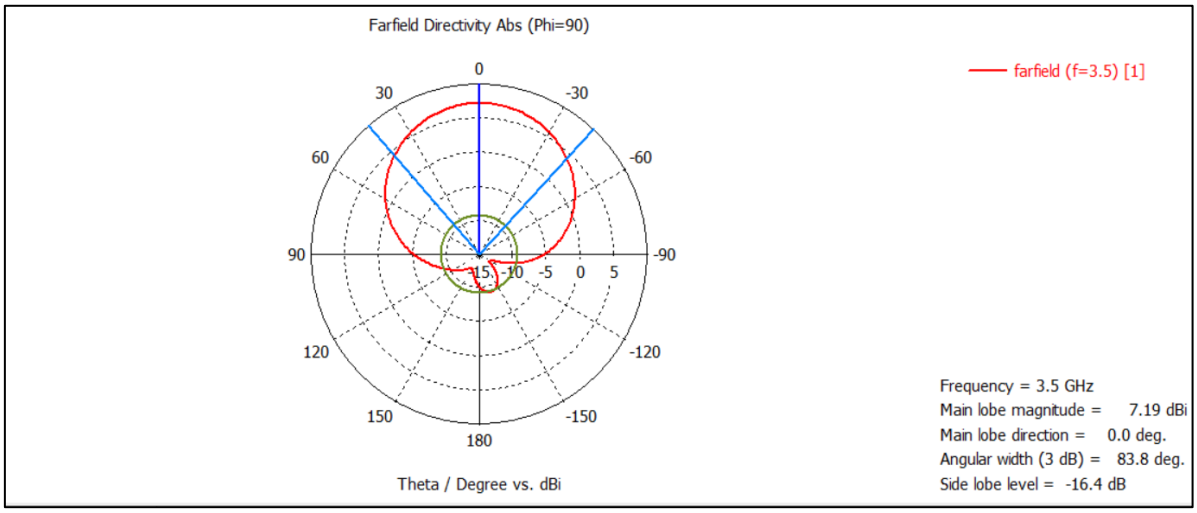

Figure 9. 11: 2D Farfield of Rogers RT5880 at 3.5 GHz when π=90

In figure 9.11, it shows 2D farfield that using Rogers RT5880. Based on that, the value of phi is 90 that shows in the farfield directivity abs. Therefore, when phi is 90, the gain is also 7.19 dB at 3.5 GHz.

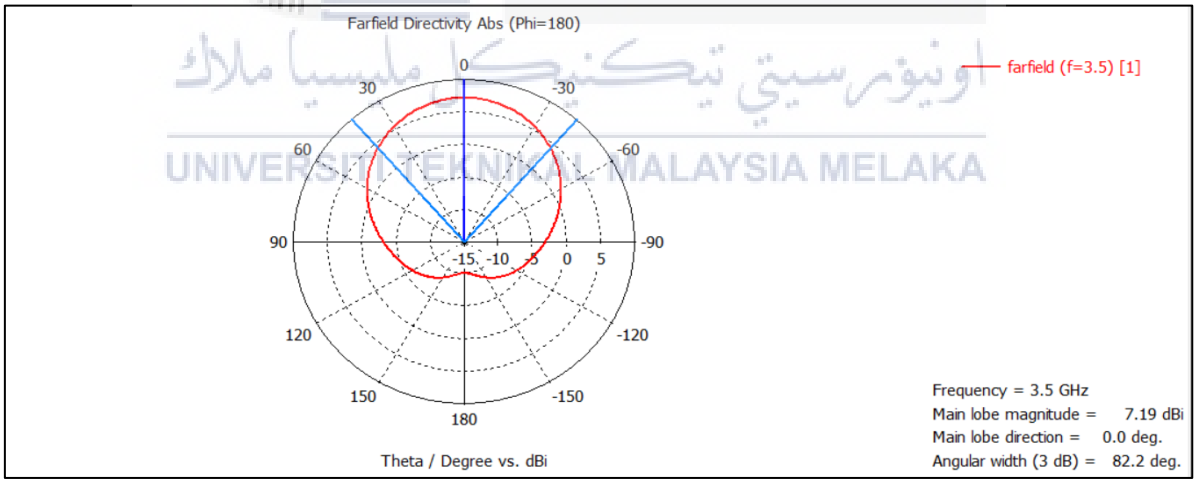

Figure 9. 12: 2D Farfield of Rogers RT5880 at 3.5 GHz when π=180

In figure 9.11, it shows 2D farfield that using Rogers RT5880. Based on that, the value of phi is 180 that shows in the farfield directivity abs. Therefore, when phi is 180, the gain is also 7.19 dB at 3.5 GHz.

4.2.3 Water and Lead Glass

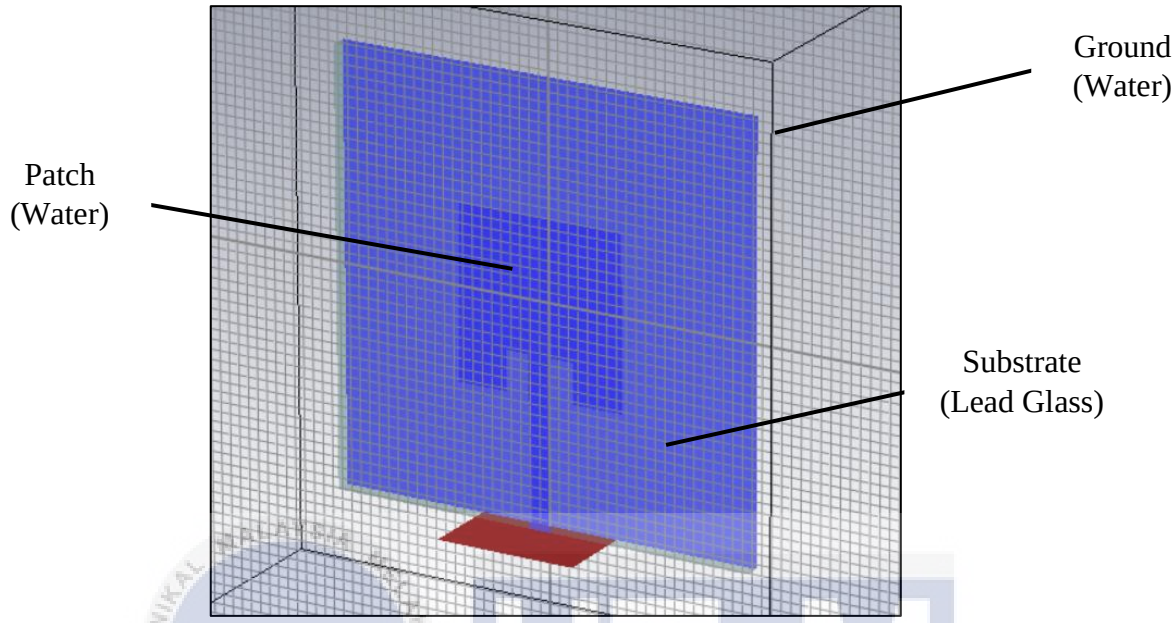

Figure 10: Transparent patch antenna using Lead Glass and Water

Calculation of Lead Glass

fr = 3.5 GHz, $\varepsilon_r = 6$, *c = 3x*10^8 *m/s, h = 1.6 mm*

$$w = \frac{c}{2fr\left(\sqrt{\frac{\varepsilon_r+1}{2}}\right)}$$

$$= \frac{3x10^8}{2(3.5\ G)\left(\sqrt{\frac{6+1}{2}}\right)}$$

$$= 0.02291\ m$$

$$= 22.91\ mm$$

$$\varepsilon_{reff} = \frac{\varepsilon_r+1}{2} + \frac{\varepsilon_r-1}{2}\left[1 + 12\left(\frac{h}{w}\right)\right]^{-\frac{1}{2}}$$

$$= \frac{6+1}{2} + \frac{6-1}{2}\left[1 + 12\left(\frac{1.6}{22.91}\right)\right]^{-\frac{1}{2}}$$

$$= 5.34$$

$$L_{eff} = \frac{c}{2fr(\sqrt{\varepsilon_{reff}})}$$

$$= \frac{3x10^8}{2(3.5\ G)(\sqrt{5.34})}$$

$$= 0.0185\ m$$

$$= 18.55\ mm$$

$$\Delta L = 0.412\ h\ \left[\frac{(\varepsilon_{reff}+0.3)(\frac{w}{h}+0.264)}{(\varepsilon_{reff}-0.258)(\frac{w}{h}+0.8)}\right]$$

$$= 0.412(1.6)\ \left[\frac{(5.34+0.3)(\frac{22.91}{1.6}+0.264)}{(5.34-0.258)(\frac{22.91}{1.6}+0.8)}\right]$$

$$= 0.7056\ mm$$

$$L_p = L_{eff} - 2\Delta L$$

$$= 18.55 - 2(0.7056)$$

$$= 17.14\ mm$$

$$w_g = L_g = w_s = L_s = \frac{c}{2f_r}$$

$$= \frac{3x10^8}{2(3.5\ G)}$$

$$= 42.86\ mm$$

$$DL = \frac{L_s}{2} - \frac{L_p}{2}$$

$$= \frac{42.86}{2} - \frac{17.14}{2}$$

$$= 12.86\ mm$$

Table 8: Comparison value of parameters using lead glass

Parameters	Theocratical Calculation Value (mm)	Simulation Value (mm)
Patch Height, Hp	0.035	0.035
Substrate Height, Hs	1.600	1.600
Feed Width, Wf	3.065	2.243
Insert Length, Yo	4.000	4.000
Patch Length, Lp	17.140	17.140
Patch Width, Wp	22.910	16.910
Substrate Width, Ws	42.860	42.860
Substrate Length, Ls	42.860	42.860
Delta L, DL	12.860	12.860

In table 8, it shows the comparison value of parameters between values of theoretical calculation and values of simulation using lead glass. Based on the values of table, there are slightly difference between theoretical calculation value and simulation value. It is because it effects from sensitivity of human error and numerical error when doing this simulation.

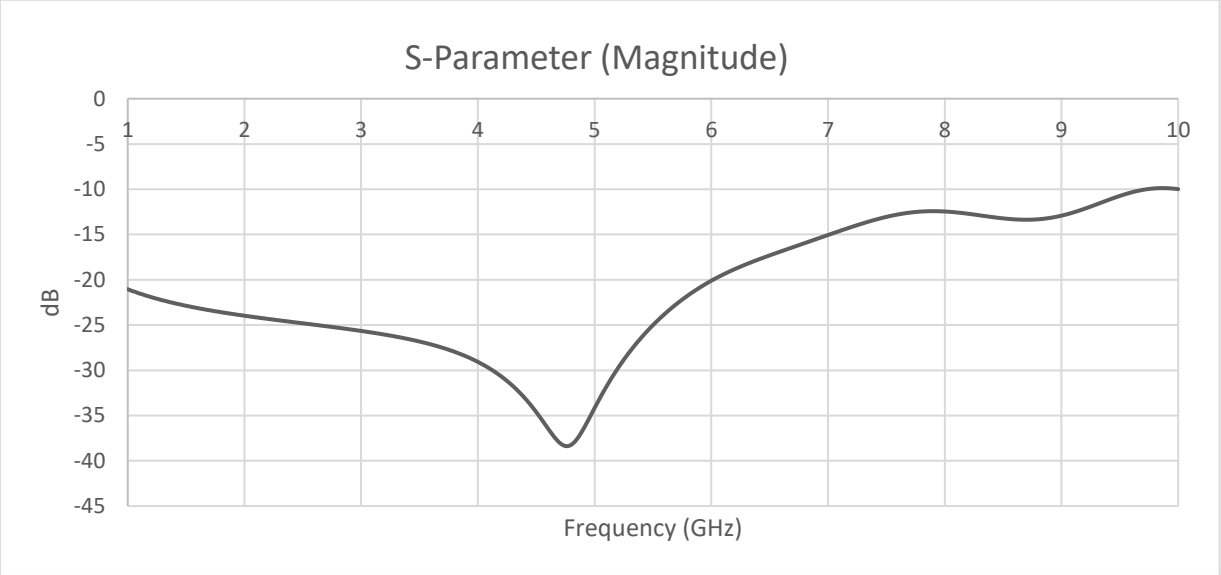

Figure 10. 1: S-Parameter |S11| of Lead Glass at 3.5 GHz

In figure 10.1, it shows the S-Parameter |S11| that using material which is lead glass at resonant frequency that chooses is 3.5 GHz. When the performance gets below -10 dB, it shows the better performance because it depends on the measurement value of return loss that we get in the measurement of simulation. Therefore, the return loss of simulate for this transparent antenna using lead glass is below -10 dB which is -38.50 dB at 4.85 GHz. From the result of S-Parameter, it shows the value of simulation and measurement difference. It is because of error of simulation in CST Software and it also depends on the type of material that using in this simulation because it different at value of epsilon of material. Based on simulation, the value of frequency is 4.85 GHz while the value of measurement frequency is 3.5 GHz.

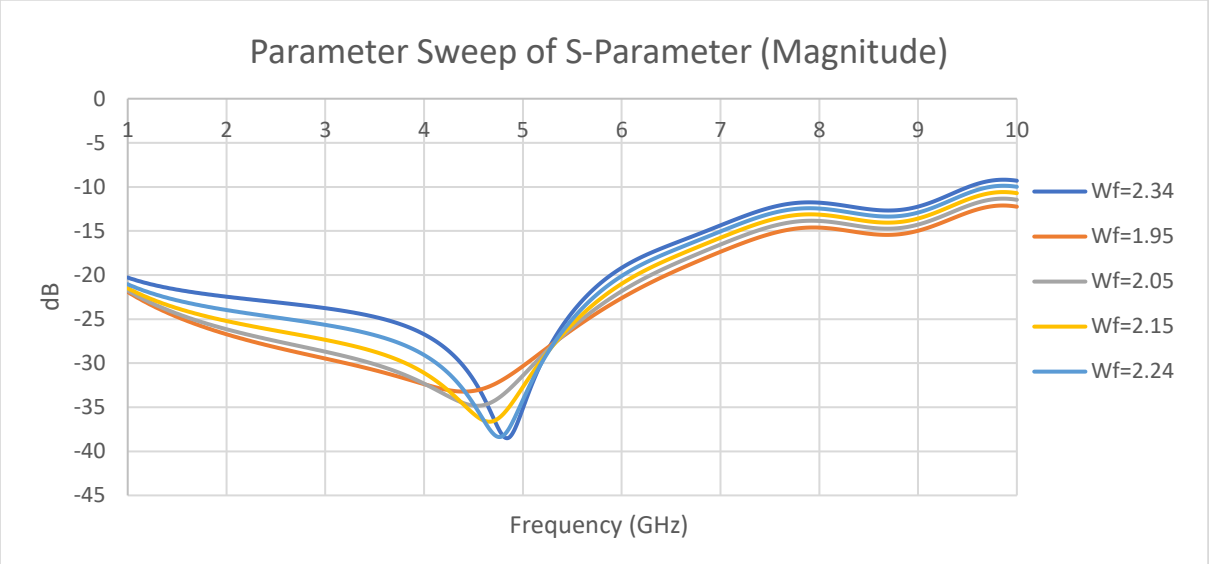

Figure 10. 2: Parameter Sweep of Lead Glass at 3.5 GHz

In figure 10.2, it shows the parameter sweep using lead glass with difference value of return loss. It is because of using difference value of length of patch that to see the difference value of return loss. Based on calculation above, the value of length patch is 17.14 mm. Therefore, using varified the value of length patch is to show the difference value of variety return loss that must below -10 dB which is -33.16, -34.79, -36.63, -38.37 and -38.50.

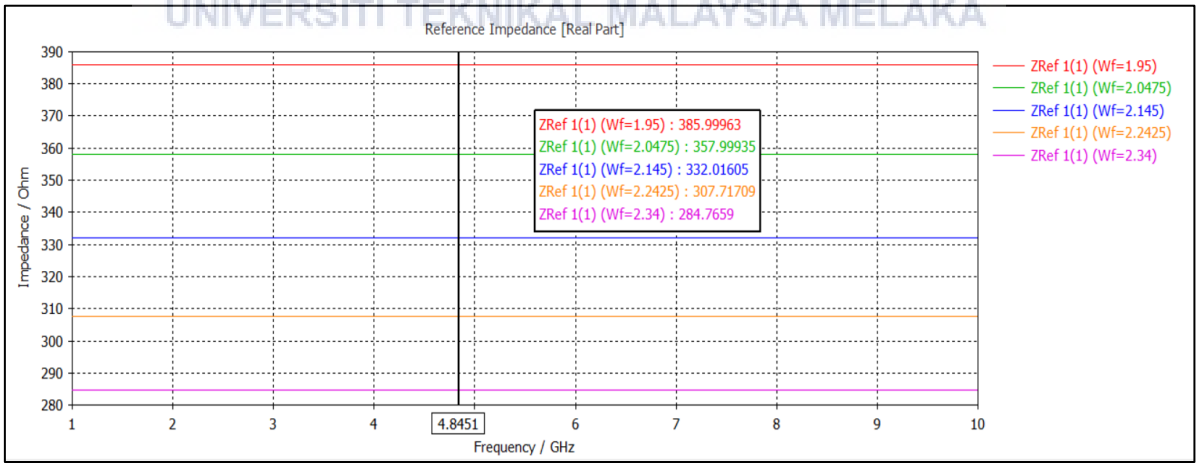

Figure 10. 3: Reference Impedance of Lead Glass at 3.5 GHz

In figure 10.3, it shows the reference impedance that using lead glass. The exactly value of impedance in antenna is 50 Ohm. The results that get in the simulation is also difference because of error. Therefore, there are difference value of impedance which are 385.99, 357.99, 332.02, 307.72 and 284.77.

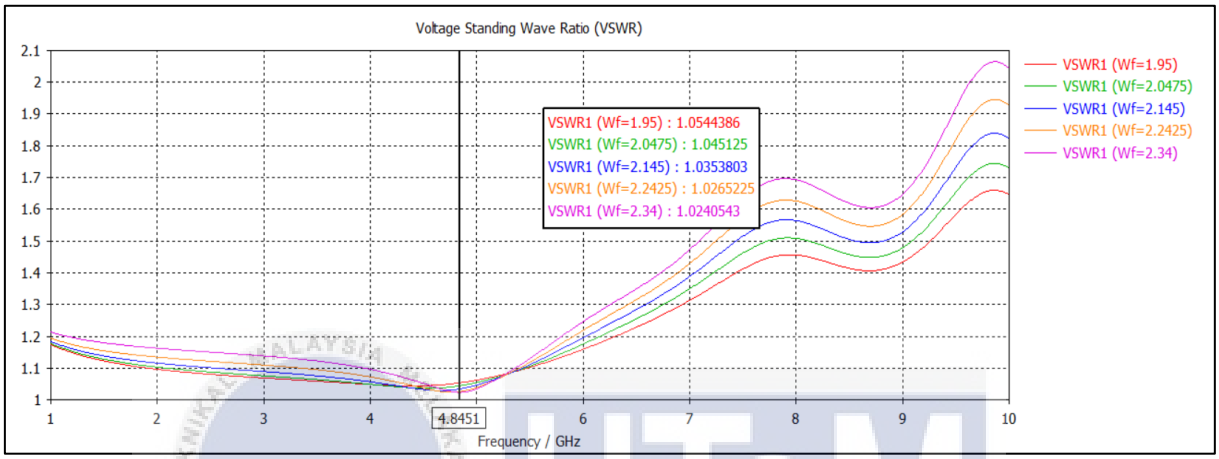

Figure 10. 4: VSWR of Lead Glass at 3.5 GHz

In figure 10.4, it shows the voltage standing wave radio that using lead glass. It is a measurement of the performance of radio frequency power transmission from a power source to a load through a transmission line. The value of voltage standing wave radio is must below 2. Therefore, the value of simulation of voltage standing wave radio is 1.06, 1.05, 1.04, 1.03 and 1.02.

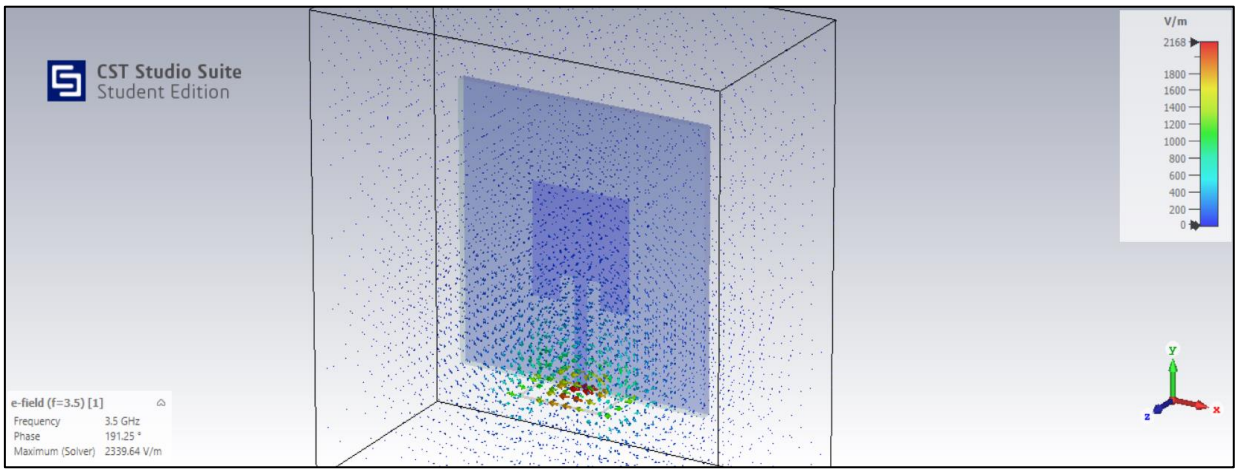

Figure 10. 5: E-field of Lead Glass at 3.5 GHz

In figure 10.5, it shows the e-field that using lead glass. E-field is standing for electric field that surrounds electrically charged particles and interacts to either attract or repel all other charged particles in the field. Therefore, at 3.5 GHz, the maximum value of e-field in this simulation is 2339.64 V/m.

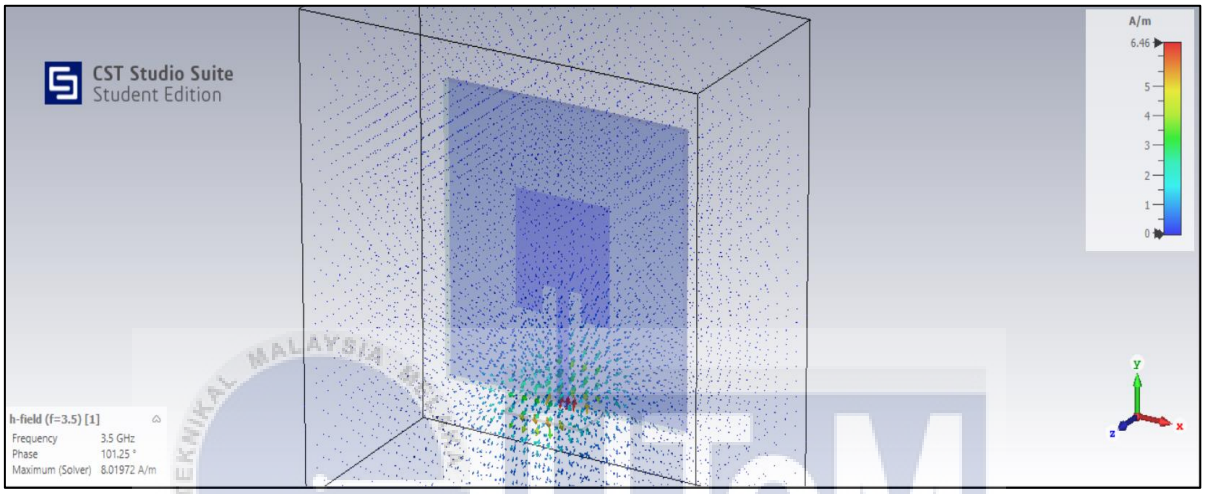

Figure 10. 6: H-field of Lead Glass at 3.5 GHz

In figure 10.6 GHz, it shows the h-filed that using lead glass. H-filed is standing for magnetic fields that what shows the antenna's greatest radiation direction. Therefore, the maximum value of h-field in this simulation at 3.5 GHz is 8.02 A/m.

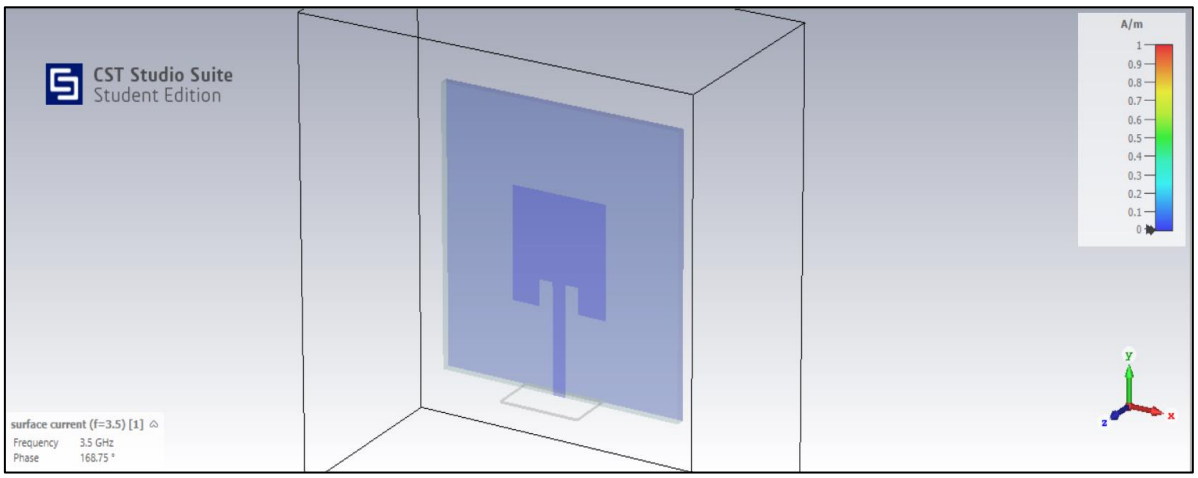

Figure 10. 7: Surface Current of Lead Glass at 3.5 GHz

In figure 10.7 GHz, it shows the surface current that using lead glass. It is an electromagnetic field that used to create a real electric current. Therefore, the maximum value of surface current in this simulation at 3.5 GHz is 168.75 A/m.

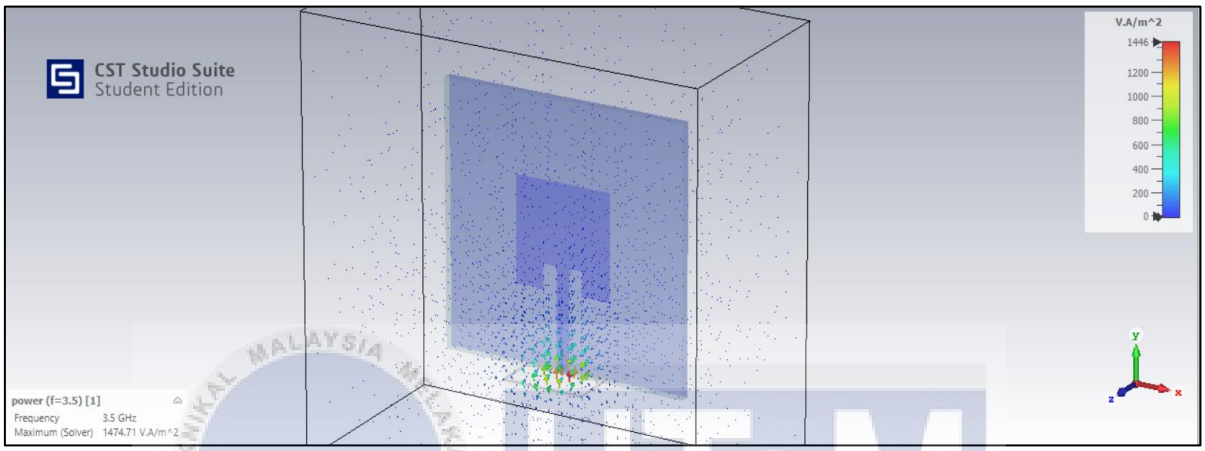

Figure 10. 8: Power of Lead Glass at 3.5 GHz

In figure 10.8, it shows the power that using lead glass. It is showing how the antenna obtains energy by radiating energy into space. Therefore, the maximum value of power in this simulation at 3.5 GHz is 1474.71 VA/m^2.

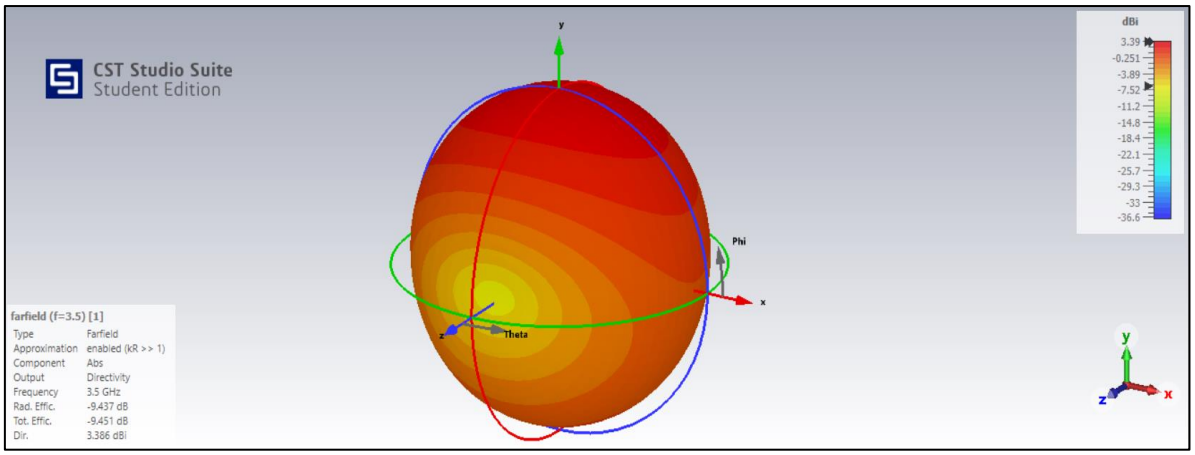

Figure 10. 9: 3D Farfield of Lead Glass at 3.5 GHz

In figure 10.9, it shows the 3D farfield that using lead glass. It shows the region where the antenna radiation pattern has a polarity variation and is independent of distance from the antenna is typically thought to be this one. Based on that, it can see the polar of theta and phi at 3.5 GHz. Therefore, the value of efficiency is -9.45 dB and the value of directivity is 3.34 dB.

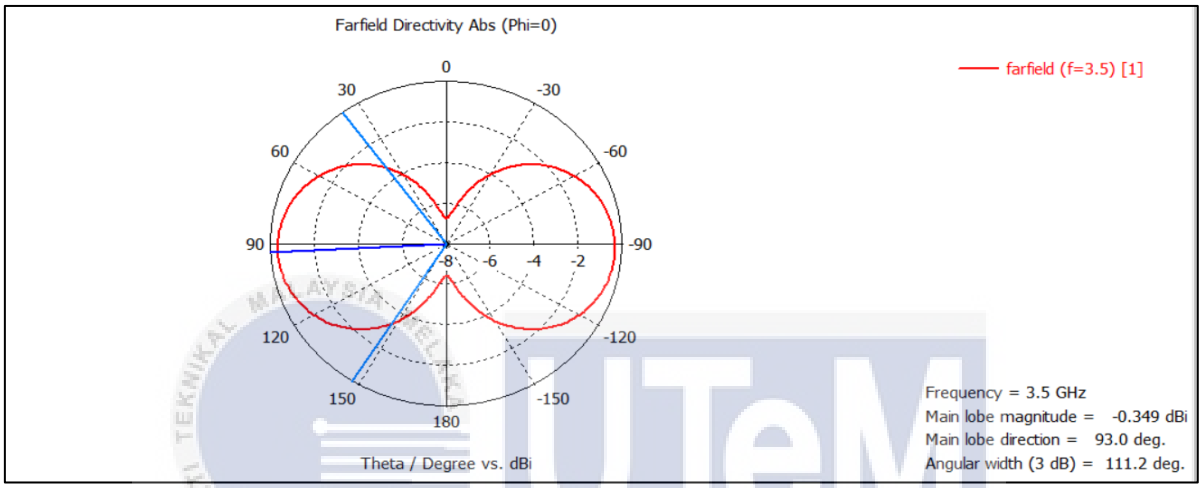

Figure 10. 10: 2D Farfield of Lead Glass at 3.5 GHz when π=0

In figure 10.10, it shows 2D farfield that using lead glass. Based on that, the value of phi is 0 that shows in the farfield directivity abs. Therefore, when phi is 0, the gain is -0.349 dB at 3.5 GHz.

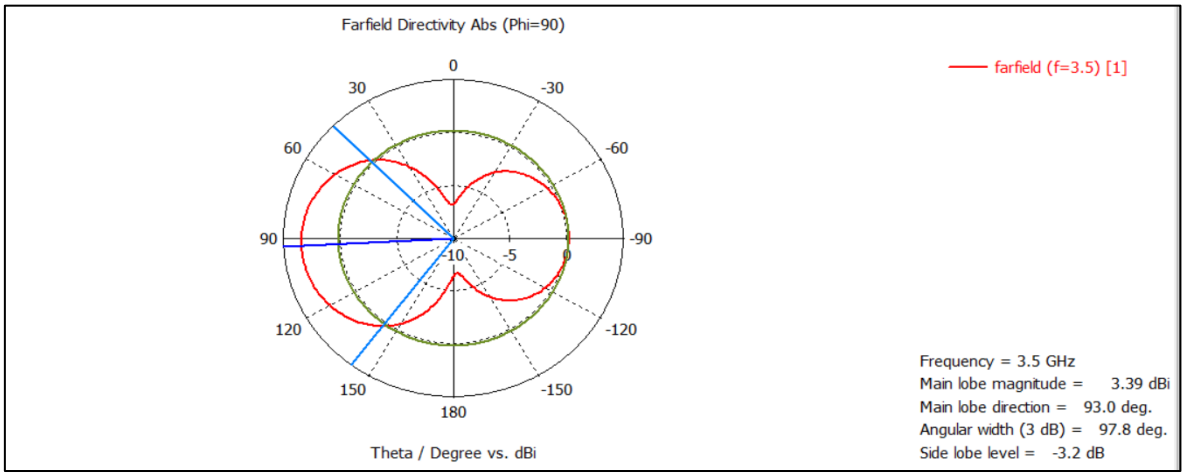

Figure 10. 11: 2D Farfield of Lead Glass at 3.5 GHz when π=90

In figure 10.11, it shows 2D farfield that using lead glass. Based on that, the value of phi is 90 that shows in the farfield directivity abs. Therefore, when phi is 90, the gain is 3.39 dB at 3.5 GHz.

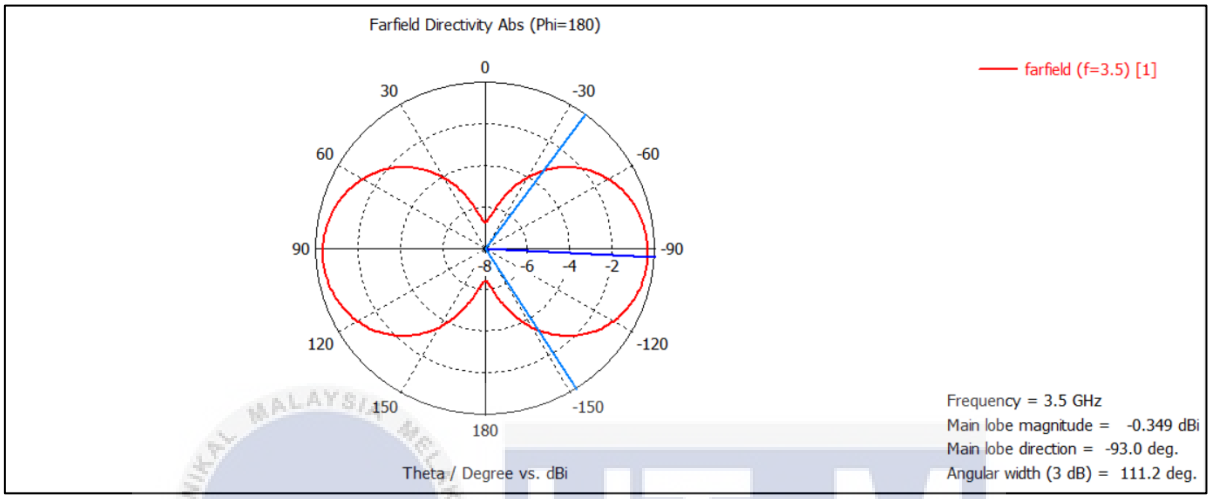

Figure 10. 12: 2D Farfield of Lead Glass at 3.5 GHz when π=180

In figure 10.12, it shows 2D farfield that using lead glass. Based on that, the value of phi is 180 that shows in the farfield directivity abs. Therefore, when phi is 180, the gain is -0.349 dB at 3.5 GHz.

4.3 Measurement of Water Samples

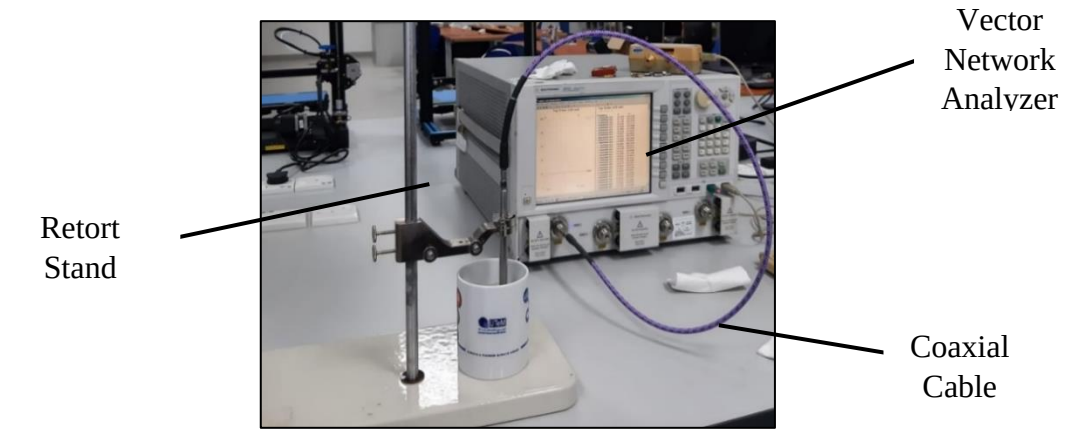

(a)Top view

(b)Side view

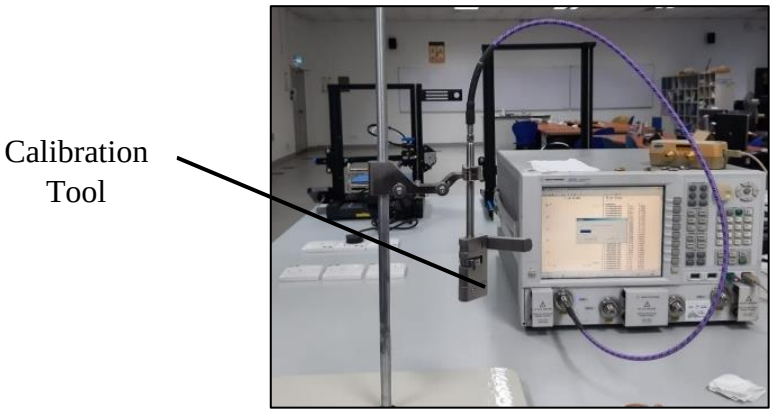

(c)Whole view

Figure 11: Equipment to measure permittivity of samples water

Figure 11, it shows the equipment to measure permittivity using six samples of water. The water samples that used are coway water, rain water, river water, sea water, sugar in water and tap water. The readings of permittivity when using difference water samples are showing in the vector network analyzer. Therefore, the dielectric probe is connecting to vector network analyzer from water samples using coaxial cable to measure the permittivity of water samples.

Furthermore, before doing measurement of permittivity using difference water samples, the dielectric probe must have to calibrate to avoid the error of readings. It is because when not doing the calibration, the readings of permittivity using difference water samples will be affected.

To calculate the conductivity, the equation is based on values of complex permittivity in readings of samples water. The equation of conductivity is based on below:

$$\varepsilon'' = \frac{\sigma'}{\omega}$$

ε'' = Complex Permittivity $\left({}^{\mathrm{F}}/_{\mathrm{m}}\right)$

σ' = Conductivity of Water $\left({}^{\mathrm{S}}/_{\mathrm{m}}\right)$

ω = angular frequency $\left({}^{rad}/_{s} = 2\pi \mathrm{f}\right.$

4.3.1 Coway Water

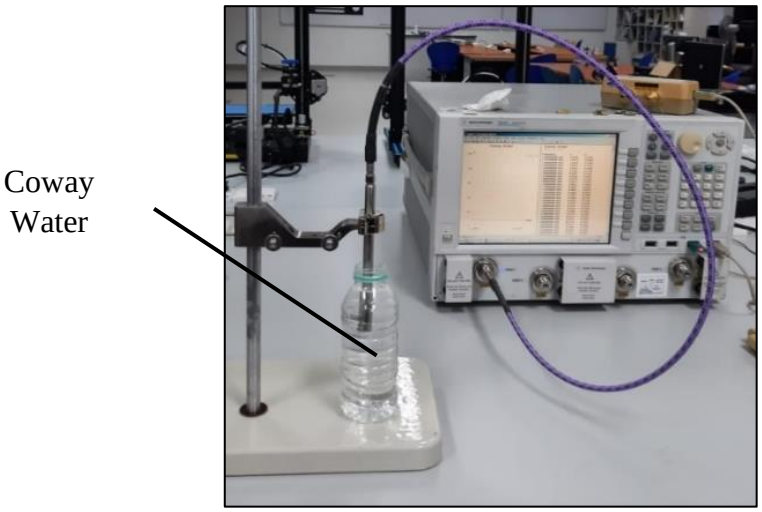

Figure 12: Measurement of coway water

In figure 12, it shows the method to measure the permittivity using water samples which is coway water. Based on the measurement, the dielectric probe was entered in the coway water and the result of readings was shown in the vector network analyzer.

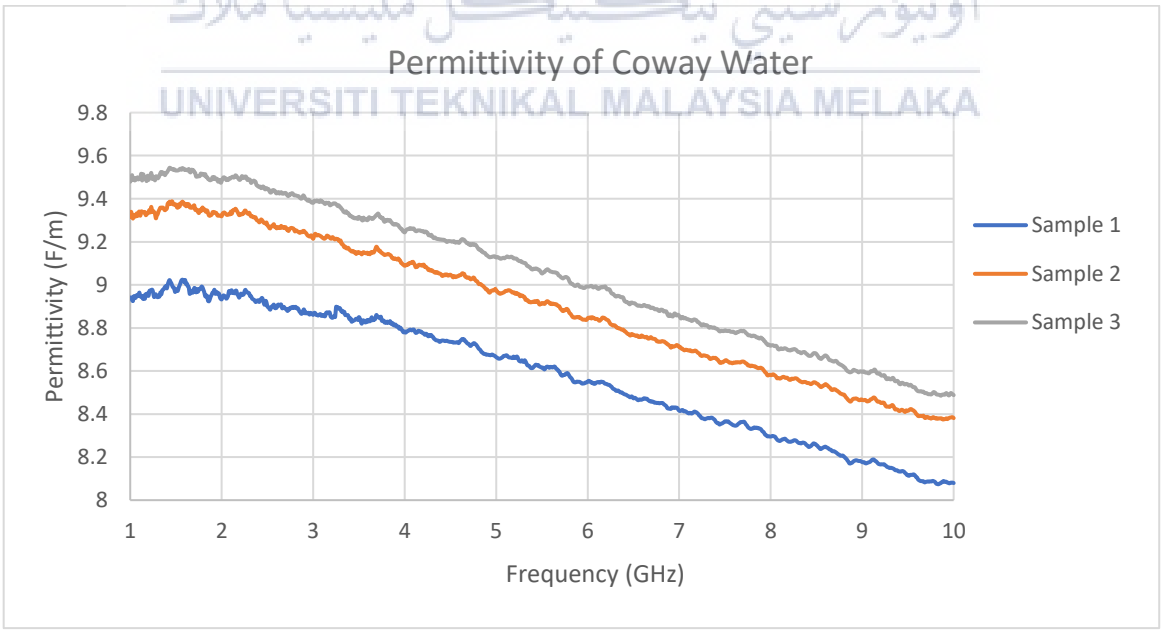

Figure 12. 1: Graph of permittivity using coway water

In figure 12.1, it shows the graph of permittivity using coway water. Based on the graph, the readings of permittivity using coway water was taken with three samples to see the difference of results. Therefore, the readings with three samples of permittivity were plotted in Microsoft Excel based on the data. From the readings, the average permittivity from three samples that was taken using coway water is 8.8483.

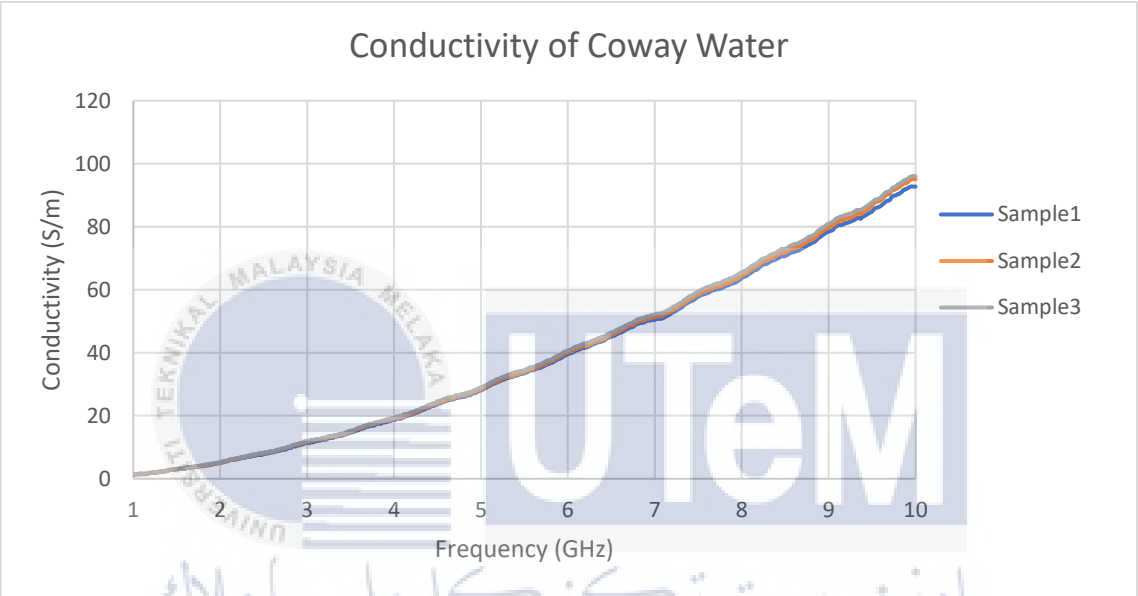

Figure 12. 2: Graph of conductivity using coway water

In figure 12.2, it shows the graph of conductivity using coway water. Based on the graph, the results of conductivity are calculating based on the equation that are given above. It plotted with three samples to see the difference of results. Therefore, the readings with three samples of conductivity were plotted in Microsoft Excel based on the data of complex permittivity and frequency on the readings of measurement. From the readings, the average of conductivity from three samples that was taken using coway water is 38.5817.

4.3.2 Rain Water

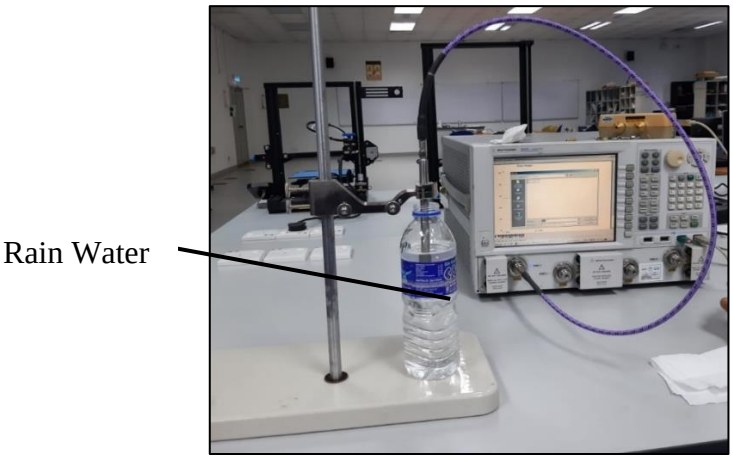

Figure 13: Measurement of rain water

In figure 13, it shows the method to measure the permittivity using water samples which is rain water. Based on the measurement, the dielectric probe was entered in the river water and the result of readings was shown in the vector network analyzer.

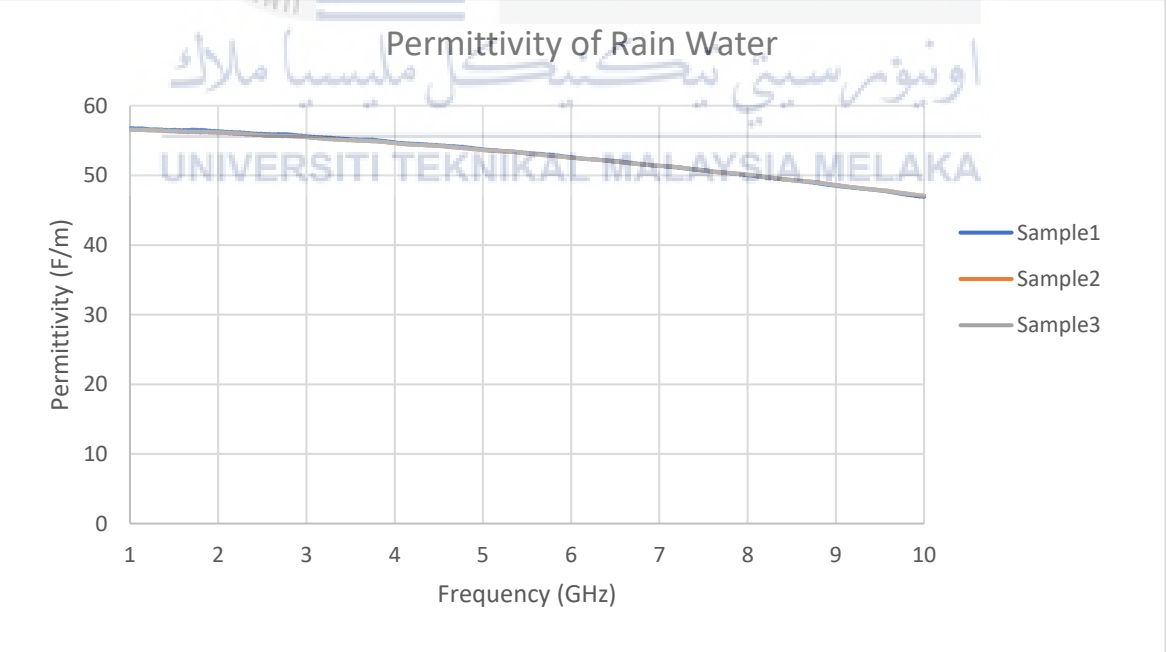

Figure 13. 1: Graph of permittivity using rain water

In figure 13.1, it shows the graph of permittivity using rain water. Based on the graph, the readings of permittivity using rain water was taken with three samples to see the difference of results. Therefore, the readings with three samples of permittivity were plotted in Microsoft Excel based on the data. From the readings, the average of permittivity from three samples that was taken using rain water is 52.7312.

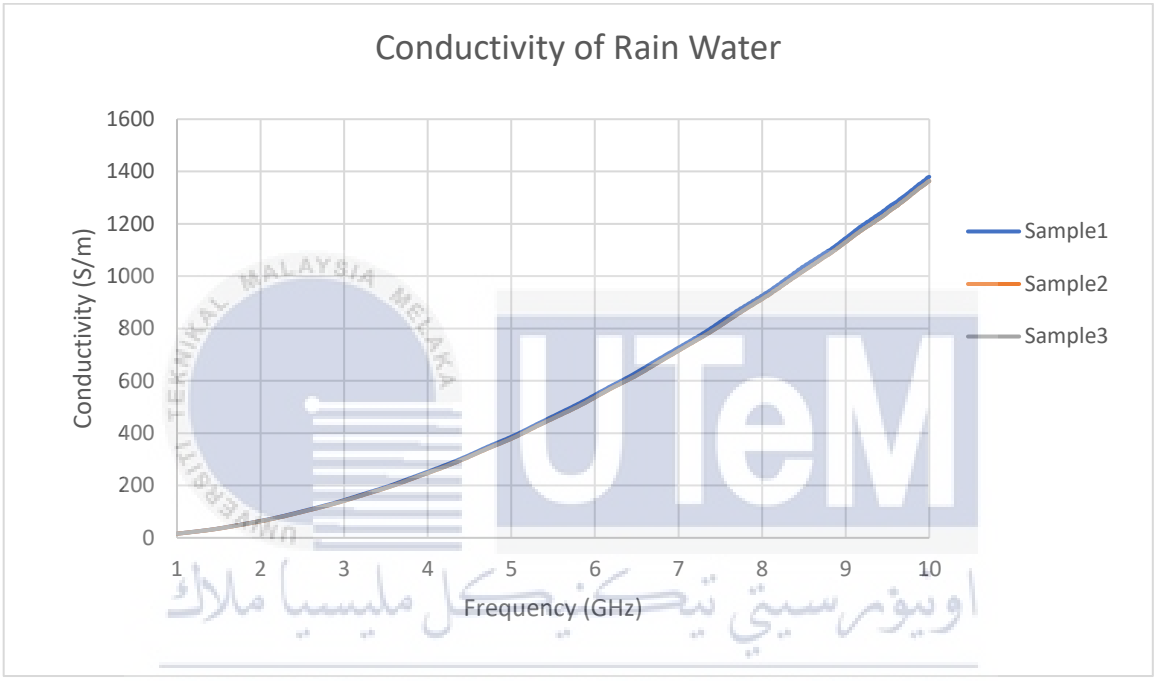

Figure 13. 2: Graph of conductivity using rain water

In figure 13.2, it shows the graph of conductivity using rain water. Based on the graph, the results of conductivity are calculating based on the equation that are given above. It plotted with three samples to see the difference of results. Therefore, the readings with three samples of conductivity were plotted in Microsoft Excel based on the data of complex permittivity and frequency on the readings of measurement. From the readings, the average of conductivity from three samples that was taken using rain water is 536.1499.

4.3.3 River Water

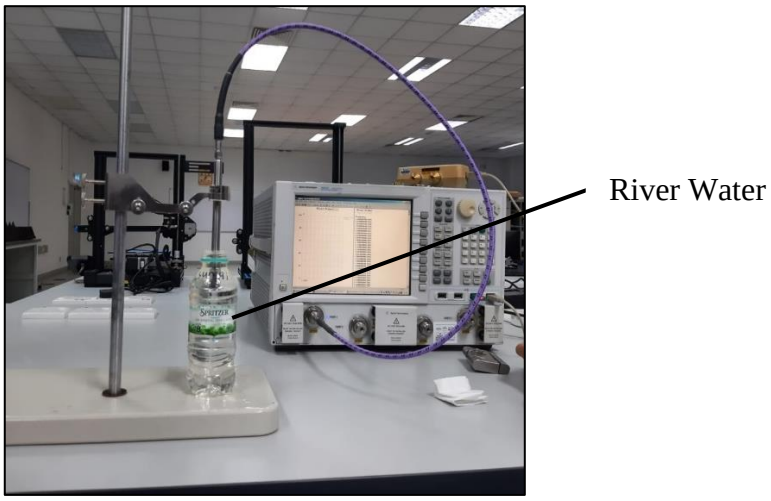

Figure 14: Measurement of river water

In figure 14, it shows the method to measure the permittivity using water samples which is river water. Based on the measurement, the dielectric probe was entered in the river water and the result of readings was shown in the vector network analyzer.

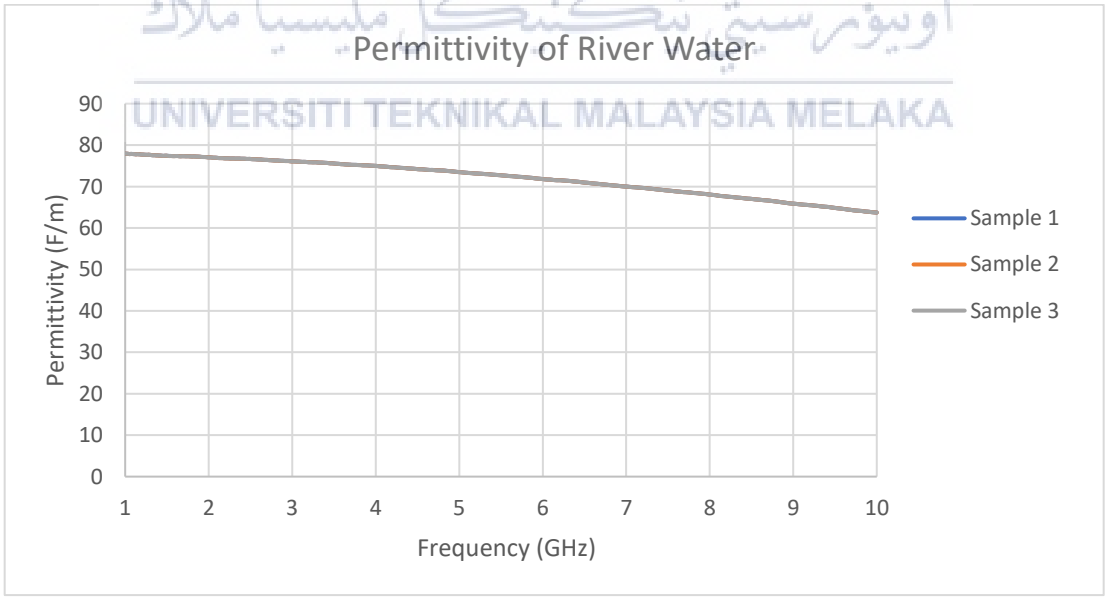

Figure 14. 1: Graph of permittivity using river water

In figure 14.1, it shows the graph of permittivity using river water. Based on the graph, the readings of permittivity using river water was taken with three samples to see the difference of results. Therefore, the readings with three samples of permittivity were plotted in Microsoft Excel based on the data. From the readings, the average of permittivity from three samples that was taken using river water is 72.0339.

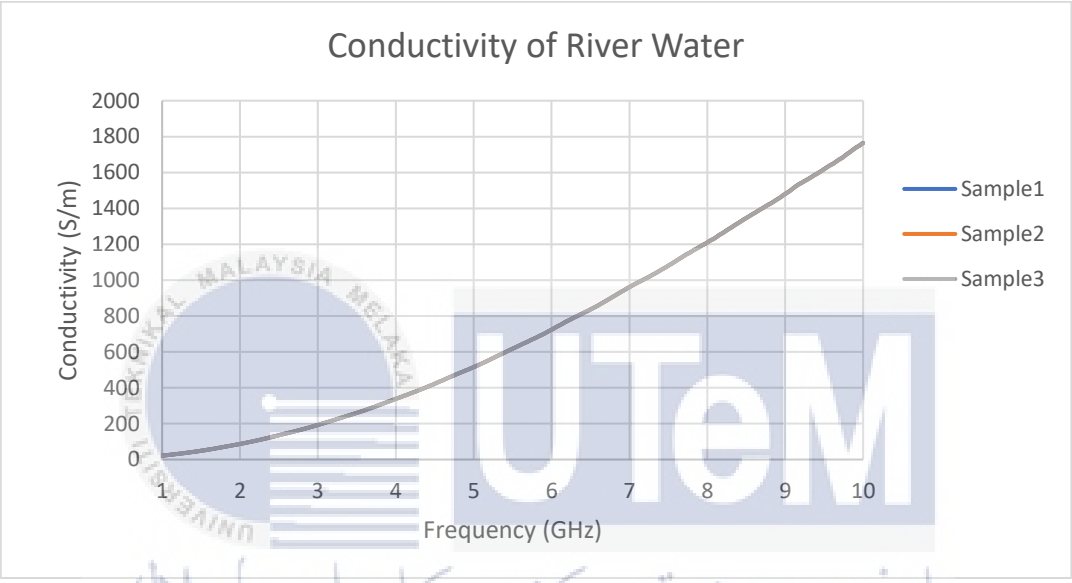

Figure 14. 2: Graph of conductivity using river water

In figure 14.2, it shows the graph of conductivity using river water. Based on the graph, the results of conductivity are calculating based on the equation that are given above. It plotted with three samples to see the difference of results. Therefore, the readings with three samples of conductivity were plotted in Microsoft Excel based on the data of complex permittivity and frequency on the readings of measurement. From the readings, the average of conductivity from three samples that was taken using river water is 708.9143.

4.3.4 Sea Water

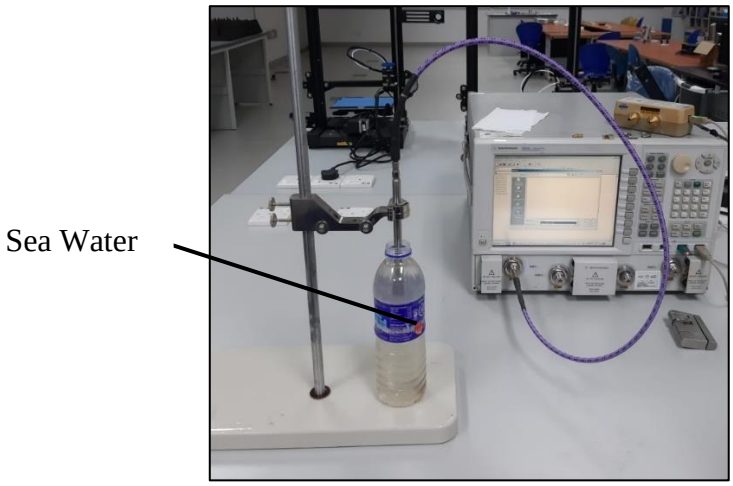

Figure 15: Measurement of sea water

In figure 15, it shows the method to measure the permittivity using water samples which is sea water. Based on the measurement, the dielectric probe was entered in the sea water and the result of readings was shown in the vector network analyzer.

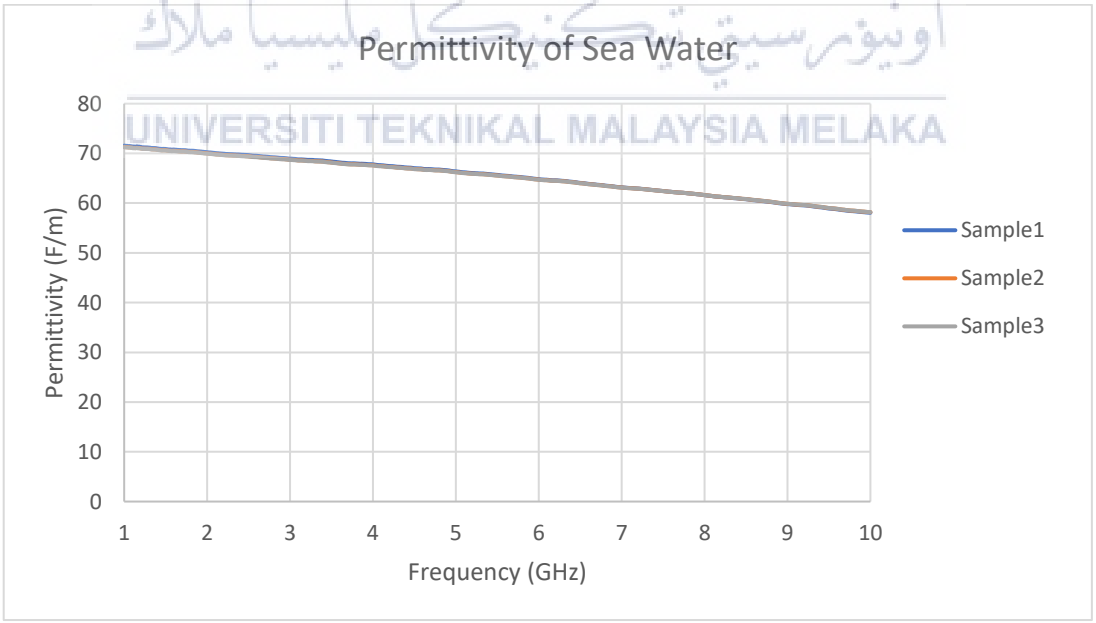

Figure 15. 1: Graph of permittivity using sea water

In figure 15.1, it shows the graph of permittivity using sea water. Based on the graph, the readings of permittivity using sea water was taken with three samples to see the difference of results. Therefore, the readings with three samples of permittivity were plotted in Microsoft Excel based on the data. From the readings, the average of permittivity from three samples that was taken using sea water is 65.2284.

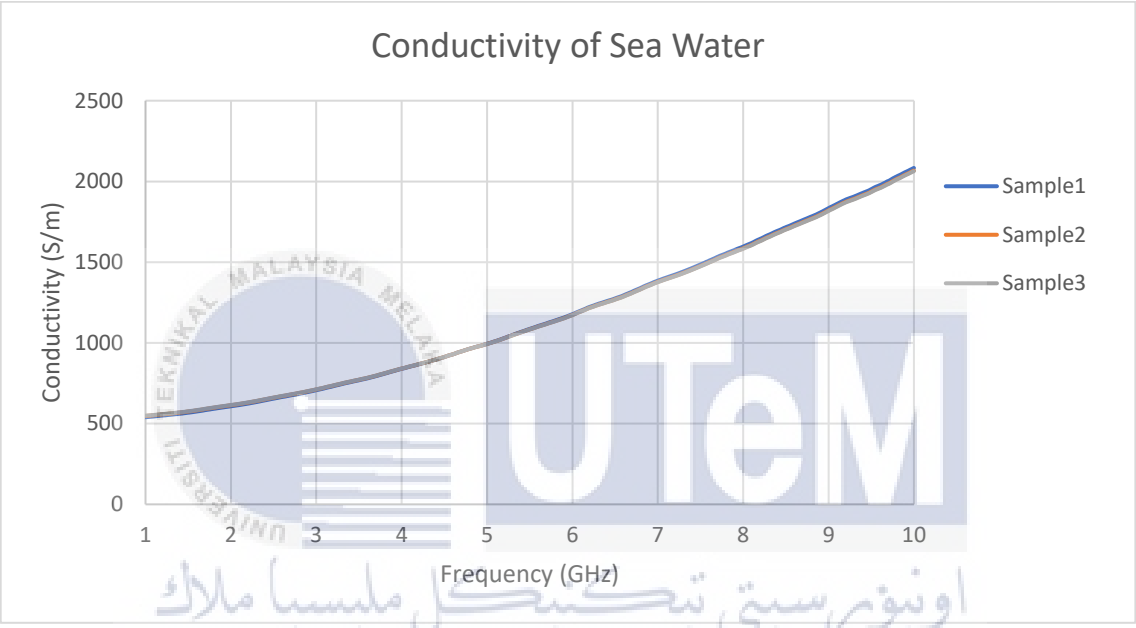

Figure 15. 2: Graph of conductivity using sea water

In figure 15.2, it shows the graph of conductivity using sea water. Based on the graph, the results of conductivity are calculating based on the equation that are given above. It plotted with three samples to see the difference of results. Therefore, the readings with three samples of conductivity were plotted in Microsoft Excel based on the data of complex permittivity and frequency on the readings of measurement. From the readings, the average of conductivity from three samples that was taken using sea water is 1157.0030.

4.3.5 Sugar in Water

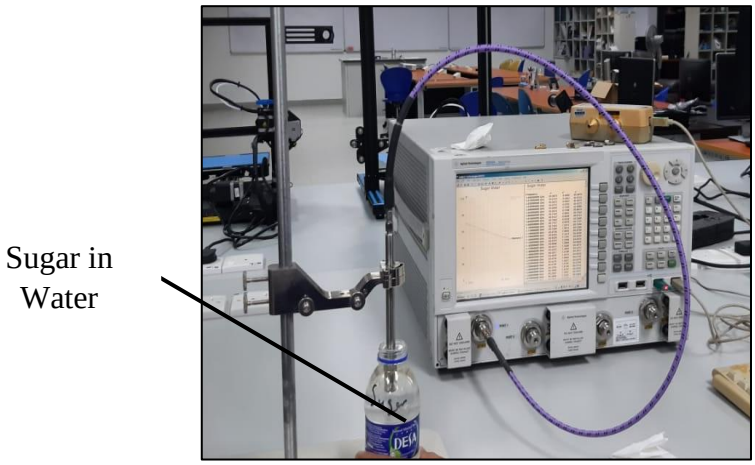

Figure 16: Measurement of sugar in water

In figure 16, it shows the method to measure the permittivity using water samples which is seven teaspoon of sugar was added in 250 ml water. Based on the measurement, the dielectric probe was entered in the sugar that added in water and the result of readings was shown in the vector network analyzer.

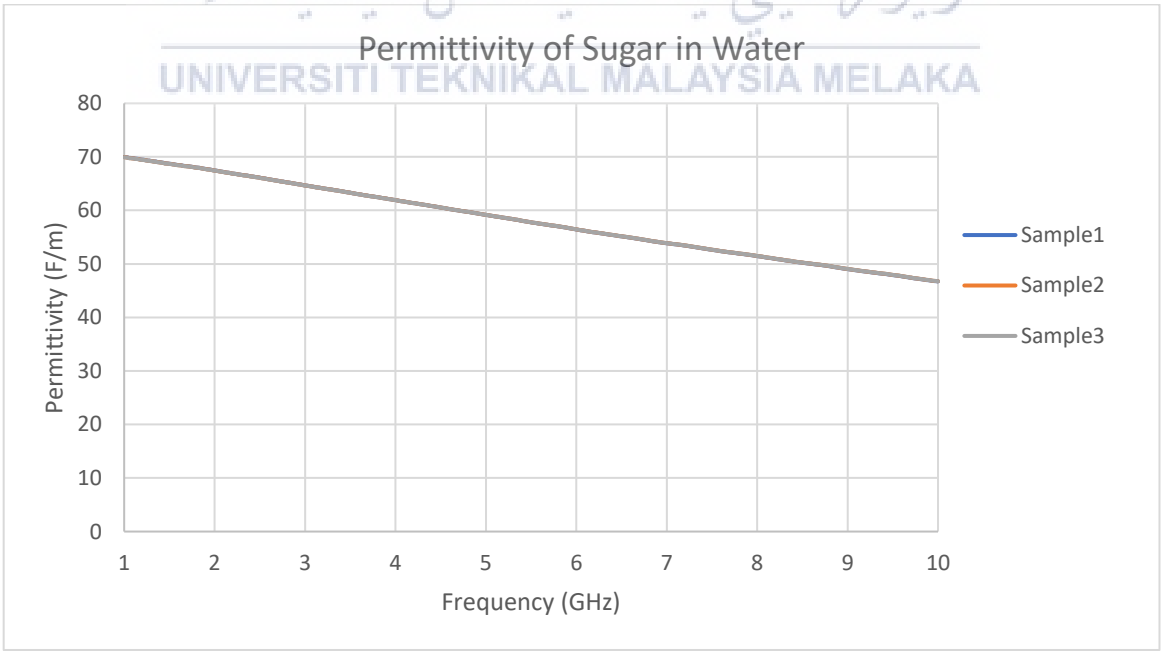

Figure 16. 1: Graph of permittivity using sugar in water

In figure 16.1, it shows the graph of permittivity using sugar that added in water. Based on the graph, the readings of permittivity using sugar that added in water was taken with three samples to see the difference of results. Therefore, the readings with three samples of permittivity were plotted in Microsoft Excel based on the data. From the readings, the average of permittivity from three samples that was taken using sugar that added in water is 58.0498.

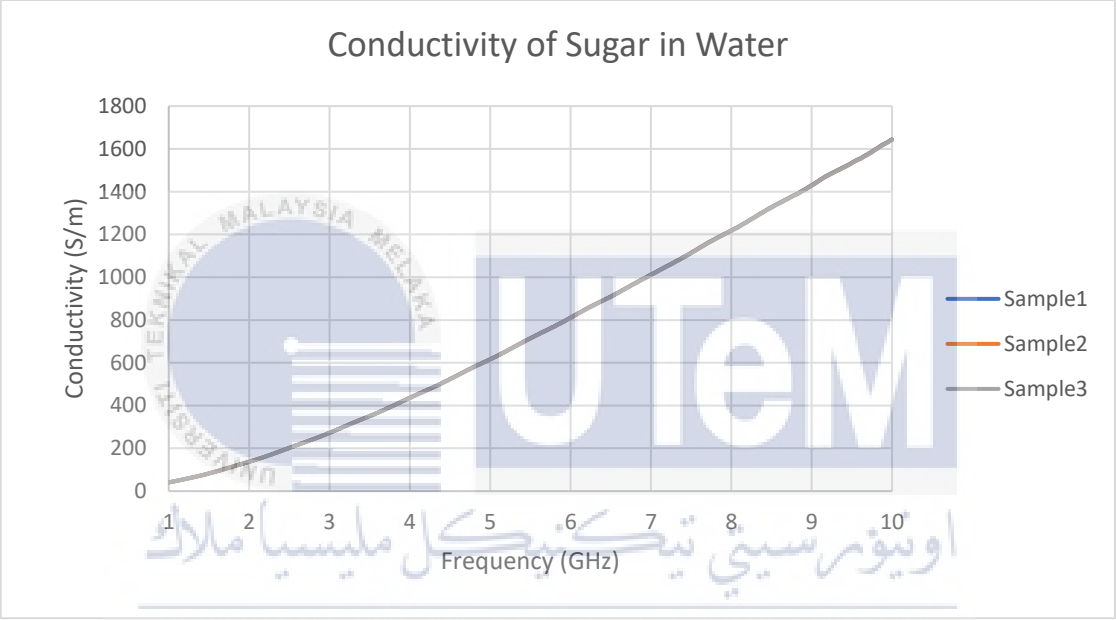

Figure 16. 2: Graph of permittivity using sugar in water

In figure 16.2, it shows the graph of conductivity using sugar in water. Based on the graph, the results of conductivity are calculating based on the equation that are given above. It plotted with three samples to see the difference of results. Therefore, the readings with three samples of conductivity were plotted in Microsoft Excel based on the data of complex permittivity and frequency on the readings of measurement. From the readings, the average of conductivity from three samples that was taken using sugar in water is 751.4808.

4.3.6 Tap Water

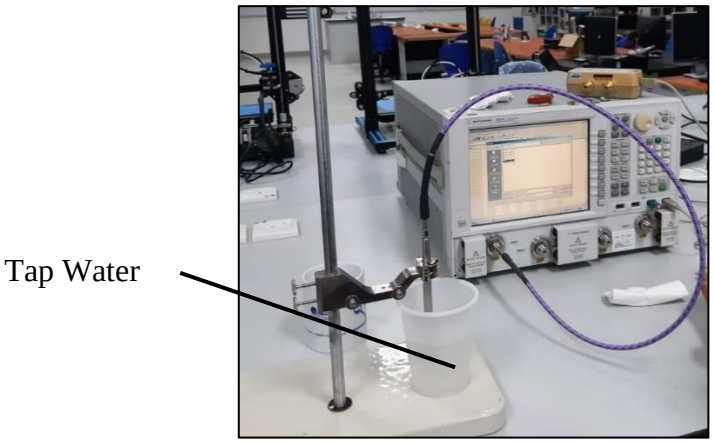

Figure 17: Measurement of tap water

In figure 17, it shows the method to measure the permittivity using water samples which is tap water. Based on the measurement, the dielectric probe was entered in the tap water and the result of readings was shown in the vector network analyzer.

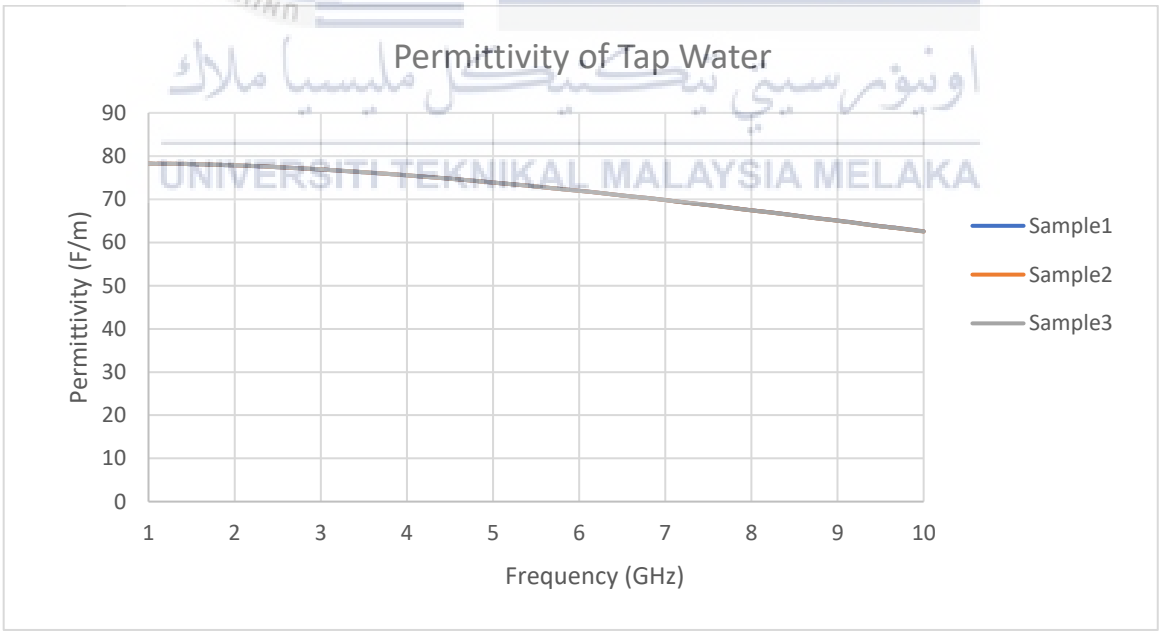

Figure 17. 1: Graph of permittivity using tap water

In figure 17.1, it shows the graph of permittivity using tap water. Based on the graph, the readings of permittivity using tap water was taken with three samples to see the difference of results. Therefore, the readings with three samples of permittivity were plotted in Microsoft Excel based on the data. From the readings, the average of permittivity from three samples that was taken using tap water is 72.1131.

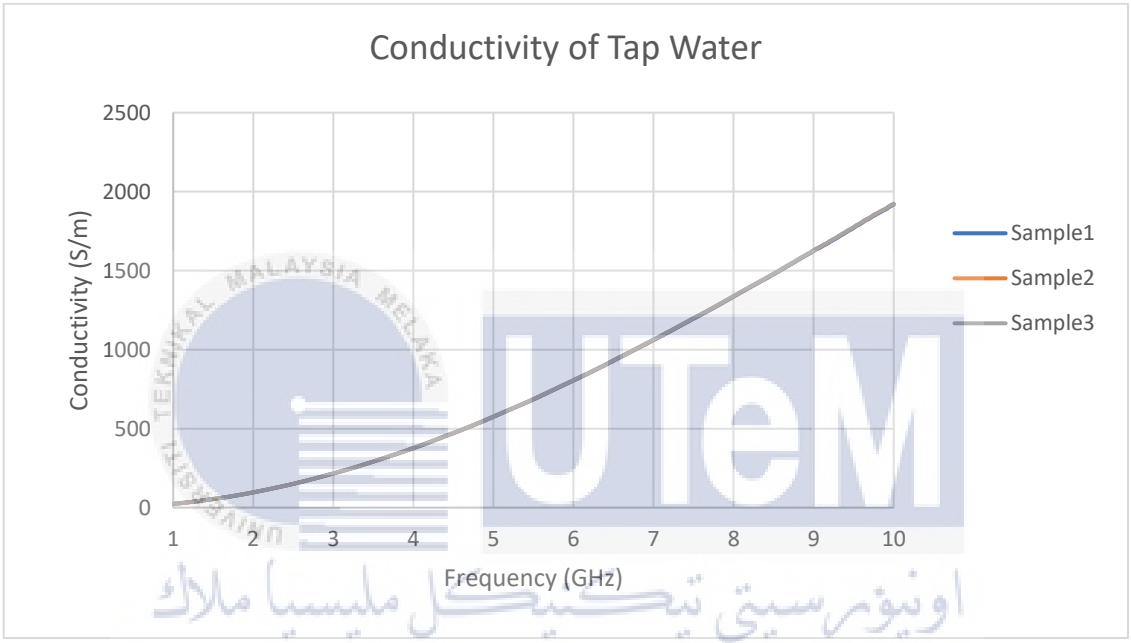

Figure 17. 2: Graph of conductivity using tap water

In figure 17.2, it shows the graph of conductivity using tap water. Based on the graph, the results of conductivity are calculating based on the equation that are given above. It plotted with three samples to see the difference of results. Therefore, the readings with three samples of conductivity were plotted in Microsoft Excel based on the data of complex permittivity and frequency on the readings of measurement. From the readings, the average of conductivity from three samples that was taken using tap water is 783.3277.

4.4 Summary

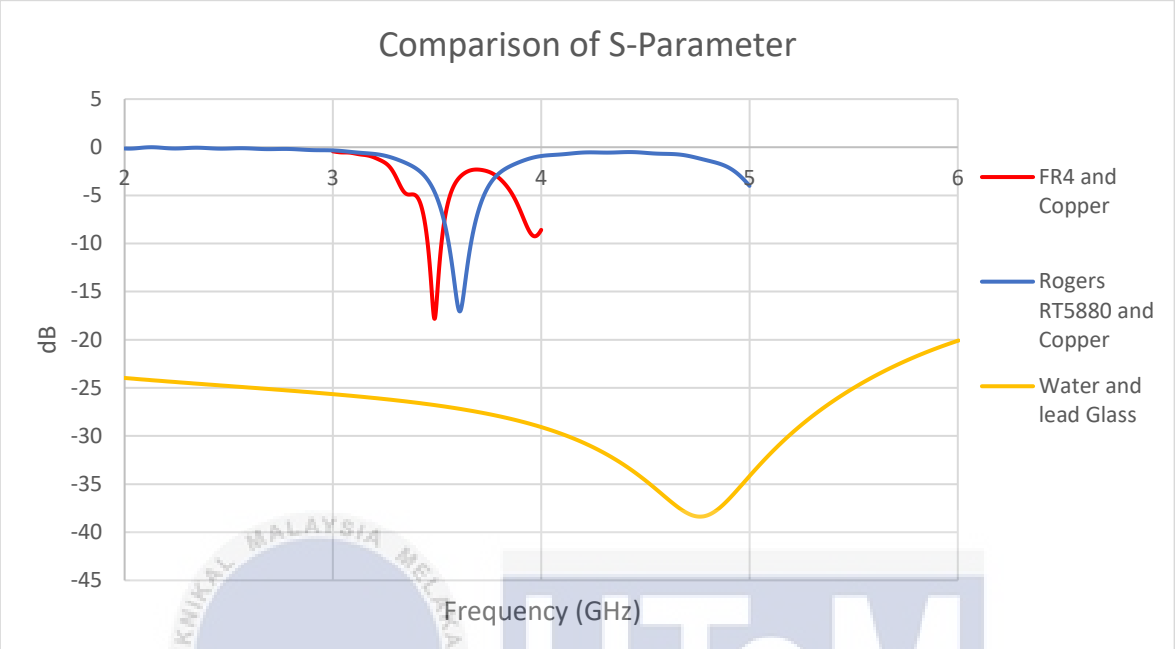

Figure 18: Graph Comparison of S-Parameter

In figure 18, it shows the graph comparison of S-Parameter using difference material which is FR4 and copper, Rogers RT5880 and copper, water and lead glass. Based on the results, material that shows the better performance is Rogers RT5880 and copper. It is because the slope of return loss sharpens than others and also the curves nearer to 3.5 GHz.

Table 9: Comparison values of difference material

	FR4 and Copper	**Rogers RT5880 and Copper**	**Water and Lead Glass**
S_{11} (return loss)	-16.88 dB	-20.23 dB	-38.50 dB
References Impedance	49.22 Ohm	49.79 Ohm	284.77 Ohm
VSWR	1.32	1.22	1.02
Gain	1.78	7.19	-0.35
Directivity	4.72	7.19	3.39
Efficiency	19.36%	90.57%	11.40%
HPBW	127.80°	82.20°	111.20°

In table 9, it shows the comparison values of difference material from the simulation results in CST Software. At FR4 and copper, the return loss is -16.88 dB, the reference impedance is 49.22 Ohm, VSWR is 1.32, gain is 1.78, directivity is 4.72, efficiency is 19.36% and HPBW is 127.80°.

In addition, at Rogers RT5880 and copper, the return loss is -20.23 dB, the reference impedance is 49.79 Ohm, VSWR is 1.22, gain is 7.19, directivity is 7.19, efficiency is 90.57% and HPBW is 82.20°. At water and lead glass, the return loss is -38.50 dB, the reference impedance is 284.77 Ohm, VSWR is 1.02, gain is -0.35, directivity is 3.39, efficiency is 11.40% and HPBW is 111.20°.

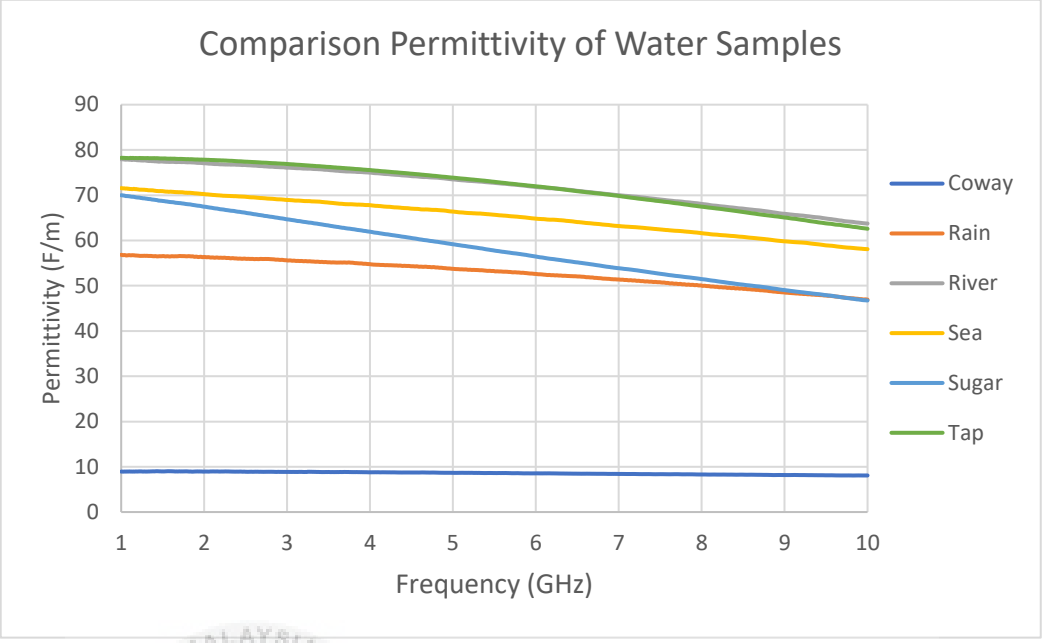

Figure 18. 1: Graph Comparison Permittivity of Water Samples

In figure 18.1, it shows the graph comparison of permittivity using six water samples such as coway water, rain water, river water, sea water, sugar in water and tap water. Therefore, based on the results of permittivity, the better permittivity is coway water because it is lowest while the highest permittivity is tap water.

Table 10: Comparison permittivity of water sample

Samples of Water	**Permittivity of Water (F/m)**
Coway Water	8.8423
Rain Water	55.1730
River water	75.5551
Sea Water	68.3518
Sugar in Water	63.2682
Tap Water	76.2388

In table 10, it shows the comparison measurement value of permittivity using six water samples such as coway water, rain water, river water, sea water, sugar in water and tap water. Based on the table, the value of permittivity was taken at 3.5 GHz. Therefore, the highest value of permittivity is tap water which is 76.2388 while the lowest permittivity is coway water which is 8.8423.

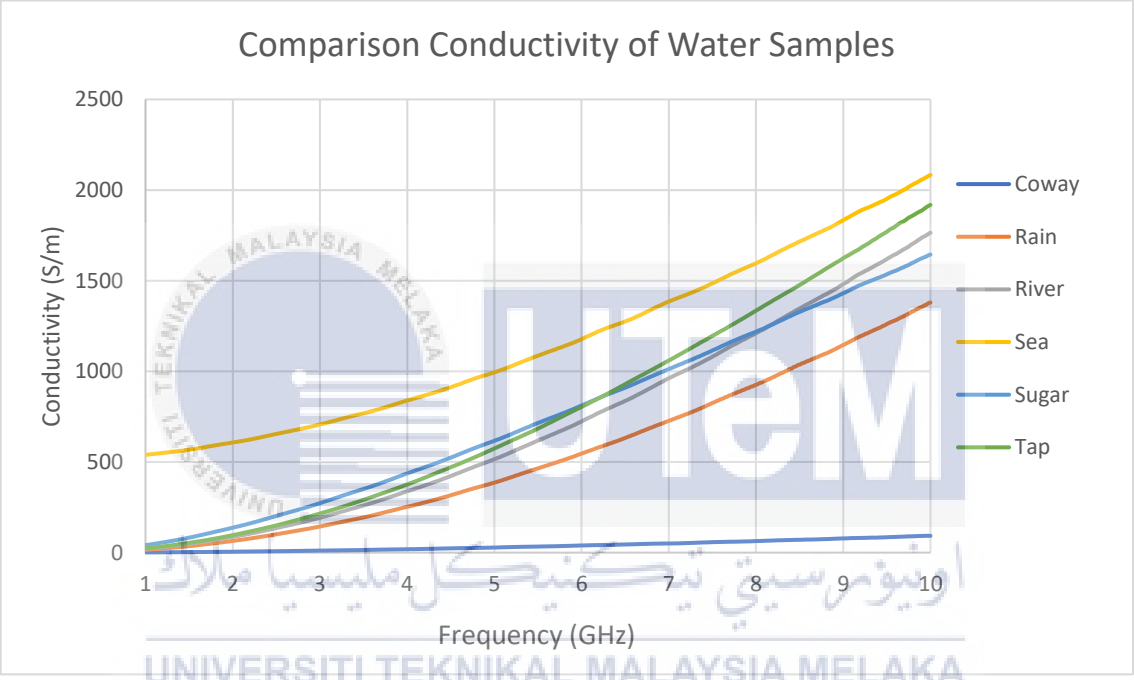

Figure 18. 2: Graph Comparison Conductivity of Water Samples

In figure 18.2, it shows the graph comparison of conductivity using six water samples such as coway water, rain water, river water, sea water, sugar in water and tap water. Therefore, based on the results of conductivity, the highest conductivity is sea water because and lowest conductivity is coway water.

Table 11: Comparison conductivity of water sample

Samples of Water	Conductivity of Water (S/m)
Coway Water	14.6194
Rain Water	194.3236
River water	260.2990
Sea Water	768.6837
Sugar in Water	351.3673
Tap Water	291.2533

In table 11, it shows the comparison measurement value of conductivity using six water samples such as coway water, rain water, river water, sea water, sugar in water and tap water. Based on the table, the value of permittivity was taken at 3.5 GHz. Therefore, the highest value of conductivity is sea water which is 768.6837 while the lowest conductivity is coway water which is 14.6194.

CHAPTER 5

CONCLUSION AND RECOMMENDATIONS

5.1 Conclusion

In conclusion, the design and simulation of a microstrip patch antenna for a 6GHz 5G communication system using CST was conducted. However, the antenna was also designed for a water-based application at 3.5GHz. The water-based antenna was able to measure the conductivity of various types of water, including sea water, rain water, river water, sugar water, coway water and tap water. The results showed that sea water had the highest conductivity while coway water had the lowest permittivity.

In addition to measuring return loss, the proposed water-based antenna materials, FR4, Rogers RT5880, and water using substrate glass, were also tested in CST Software. The results showed that Rogers RT5880 had the better performance in return loss due to its sharp curve in the s-parameter. However, water using substrate glass gave the highest value in the return loss though the curve was not as sharp.

Based on the results, it is recommended to use Rogers as the material for the proposed antenna due to its better performance in return loss. Additionally, sea water was found to be the best choice for its high conductivity. The proposed water-based antenna, using Rogers RT5880 and sea water, has the potential to be used in various applications such as water quality monitoring and wireless communication in marine environments. Overall, the results of this study provide valuable information for the design and optimization of water-based antennas in future research.

5.2 Future Works

Future work that can be done on water-based antennas includes:

i. Experimentally validating the simulation results: The simulation results of the water-based antenna should be validated experimentally to ensure their accuracy and to identify any discrepancies between the simulation and actual performance.
ii. Optimizing the antenna geometry: The geometry of the water-based antenna can be optimized to improve its performance in terms of gain, directivity, and radiation pattern.
iii. Investigating other water-based materials: Other materials that can be used as a substrate for water-based antennas can be investigated to see if they offer any performance improvements over the materials used in this study.
iv. Investigating other frequency ranges: The antenna can be designed to operate in different frequency ranges, such as in the millimetre-wave band for 5G applications, to see if it can be used in other wireless communication systems.
v. Developing a practical application: The water-based antenna can be integrated into a practical application, such as a water quality monitoring system or wireless communication system in marine environments, to demonstrate its potential use in real-world scenarios.
vi. Study the effect of temperature, humidity and pressure on the antenna performance.
vii. Study the effect of different conductivity of water on the antenna performance.
viii. Study the effect of different dielectric constant of water on the antenna performance.
ix. Study the effect of different permittivity of water on the antenna performance.

All of these studies will provide valuable information for the design and optimization of water-based antennas in future research.

REFERENCES

[1] J. Yi, W. Li, L. Wang, and Z. Wen, "The simulation of frequency-capacitance characteristics of fresh water conductivity sensor," *4th IEEE Int. Conf. Nano/Micro Eng. Mol. Syst. NEMS 2009*, no. d, pp. 29–32, 2009, doi: 10.1109/NEMS.2009.5068520.

[2] S. Hong, Y. Kim, and C. Won Jung, "Transparent Microstrip Patch Antennas with Multilayer and Metal-Mesh Films," *IEEE Antennas Wirel. Propag. Lett.*, vol. 16, no. c, pp. 772–775, 2017, doi: 10.1109/LAWP.2016.2602389.

[3] C. Ding, L. Liu, and K. M. Luk, "An optically transparent dual-polarized stacked patch antenna with metal-mesh films," *IEEE Antennas Wirel. Propag. Lett.*, vol. 18, no. 10, pp. 1981–1985, 2019, doi: 10.1109/LAWP.2019.2935694.

[4] Y. Li and K. M. Luk, "A Water Dense Dielectric Patch Antenna," *IEEE Access*, vol. 3, pp. 274–280, 2015, doi: 10.1109/ACCESS.2015.2420103.

[5] J. Sun and K. M. Luk, "A Circularly Polarized Water Patch Antenna," *IEEE Antennas Wirel. Propag. Lett.*, vol. 19, no. 6, pp. 926–929, 2020, doi: 10.1109/LAWP.2020.2982690.

[6] J. Serrao and A. Fakih, "Design and analysis of a broadband low profile monopolar patch antenna," *Proc. - 2014 6th Int. Conf. Comput. Intell. Commun. Networks, CICN 2014*, pp. 46–50, 2014, doi: 10.1109/CICN.2014.22.

[7] Z. Hu, S. Wang, Z. Shen, and W. Wu, "Broadband Polarization-Reconfigurable Water Spiral Antenna of Low Profile," *IEEE Antennas Wirel. Propag. Lett.*, vol. 16, pp. 1377–1380, 2017, doi: 10.1109/LAWP.2016.2636923.

[8] Z. Ren, S. S. Qi, Z. Hu, Z. Shen, and W. Wu, "Wideband Water Helical Antenna of Circular Polarization," *IEEE Trans. Antennas Propag.*, vol. 67, no. 11, pp. 6770–6777, 2019, doi: 10.1109/TAP.2019.2922846.

[9] Y. Guo, M. Yan, W. Chia, Z. N. Chen, and K. Luk, "0 : 475 0)," vol. 52, no. 4, pp. 1115–1116, 2004.

[10] L. Xing, Y. Huang, Q. Xu, S. Alja'Afreh, and T. Liu, "A Broadband Hybrid Water Antenna for Hand-Portable Applications," *IEEE Antennas Wirel. Propag. Lett.*, vol. 15, pp. 174–177, 2016, doi: 10.1109/LAWP.2015.2436692.

[11] W. Lin and H. Wong, "Circularly polarized conical-beam antenna with wide bandwidth and low profile," *IEEE Trans. Antennas Propag.*, vol. 62, no. 12, pp. 5974–5982, 2014, doi: 10.1109/TAP.2014.2360223.

[12] L. Ge and K. M. Luk, "Frequency-reconfigurable low-profile circular monopolar patch antenna," *IEEE Trans. Antennas Propag.*, vol. 62, no. 7, pp. 3443–3449, 2014, doi: 10.1109/TAP.2014.2318077.

[13] Y. Shi and J. Liu, "Wideband and Low-Profile Omnidirectional Circularly Polarized Antenna With Slits and Shorting-Vias," *IEEE Antennas Wirel. Propag. Lett.*, vol. 15, no. c, pp. 686–689, 2016, doi: 10.1109/LAWP.2015.2469277.

[14] J. Sun and K. M. Luk, “A compact-size wideband optically-transparent water patch antenna incorporating an annular water ring,” *IEEE Access*, vol. 7, pp. 122964–122971, 2019, doi: 10.1109/ACCESS.2019.2936458.

[15] Z. Ren, S. S. Qi, W. Wu, and Z. Shen, “Pattern-reconfigurable water horn antenna,” *IEEE Trans. Antennas Propag.*, vol. 69, no. 8, pp. 5084–5089, 2021, doi: 10.1109/TAP.2021.3064036.

[16] J. Sun and K. M. Luk, “A fully transparent wideband water patch antenna with L-shaped feed,” *IEEE Open J. Antennas Propag.*, vol. 2, no. July, pp. 968–975, 2021, doi: 10.1109/OJAP.2021.3111700.

[17] C. Hua *et al.*, “Reconfigurable Antennas Based on Pure Water,” *IEEE Open J. Antennas Propag.*, vol. 2, no. March, pp. 623–633, 2021, doi: 10.1109/OJAP.2021.3079353.

[18] Samsuzzaman, M. T. Islam, N. Rahman, and M. S. J. Singh, “Detection of salt and sugar contents in water on the basis of dielectric properties using microstrip antenna-based sensor,” *IEEE Access*, vol. 6, pp. 4118–4126, 2018, doi: 10.1109/ACCESS.2017.2787689.

[19] C. Hua, Z. Shen, and J. Lu, “High-efficiency sea-water monopole antenna for maritime wireless communications,” *IEEE Trans. Antennas Propag.*, vol. 62, no. 12, pp. 5968–5973, 2014, doi: 10.1109/TAP.2014.2360210.

[20] L. Xing, Y. Huang, Q. Xu, S. Alja’Afreh, and T. Liu, “Complex permittivity of water-based liquids for liquid antennas,” *IEEE Antennas Wirel. Propag. Lett.*, vol. 15, no. c, pp. 1626–1629, 2016, doi: 10.1109/LAWP.2016.2519542.

[21] D. Wang, N. Jin, J. Ma, and Y. Ren, “Measurement of Water Holdup in Oil-Gas-Water Slug Flow Using Microstrip Antenna,” *IEEE Trans. Instrum. Meas.*, vol. 70, 2021, doi: 10.1109/TIM.2021.3096574.